

# ***Energy Mines and Resources – YTG***

---

## ***Mount Nansen Bioremediation Assessment***



*February 2006*

***DRAFT***



# ***Table of Contents***

---

# *Table of Contents*

---

<b>TABLE OF CONTENTS</b> .....	i
<b>1. INTRODUCTION</b> .....	1-1
<b>2. BACKGROUND</b> .....	2-1
<b>3. DISCUSSIONS</b> .....	3-1
3.1 TAILINGS POND .....	3-1
3.2 BROWN MCDADE PIT LAKE .....	3-15
<b>4. CONCLUSIONS AND RECOMMENDATIONS</b>	
4.1 TAILINGS POND .....	4-1
4.2 PIT LAKE .....	4-2
4.3 RECOMMENDATIONS .....	4-4
<b>REFERENCES</b> .....	R-1
 <b>APPENDIX A:</b> MINERALOGY OF TAILINGS FROM THE MOUNT NANSEN SITE, YUKON	

## LIST OF TABLES

<b>TABLE 3-1</b>	DILUTION AND BASE FLOW CALCULATIONS FOR DOME CREEK .....	3-9
<b>TABLE 3-2</b>	DILUTION AND BASE FLOW CALCULATIONS FOR VICTORIA CREEK.....	3-9

## LIST OF FIGURES

<b>FIGURE 3-1</b>	AMMONIA AND SODIUM IN THE MOUNT NANSEN TAILINGS POND THROUGH THE OPEN WATER PERIOD OF 2005 .....	3-2
<b>FIGURE 3-2</b>	NITRATE, NITRITE AND AMMONIA (AS N) IN THE MOUNT NANSEN TAILINGS POND THROUGH THE OPEN WATER PERIOD OF 2005 .....	3-3
<b>FIGURE 3-3</b>	AMMONIA (AS N) AND TOTAL ALKALINITY IN THE MOUNT NANSEN TAILINGS POND THROUGH THE OPEN WATER PERIOD OF 2005 .....	3-4
<b>FIGURE 3-4</b>	TOTAL AND WAD CYANIDE IN THE MOUNT NANSEN TAILINGS POND THROUGH THE 2005 SAMPLING YEAR.....	3-6
<b>FIGURE 3-5</b>	THIOCYANATE IN THE MOUNT NANSEN TAILINGS POND THROUGH THE OPEN WATER PERIOD OF 2005 .....	3-7
<b>FIGURE 3-6</b>	SULPHATE IN THE TAILINGS POND, SEEPAGE POND, DOME CREEK AND VICTORIA CREEK DURING THE 2005 FIELD SAMPLING. ....	3-8
<b>FIGURE 3-7</b>	DISSOLVED ARSENIC IN THE TAILINGS POND AND SEEPAGE POND DURING THE 2005 FIELD SAMPLING .....	3-11
<b>FIGURE 3-8</b>	THE MOUNT NANSEN TAILINGS POND AND COLLECTION SITES FOR SURFACE TAILINGS GRAB SAMPLES.....	3-12
<b>FIGURE 3-9</b>	SAMPLE 006 IN PLAIN TRANSMITTED LIGHT, WIDTH OF FIELD 2.6 MM, SHOWING A LARGE PARTICLE OF REDDISH, HETEROGENEOUS FE OXYHYDROXIDE .....	3-13
<b>FIGURE 3-10</b>	SAMPLE 006 IN PLAIN REFLECTED LIGHT, WIDTH OF FIELD 0.625 MM, SHOWING FE-OXYHYDROXIDE RIMS ON PYRITE. THE ADJACENT WHITE PRISMATIC GRAIN SOUTHEAST OF THE ALTERED PYRITE IS ARSENOPYRITE .....	3-14
<b>FIGURE 3-11</b>	BACKSCATTERED-ELECTRON IMAGE OF SAMPLE 005 SHOWING A GRAIN OF ARSENOPYRITE WITH A READILY VISIBLE ALTERATION RIM (FE ARSENATE) .....	3-14
<b>FIGURE 3-12</b>	STATION LOCATIONS AND APPROXIMATE WATER DEPTH WITHIN THE BROWN MCDADE PIT LAKE .....	3-15
<b>FIGURE 3-13</b>	DISSOLVED CA AND SULPHATE IN THE BROWN-MCDADE PIT LAKE DURING THREE SEPARATE SURVEYS AT STATION SP1 .....	3-16
<b>FIGURE 3-14</b>	DISSOLVED MN AND NITRATE IN THE BROWN-MCDADE PIT LAKE DURING THREE SEPARATE SURVEYS AT STATION SP1 .....	3-17
<b>FIGURE 3-15</b>	DISSOLVED ZN AND CD IN THE BROWN-MCDADE PIT LAKE DURING THREE SEPARATE SURVEYS AT STATION SP1.....	3-17
<b>FIGURE 3-16</b>	SOUTHERN-MOST SHORE OF THE BROWN-MCDADE PIT LAKE SHOWING THE PRESENCE OF AN ALGAL MAT BLANKETING THE SHALLOW LAKE FLOOR.....	3-18

# ***1. Introduction***

---

# **1. Introduction**

---

The Mount Nansen gold mine operated between 1997 and 1999. Oxide and sulphide ores were mined from the Brown-McDade Pit, producing approximately 250,000 tonnes of arsenic- and cyanide-bearing tailings which were stored in an impoundment within the Dome Creek watershed down-gradient of the mill. Water quality in the tailings pond has only been measured accurately since the beginning of 2005, but shows evidence of elevated concentrations of some parameters associated with the break-down of cyanide compounds. The pit has partially flooded since mine closure, and now hosts a shallow lake hosting elevated concentrations of zinc, cadmium and nitrate.

In order to assess the potential to further improve water quality within both the tailings and pit lake facilities, Lorax was commissioned to examine the existing data and assess the potential for viable treatment strategies with emphasis on bioremediation.

The following report presents an assessment of the data and defines the governing geochemical mechanisms active in each of these facilities with special reference to the advantages and liabilities associated with bioremediation programs. Following a presentation of background information in Chapter 2, which summarizes the parameters of concern and relevant geochemical processes, the results of the data interpretation for both the tailings pond and pit lake and discussed (Chapter 3). The report concludes with a discussion of the salient conclusions and recommendations (Chapter 4).

## ***2. Background***

---

## 2. Background

---

There are two facilities under consideration for water treatment at the Mount Nansen Mine site, the tailings pond and the Brown-McDade pit lake. The Mount Nansen tailings pond hosts a suite of nitrogenous species most notably cyanide, thiocyanate and ammonia whereas the Brown-McDade pit lake hosts elevated nitrate. More importantly in the pit lake is the presence of elevated concentrations of dissolved zinc. In all cases, the parameters of interest are candidates for mitigation through bioremediation. However, in order to understand which treatment options are most viable, the geochemistry of relevant species and the notion of bioremediation must be defined. These factors are summarized below.

### ***Bioremediation***

Biological production (*i.e.*, algal/phytoplankton growth) in fresh water lakes and streams is typically limited by available phosphorus (P) (Schindler, 1977); this is likely true for the Mount Nansen Tailings Pond where P-limitation allows excess ammonia to build up rather than being consumed by algal growth. The intentional addition of phosphate (and other nutrients) can act to enhance algal productivity in a tailings pond, potentially leading to a series of ameliorative effects including: 1) the consumption of nitrogenous species from the water column (most notably nitrate, nitrite and ammonia) through the assimilation and growth of phytoplankton; 2) the assimilation and sorption of Cu, Zn and other trace elements by phytoplankton and subsequent removal from the water column via particle settling; 3) the development of ephemeral reducing conditions in the water column or at the sediment-water interface, leading to the removal of trace metals from solution via the formation of sulphide minerals; and 4) production of alkalinity through the uptake of nitrate and carbon dioxide by primary producers (McNee, 2003). Such alterations to biological production (bioremediation) have the potential to greatly reduce water column concentrations of ammonia in addition to Cu and Zn via particle removal, as well as to foster the conditions necessary for the permanent removal of Cu and Zn via sulphide precipitation.

### ***Nitrogen Geochemistry***

Cyanide is typically used in the processing of gold-bearing ore; thus, while cyanide can be produced naturally, the primary source in the Mount Nansen tailings pond would have been associated with the tailings discharge. Since abandonment, the primary source of cyanide to the tailings pond should no longer exist. However, it is possible that residual cyanide in the tailings porewater contributes to the cyanide inventory in pond water column and the seepage collection pond immediately down-stream of the tailings pond.

Cyanide is not a persistent chemical as it is subject to a suite of destructive/alteration processes including: UV photo-oxidation, microbial oxidation, hydrolysis, volatilization and complexation. All of these processes are important from the perspective of its progressive loss from tailings pond waters; however, the oxidation and hydrolysis mechanisms are particularly important as a primary by-product of those processes is ammonia.

Specifically, the destruction of cyanide in INCO SO<sub>2</sub>-Air processing (Devuyst *et al.*) results in the production of cyanate, which in turn hydrolyzes in basic mill effluents to produce ammonia via:



Free cyanide will also hydrolyze in neutral waters to form ammonium at circum-neutral pH via:



Both hydrogen cyanide and ammonia can volatilize from surface water to the atmosphere although these processes are strongly pH and temperature dependent (Emerson *et al.*, 1975), as well as inhibited by ice cover. Specifically, the volatilization of ammonia to the atmosphere is only effective at alkaline pH (pH>9). Further, the increased residence time of cyanide compounds during under-ice conditions, and their subsequent breakdown, contribute to increased ammonia concentrations during winter periods.

### ***Ammonia, Nitrite, Nitrate***

The concentrations of all nitrogenous species are governed by the balance between their inputs, transformations and ultimate loss from the system. Therefore, an understanding of the dominant transformations is central to adopting an effective treatment strategy for the Mount Nansen tailings pond. In the following paragraphs, relevant processes relating to nitrogen cycling are discussed.

Ammonium is not thermodynamically stable in oxygenated waters, and depending on the prevailing conditions, it may be transformed into other nitrogen species by oxidation reactions or, under more basic pH conditions (pH>9), may volatilize from the pond surface. In addition, ammonia, nitrite and nitrate can be assimilated by algae as primary nutrient sources. Thus, possible removal mechanisms for ammonia include:

- Assimilation by algae;
- Adsorption to minerals surfaces on resuspended sediments and substrates;
- Oxidization to nitrite and nitrate in the two-step process of nitrification; and
- Conversion to ammonia (NH<sub>3</sub>) under alkaline conditions (pH>9) and volatilized.

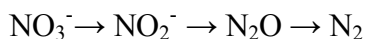
Under low oxygen conditions (*i.e.*, low redox potential), ammonia will not be oxidized. However, nitrate may be removed from the tailings pond water by denitrification in suboxic settings which may develop during ice-covered periods. Suboxic sediments can also serve as a sink for nitrate through nitrate reduction in near-surface porewaters (Van der Weijden, 1992).

Under oxygenated conditions, nitrification is the most common nitrogen transformation process in surface waters and soils. In this process, ammonium is oxidized first to nitrite and then (typically) rapidly further oxidized to nitrate according to the following:



Nitrite occurs as an intermediate and under typical conditions does not accumulate and is rapidly oxidized to nitrate.

Conversely, under low oxygen conditions, nitrate may be removed from water by denitrification, which involves the bacterially-mediated reduction of nitrate to nitrogen gas via the process:



While nitrite ( $\text{NO}_2^-$ ) is not an end product in any of the above transformations, it is a meta-stable intermediate, meaning that it is formed during the transformation from one species to another (*e.g.*,  $\text{NH}_4^+ \rightarrow \text{NO}_2^- \rightarrow \text{NO}_3^-$ ). Accordingly, the concentration of nitrite is determined by the balance of its production (*i.e.*, the oxidation of  $\text{NH}_4^+$ ) minus its loss through transformation to other species (*i.e.*, further oxidation to  $\text{NO}_3^-$ ). The same holds true for the reduction reactions (denitrification). Thus, accumulation of nitrite often implies that there is some inhibition of the processes contributing to its loss (*i.e.*, the latter stages of either nitrification or denitrification).

The kinetics of nitrogen oxidation in nitrification are largely controlled by temperature, pH and dissolved oxygen. Rates of nitrification are generally higher in summer than in winter. The optimum pH for nitrification is 8.2 to 8.6, with lower rates both above and below this range (Viessman and Hammer, 1993). In contrast, rates of under-ice denitrification in the tailings pond are probably limited by temperature.

### ***Thiocyanate***

Thiocyanate (SCN) is a common constituent found in tailings ponds in which cyanide is used for gold extraction. It is generally formed in the mill by reaction of cyanide with polysulphides, and although considerably less toxic than cyanide, it is often considered a problematic parameter.

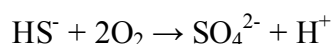
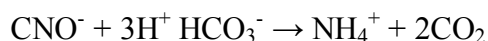
Thiocyanate can undergo microbial degradation; however, it is removed more slowly than cyanide and its biological removal is further hindered by the presence of ammonium

ion (Ludzack and Shaffer, 1960; Stafford and Callely, 1969). Indeed, the residual presence of ammonium in tailings ponds often accounts for concurrent concentrations of thiocyanate.

Thiocyanate undergoes biodegradation via one of two pathways, via a carbonyl pathway to ammonia:



or through a cyanate pathway with sulphide and cyanate as intermediate products:



In either case, biological productivity would be stimulated by the addition of phosphorus with the notion that thiocyanate would be consumed once ammonia concentrations have been reduced sufficiently.

### ***Metal Remediation***

Bioremediation has been used in tailings ponds and lakes for the management of elevated metal concentrations; the managed growth of algae in water bodies can draw down metal concentrations in a variety of fashions. Specifically, bioremediation through fertilization can remove metals through indiscriminant algal assimilation of metals, through adsorption onto algal surfaces and through the formation of secondary mineral phases in association with alterations to redox conditions in the water column or surface sediments.

Such remediation strategies have worked extremely well in pit lake systems where relatively large volumes of water require treatment and the structure of the water column is defined by seasonally-driven lake physics. Similar approaches have worked in comparatively shallower tailings ponds. However, given the higher surface area to water-depth ratio of tailings ponds, the exchange of solutes across the sediment-water interface has a greater potential to influence water column chemistry. Accordingly, bioremediation strategies must consider the potential for the remobilization of redox-sensitive phases under conditions of enhanced algal productivity. Most notably, secondary oxidation products such as Fe and Mn oxyhydroxides present phases of potential concern, as they may be subject to reductive dissolution under more reducing conditions at the sediment-water interface. Specifically, given that numerous trace elements strongly sorb to Fe and Mn oxyhydroxides, the remobilization of such phases can result in the release of associated trace metals to the water column (*e.g.*, Cu, Ni, Zn, As) (Tessier *et al.*, 1985).

### **Background Zinc**

In oxygenated waters at neutral pH, zinc exists as a divalent cation ( $Zn^{2+}$ ), and depending on the environment, is associated with various inorganic and organic complexes. Inorganic complexes typical to freshwaters include free hydrated aquo ions (*e.g.*,  $Zn^{2+} \cdot xH_2O$ ), carbanoto species (*e.g.*,  $ZnCO_3$ ) and hydroxy complexes (*e.g.*,  $ZnOH^+$ ) (Stumm and Morgan, 1981). Associations with organic ligands (*e.g.*, phytoplankton metabolites, proteins, humic acids, mill reagents, *etc.*) have also been shown to be important for this trace metal (Donat and Bruland, 1995).

The involvement of many trace elements in biological cycles can strongly influence their distribution in both natural systems and artificially created pit lakes. Metals such as zinc, cadmium and copper, for example, are required micronutrients which are actively assimilated by phytoplankton (Morel and Hudson, 1985). In addition, metals can become complexed with biogenic particles via indiscriminate algal uptake and sorption to biological surfaces. Metal scavenging by organics and subsequent gravitational settling, therefore, provides an important transport mechanism of metals (as metal-organic complexes) to bottom sediments.

In deeper aquatic systems, such as pit lakes, the oxidation of organic matter occurs both in the water column and at the sediment-water interface. The degradation of organic matter often results in the remobilization of associated trace metals and subsequent metal release to solution. Such metal recycling has been observed for nickel, copper, zinc, cadmium and lead in a variety of natural marine and lake environments (*e.g.*, Reynolds and Hamilton-Taylor, 1992; Westerlund *et al.*, 1986; Morfett *et al.*, 1988; McKee, 1989).

The reactivity of zinc towards sulphide ( $S^{2-}$ ) presents an additional control in subaqueous systems; zinc reacts with  $S^{2-}$  to form insoluble sulphide mineral phases (Heurta-Diaz and Morse, 1990). The precipitation of metals as their respective sulphides (*e.g.*,  $ZnS$ ) has been shown to provide an effective sink for dissolved metals in several lake and marine environments (Emerson *et al.*, 1983; Jacobs and Emerson, 1982), including meromictic lakes (*e.g.*, Green *et al.*, 1989).

Dissolved Zn responds particularly well to bioremediation through both biological uptake and through the process of sulphide formation. In the context of short-term remediation, biological uptake is perhaps the most important mechanism as Zn is sorbed to the organic functional groups on algal cells in addition to adsorption onto the silica frustules of diatoms. In previous bioremediation experiments (*e.g.*, Equity Silver Pit Lakes and Grum Pit Lake), Zn sorption to algal cells was capable of removing substantial concentrations of dissolved Zn from the water column bringing concentrations of several mg/L down by more than two orders of magnitude.

### **3. *Discussions***

---

## 3. Discussions

---

The ultimate objective of the assessment herein is to examine the potential for bioremediation in improving water quality for both the tailings pond and the Brown-McDade pit lake. The approach in both cases is to understand the geochemistry and physical dynamics governing the behaviour of the contaminants of concern for each system and then determine first, whether bioremediation is feasible, and secondly, whether there are any environmental liabilities associated with such an approach. These issues are discussed below in turn for the tailings pond and pit lake.

### 3.1 Tailings Pond

The Mount Nansen tailings facility is relatively small (~4 ha) residing in the Dome Creek watershed down-valley from the mill. The facility has received tailings generated predominantly from oxide and sulphide zones within the Brown-McDade pit and cyanide leach as been used to extract gold. The resulting environmental liability therefore includes: a) residual cyanide (and associated break-down products) in the pond and seepage return pond waters; b) unoxidized sulphide minerals potentially capable of producing neutral drainage or acid-drainage problems; and c) arsenic hosting oxide phases which may be capable of release under certain redox conditions.

The current water balance for the tailings pond has involved diversion of surface waters through a ditch around the pond and back into Dome Creek immediately below the seepage return pond. However, the tailings pond appears to receive inputs from its own small catchment in addition to unknown groundwater additions. Losses from the pond include direct discharge to the Dome Creek diversion ditch (from late September to late October, 2005) at approximately 65 USG/min (~4.1 L/s) and ongoing seepage through the dam into the seepage collection pond. In previous years, seepage pond water was pumped back to the tailings pond; however, in 2005, seepage water was discharged directly to Dome Creek from mid July, 2005 onwards at a rate similar to that discharged directly from the tailings pond (*i.e.*, ~4.1 L/s).

The INCO SO<sub>2</sub>-air process has been used on the tailings pond water in the past (2004 was the last year) to reduce cyanide concentrations before discharge to the environment; however, recent concentrations have been low enough to discharge seepage pond and tailings pond water directly to the receiving environment (Dome Creek). Nevertheless, nitrogen species associated the cyanide (*i.e.*, ammonia, thiocyanate etc.) are sufficiently high to warrant considerations of bioremediation as described in Chapter 2.

***Nitrate, Nitrite and Ammonia***

The behaviour of water-borne constituents in the tailings pond is best illustrated in Figure 3-1 which compares times series for ammonium and sodium in the tailings pond waters. Sodium is a conservative tracer (it is unreactive, changing in concentration only through addition or dilution processes) whereas ammonium is intimately tied to the nitrogen cycling processes within the pond.

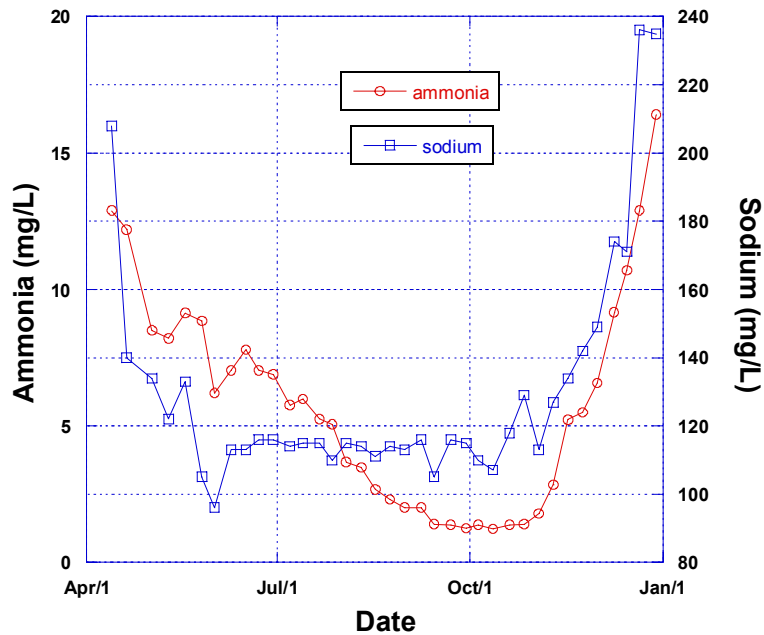


**Figure 3-1: Ammonia and sodium in the Mount Nansen Tailings Pond through the open water period of 2005.**

In the spring, both ammonia and sodium decrease in concentration markedly; however, while the sodium concentration levels out at approximately 115 mg/L from early June onwards, the ammonia concentration continues to decrease until early October. These data suggest that the primary dilution of water within the tailings pond occurs in association with spring freshet and that little dilution occurs through much of the summer (Figure 3-1). In contrast, the continual ammonia decrease between June and October 2005 can likely be attributed to the oxidation of ammonia and the concurrent formation of nitrate (discussed below).

Evidence for the process of nitrification can be seen in the temporal trends for nitrite and nitrate (Figure 3-2). A decrease in ammonia concentration occurs concomitantly with an increase in nitrate, supporting the tenet that nitrification contributes to the loss of ammonia during the summer and fall period. Under oxygenated conditions, ammonia will oxidize to nitrate through the meta-stable intermediate nitrite species. Indeed, values for

nitrite also exhibit a slight increase over the period of ammonia reduction (~July to October 2005) (Figure 3-2).

The decrease in ammonia is greater than the corresponding increase in nitrate on a molar basis suggesting that an additional ammonia removal mechanism is active. Mechanisms potentially contributing to this additional loss include: 1) volatilization to the atmosphere; 2) biological uptake; and/or 3) sorption to particles in the water column and substrates. However, given that the volatilization of ammonia is most effective at pH>9, and given that the pond exhibits only slightly alkaline pH (pH<8), it is unlikely that volatilization contributes significantly to the ammonia decrease.

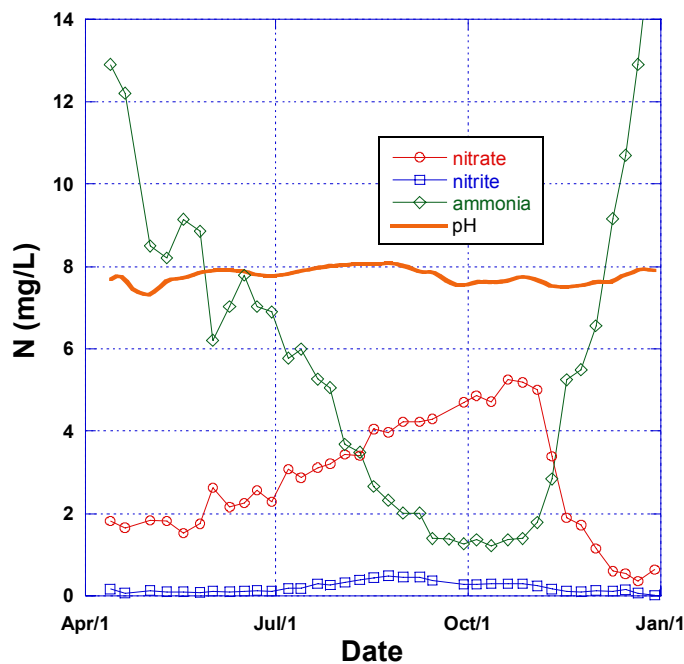


**Figure 3-2: Nitrate, nitrite and ammonia (as N) in the Mount Nansen Tailings Pond through the open water period of 2005.**

One would normally expect to see a depression in pH associated with nitrification as the oxidation of ammonia in the summer results will result in the release of protons. However, as can be seen in Figure 3-2, pH remains relatively stable very near pH 8 with only minor fluctuations through time. This behaviour can be explained by carbonate buffering within the tailings pond. In the early stages of freshet in 2005, tailings pond pH decreased slightly in response to the introduction of lower-pH melt waters. Snow melt and runoff water typically have pH values < 7. The existing carbonate species in the pond (as represented by high alkalinities on the order of 100 to 200 mg/L as CaCO<sub>3</sub>) prevent pH from diminishing further through buffering reactions associated with carbonate equilibria.

This behaviour is reflected in the alkalinity data (Figure 3-3) which illustrate an initial decrease in alkalinity associated with the inflow of freshet waters and then a near-constant value of 120 mg/L (as CaCO<sub>3</sub>), which represents the balance between carbonate dissolution (within the solid phases of the tailings) and acid generation resulting from nitrification and possibly sulphide oxidation. In essence, it is the on-going dissolution of carbonate minerals within the tailings solids that is responsible for maintaining elevated alkalinity and pH values near 8.

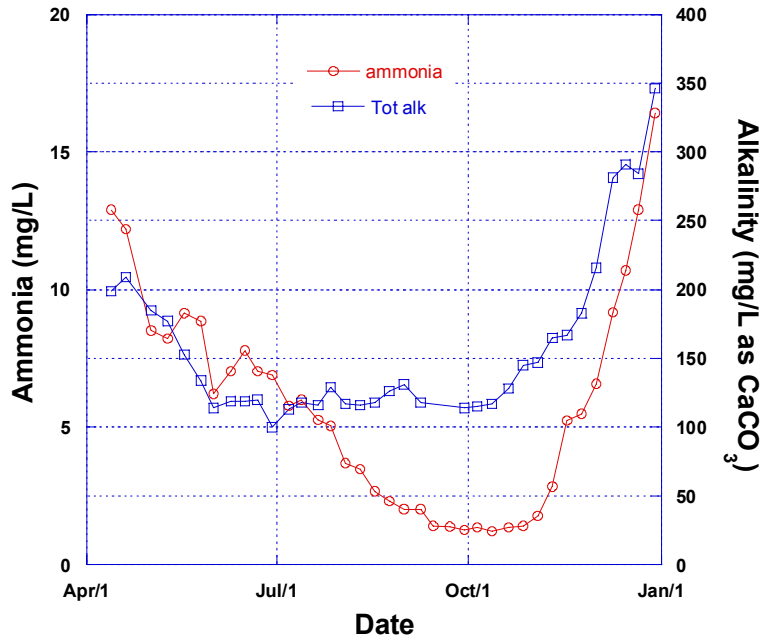


**Figure 3-3: Ammonia (as N) and total Alkalinity in the Mount Nansen Tailings Pond through the open water period of 2005.**

In late October/early November, the concentration of both ammonia and sodium increase concurrently (Figure 3-1) suggesting that mine impacted water was introduced to the pond in the late fall. Given the presence of ice on the pond at this time and a decreasing pond volume (through ongoing dewatering), it is likely that these latter inputs to the pond reflect in part the draining from porewater within the tailings into relatively small residual pond volume. This notion is supported by the fact that both ammonia and sodium are expected to be elevated in tailings porewater: the ammonia as a breakdown product of cyanide degradation and the sodium as a residual counter-ion from the NaCN introduced during gold extraction. In a situation where the pond volume was larger, the inflows of ammonia and sodium would not be expected to exert such a visible impact on water quality in the late-fall/winter.

The source of the increase in ammonia is an important consideration as it has ramifications as to the duration of ammonia loads to the facility. Porewater-derived

ammonia will have a finite inventory and will eventually be flushed from the system, whereas recycled ammonia (*i.e.*, through ammonification) may persist for longer periods of time. Indeed, ice on the pond precludes the ingress of oxygen to the water column and nitrate- and nitrite-nitrogen both decrease markedly (Figure 3-2) suggesting that either denitrification is occurring (nitrate to nitrogen gas) or ammonification is underway (nitrite to ammonia). The distinction between these two processes is important as denitrification represents a loss of N from the system where as ammonification represents internal recycling of nitrogenous species.

While it is tempting to suggest that ammonification is underway due to the fall increase in ammonia within the tailings pond, this mechanism is not supported by the data. First, ammonification requires strongly reducing conditions (in the water column and/or tailings porewaters), which are unlikely in this facility given the low abundance of organic matter. And second, the ammonification process necessitates the presence of nitrite as a meta-stable intermediate product; nitrite does not exist at this time (Figure 3-2). Rather, the data suggest that the loss of nitrate can be explained by the process of denitrification in which nitrate undergoes reduction to nitrogen gas under anaerobic conditions without the intermediate nitrite.

Interestingly, as the rate oxidation of ammonia decreases in the fall, so too does the liberation of acid. This is likely responsible for the fall/winter increase in alkalinity as carbonate dissolution (and flushing from the porewaters) continues (Figure 3-3). This ongoing process of rapid carbonate dissolution has implications for the ongoing stability of the sulphidic tailings within the facility as discussed later.

Seasonal nitrification/denitrification cycles and loss through discharge from the facility should progressively improve water quality within the facility for the nitrogen species (even though there are no discharge limits for these parameters). Further, other non-conservative removal mechanisms (volatilization, biological uptake and sorption) will also contribute to ammonia losses.

The addition of phosphorus to the tailings pond could induce growth of primary producers (phytoplankton) and increase the rate of nitrogen loss from the system through uptake of ammonia, nitrite and nitrate to satisfy nutrient requirements. The nutrient inventory would be directed to the sediments on the pond floor. While this approach could remove nitrogen from the water column, some of this inventory would be recycled back into the tailings pond thereby attenuating the loss of N from the system. Additionally, a liability exists with regard to the potential for destabilization of As-bearing solid phases within the tailings as described below.

**Cyanide (total and WAD)**

Total and WAD cyanide are regulated parameters at the Mount Nansen mine site with respective discharge limits of 0.3 and 0.1 mg/L. The concentrations in the tailings pond have decreased markedly since closure and during 2005, and, with the exception of one spurious value, have remained below their respective discharge limits in both the tailings pond and seepage pond (Figure 3-4).

The increases in total and WAD cyanide, which occur in the late fall, are commensurate with previously described increases in ammonia, and suggest that the flushing of cyanide-replete porewaters contributes to the observed trends. Despite this flushing event, concentrations of both total and WAD cyanide remain below their respective discharge limits (with the exception of one WAD-CN value as noted above). Given the generally low values, and the on-going degradation which will occur, there is no reason to anticipate future CN issues. Accordingly, it can be concluded that the decision to stop treatment for cyanide (*i.e.*, INCO SO<sub>2</sub>-air) was well-founded.

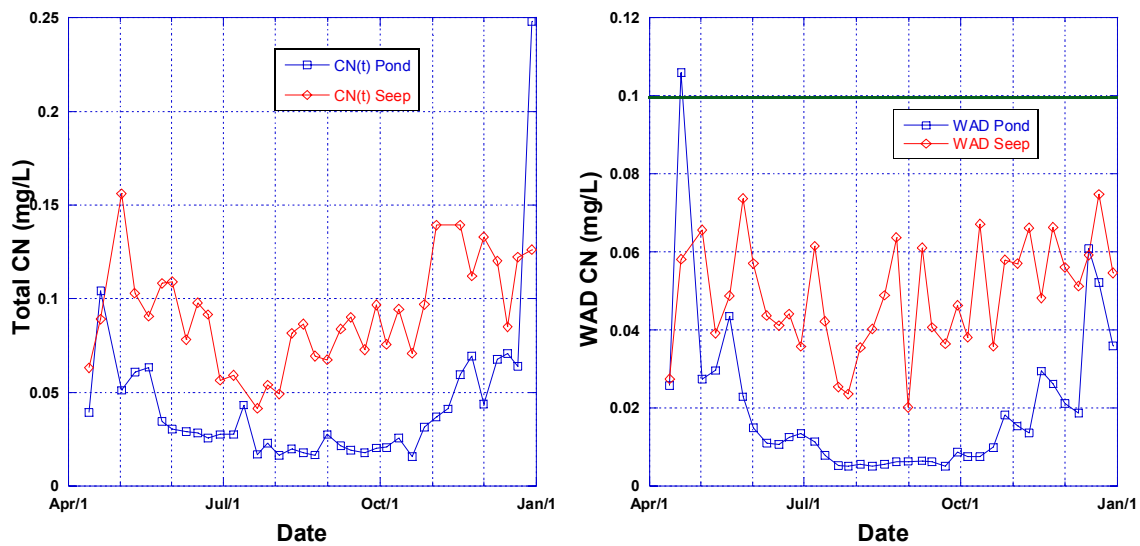


**Figure 3-4: Total and WAD cyanide in the Mount Nansen Tailings Pond through the 2005 sampling year.**

Bioremediation could conceivably further reduce the concentrations of total and WAD cyanide; however, given their already low (below guideline) concentrations in concert with liability of arsenic remobilization (described in greater detail below), natural attenuation and downstream dilution (also described below) appear to be the best approaches for the management of these parameters in the tailings pond facility.

**Thiocyanate**

Although not as toxic as the other parameters, thiocyanate is the only parameter existing at substantial concentrations (*i.e.*, up to 8 mg/L in the seepage pond). Thiocyanate is generally formed in the mill when cyanide is exposed to reduced sulphur; accordingly, it was most likely delivered to the tailings pond facility in association with the tailings slurry and thus, likely resides within the tailings porewaters.

Thiocyanate levels in the seepage pond decreased progressively through 2005 presumably in response to depleting inventories in the tailings porewaters. In contrast, thiocyanate in the tailings pond exhibits a distribution similar to that of sodium suggesting that it is responding to dilution in the spring, followed by its re-introduction to a comparatively small pond as porewaters drain into the residual tailings pond. It is unlikely that the thiocyanate decrease in the spring is related to biological utilization given the presence of ammonia in the tailings pond (ammonia is a preferred source of nitrogen for most microbes).

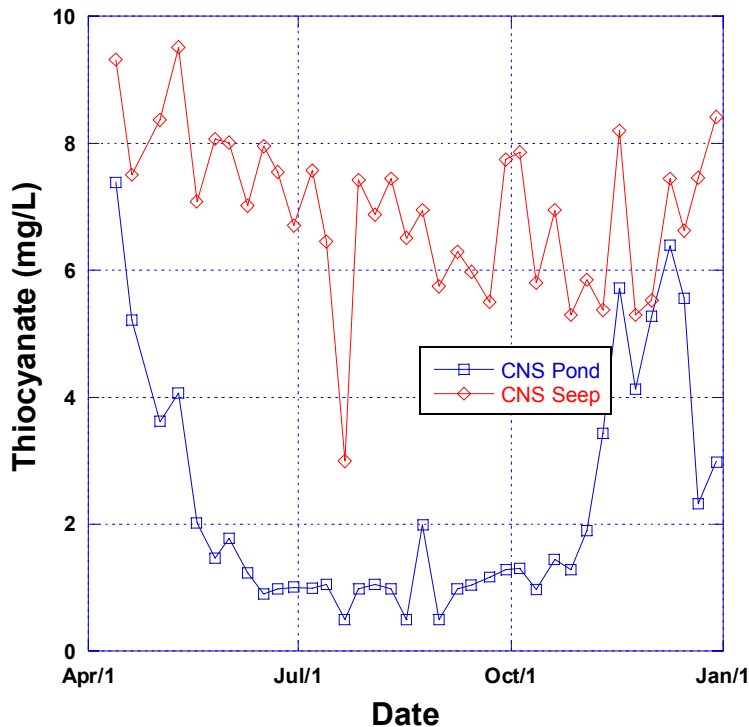


**Figure 3-5: Thiocyanate in the Mount Nansen Tailings Pond through the open water period of 2005.**

**Downstream Dilution and Impacts to Victoria Creek**

Water was discharged from the tailings facility in 2005 as effluents satisfied compliance criteria. Initially, discharge from the seepage pond commenced in mid-July at a rate of

approximately 65 USgpm (~4.1 L/s) directly into Dome Creek. This discharge configuration resulted in an insufficient lowering of the tailings pond level (Frank Patch, pers. comm.) and as a result, concurrent discharge directly from the tailings pond to the diversion ditch began in late September, 2005 at a rate similar to that from the seepage pond (*i.e.*, ~4.1 L/s). By the end of October, 2005, the tailings pond had been drained as low as possible without risking the discharge of solids. At this point, direct discharge from the pond ceased, leaving the discharge from the seepage pond as the sole release to the receiving environment. This discharge schedule is represented in the bars at the top of Figure 3-6.

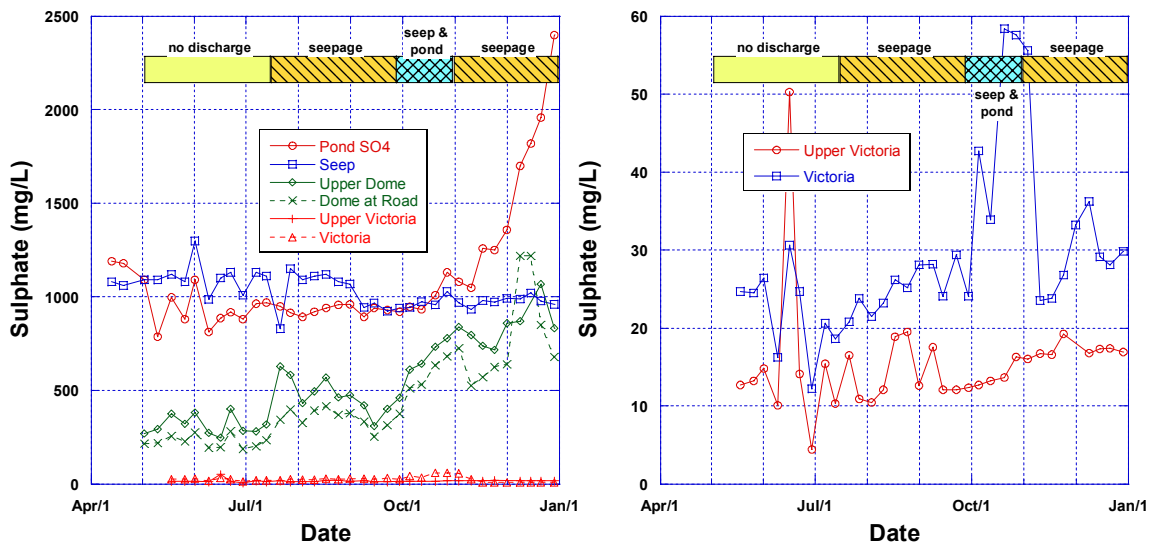


**Figure 3-6: Sulphate in the tailings pond, seepage pond, Dome Creek and Victoria Creek during the 2005 field sampling.**

Using the sequencing of discharge, the concentration of sulphate in the tailings pond and the seepage pond, and the corresponding concentrations in the receiving environment, an estimate of dilution, impact and assimilative capacity was quantified for both Dome and Victoria Creeks assuming conservative behaviour of sulphate (*i.e.*, that sulphate changes in concentration only through dilution).

Sulphate loadings from the tailings facility were monitored at Upper and Lower Dome Creek (Station Dome at Road). Knowing the effluent discharge rates from the tailings pond and the seepage pond (4.1 L/s each) and assuming a background sulphate concentration of 15 mg/L (the same value observed in Upper Victoria Creek), it is possible to develop a mass loading (flow x concentration) equation and solve for the flow gained by Dome Creek between the effluent discharge point and the lower Dome Creek. The underlying premise is that mass is conserved, thus, the load from each discharge

scenario must be preserved down the Dome Creek and any changes in sulphate concentration must be attributed to dilution.

The two discharge scenarios (*i.e.*, Seepage Pond alone and Seepage + Tailings ponds together) provide independent estimates for predicting base flow entering Dome Creek between the tailings facility and the confluence with Victoria Creek. The values used in the calculation are presented in Table 3-1.

**Table 3-1:  
Dilution and Base Flow Calculations for Dome Creek**

Discharge Scenario	Effluent Flow to Dome Cr.	*Sulphate at Upper Dome	*Sulphate at Dome at Road	Effective Dilution	Predicted Base Flow
Seepage	4.1 L/s	500 mg/L	400 mg/L	20%	0.82 L.s
Seepage+Pond	8.2 L/s	800 mg/L	700 mg/L	12%	1 L/s

\*Assumes background sulphate concentration is similar to Upper Victoria Cr (*i.e.*, ~15 mg/L)

Using the discharge flows for the two scenarios and the corresponding sulphate concentrations in upper and lower Dome Creek results in remarkably similar estimates for base flow of 0.82 and 1 L/s (Table 3-1). In other words, there appears to be an approximate 10% and 20% dilution factor for the Seepage + Tailings Pond discharge and Seepage Pond alone discharge (at 2005 discharge rates), respectively between Upper and Lower Dome Creek prior to the confluence with Victoria Creek.

Similar calculations were applied for Victoria Creek using upstream and downstream sulphate concentrations observed during both discharge scenarios (Table 3-2); Dome Creek total flows to Victoria Creek were based on the effluent flow for each discharge scenario plus 0.95 L/s base flow from the lower Dome Creek watershed.

**Table 3-2:  
Dilution and Base Flow Calculations for Victoria Creek**

Discharge Scenario	*Dome Cr flow to Victoria Cr	Sulphate at Dome at Road	Sulphate Upper Victoria	Sulphate Lower Victoria	Predicted Flow Summer
Seepage	5.05 L/s	400 mg/L	15 mg/L	25 mg/L	190 L/s
Seepage+Pond	9.15 L/s	700 mg/L	15 mg/L	45 mg/L	200 L/s

\*Values equal Effluent flow plus 0.95 L/s as an estimate for Dome Creek base flow

The mass balance calculation for the two discharge scenarios again resulted in remarkably similar values for summer flow in upper Victoria Creek with estimates of 190 and 200 L/s for Seepage alone and Seepage + Tailings Pond, respectively (Table 3-2). The agreement between the all estimates suggests that these calculations reasonably represent the flows and dilutions in Dome and Victoria Creeks. Effective dilution factors in Victoria Creek for Dome Creek with discharge from the Seepage Pond alone and Seepage + Tailings Ponds together are approximately 50-fold and 25-fold, respectively.

In other words, there appears to be a relatively large assimilative capacity for contaminants in Victoria Creek.

### ***Arsenic***

Arsenic is the primary metal of concern in the tailings pond as it exists at relatively high concentration in the tailings solids; it is also one of the regulated parameters at the Mount Nansen mine site with a discharge limit of 0.1 mg/L. Thus far, arsenic has not been particularly problematic from a discharge perspective having been below its discharge criteria when discharge was required. However, arsenic is associated both with arsenopyrite and with Fe-oxyhydroxides in the tailings (Appendix A). Arsenic in the former phase is subject release from sulphide oxidation under either pH neutral or acidic conditions, while the latter is subject to release through reductive dissolution of the Fe-oxyhydroxide matrix. Within the context of bioremediation, it is the latter mechanism that poses the greatest liability for future As release.

Evidence of arsenic release can be seen in the 2005 data (Figure 3-7). In the pond environment, dissolved As levels reach a seasonal minimum commensurate with the introduction of freshet waters. Values progressively increases over the summer period, stabilizing at a concentration of approximately 0.02 mg/L (well below the discharge criteria of 0.1 mg/L). It is conceivable that the steady increase during the summer represents release of As through the process of neutral drainage as arsenopyrite phases progressively oxidize under pH-neutral conditions. Upon ice cover in the late fall, dissolved As increases markedly to a concentration of 0.08 mg/L. This addition of arsenic is likely due to: 1) the introduction of arsenic-rich seepages to a comparatively small pond as porewaters the drain down of arsenic into the residual tailings pond (as described for sodium and ammonia); and/or 2) the reductive dissolution of arsenic-bearing Fe-oxyhydroxides. With regards to the latter, the increase in arsenic appears to follow changes in nitrogen speciation (Figure 3-2) associated with ice cover and possible alterations to the redox regime. Accordingly, it is possible that the increase in dissolved arsenic is associated with reductive dissolution of As-bearing Fe-oxyhydroxides. Indeed, these phases have been shown to be abundant through detailed mineralogical analysis. The effect on concentration is “magnified” by the relatively small volume of the tailings water cover in the early winter of 2005.

Through this same period of time, dissolved As in the seepage pond is uniformly low, typically <0.005 mg/L suggesting that fluctuations within the pond associated with oxidative or reductive release are attenuated (Figure 3-7).

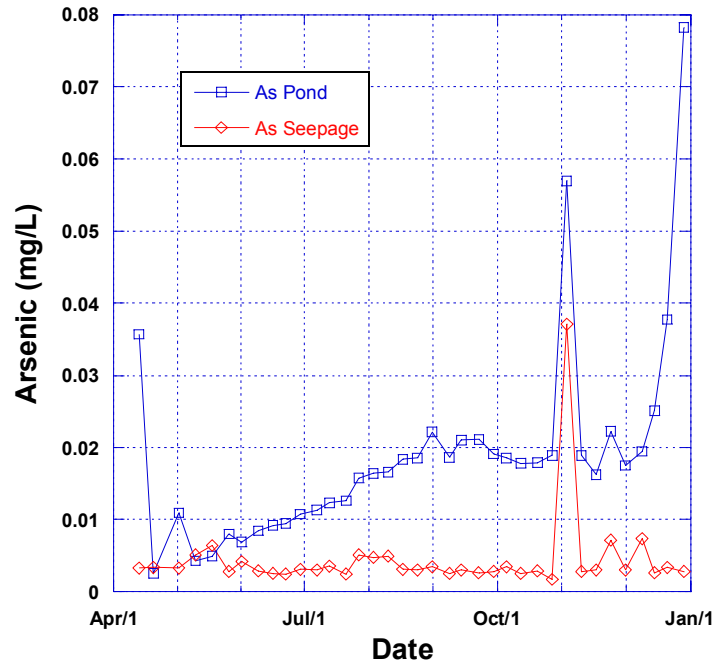


**Figure 3-7: Dissolved arsenic in the tailings pond and seepage pond during the 2005 field sampling.**

***Arsenic Liability***

In order to assess the likelihood of metal remobilization from submerged tailings deposits following pond fertilization, six tailings samples (surface deposits) were collected from various locations in the tailings pond (Figure 3-8) and submitted to LRC (Dr. John Jambor) for mineralogical analysis. The specific objective of the analysis was to identify any problematic phases which may become destabilized under more reducing sedimentary conditions. Sedimentary redox conditions are primarily governed by the accumulation rate of organic matter (OM) at the benthic boundary. The flux of OM at the sediment-water interface is driven by algal productivity (*e.g.*, phytoplankton growth), which is in turn governed by the available nutrient inventory. Accordingly, alterations to sedimentary redox conditions can occur in response to nutrient amendments (fertilization). Increased sediment-oxygen demand under conditions of enhanced algal production can lead to the destabilization of redox-sensitive solid phases (*e.g.*, Fe-oxhydroxides) and release of associated trace elements (*e.g.*, arsenic, copper, zinc). Such mechanisms have relevance to the feasibility of bioremediation options for the tailings pond.

Samples for mineralogical examination were allowed to dry at room temperature, after which a split was used for the preparation of polished thin-sections. This sections were examined in both transmitted and reflected light. Scanning electron microscopy and

energy-dispersion spectroscopic analyses (SEM–EDS) were done at 20 kV with a Philips XL-30 instrument and a coupled Princeton Gamma Tech IMIX-4 analyzer, at the Department of Earth and Ocean Sciences, University of British Columbia (UBC). X-ray diffractometry was done with a Siemens rotating-anode instrument at UBC. The complete results of the mineralogical analysis are presented in Appendix A, and summarized below.

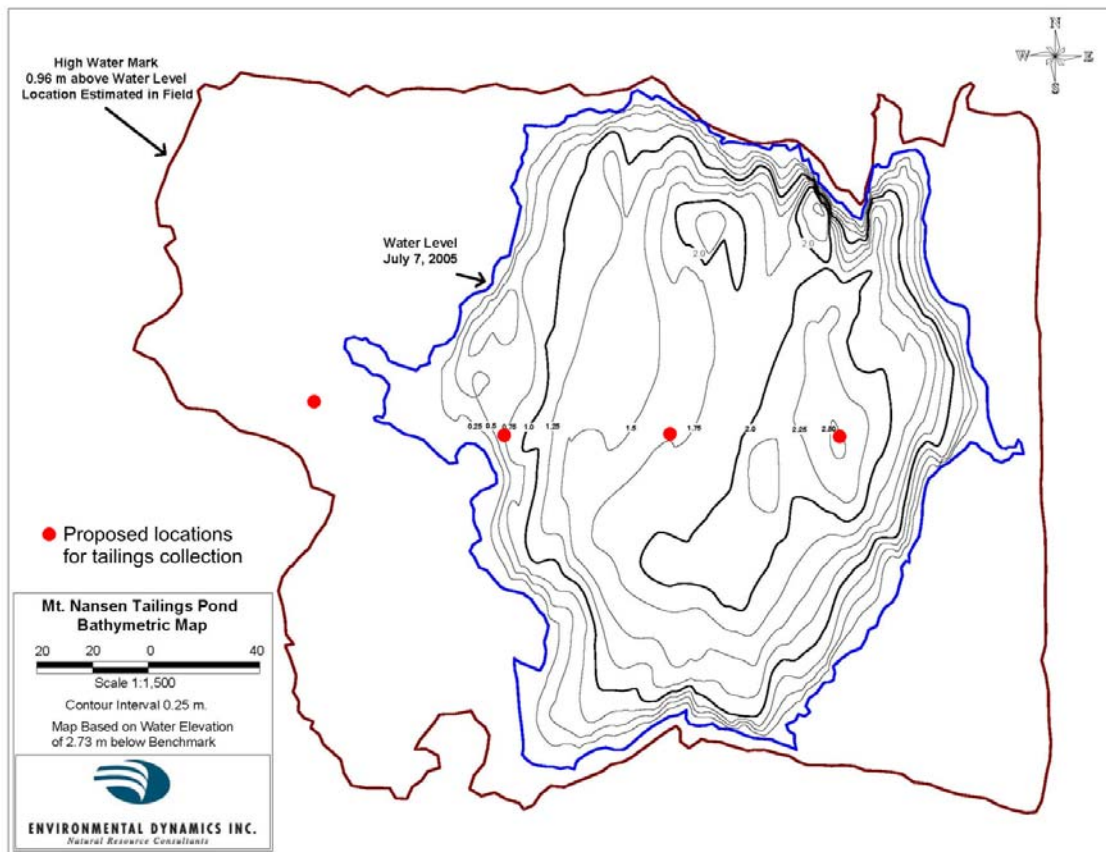


**Figure 3-8: The Mount Nansen Tailings Pond and collection sites for surface tailings grab samples.**

All tailings samples are quartz-rich, with the majority of samples containing major amounts of carbonate minerals. The sulphide mineral assemblage is dominated by pyrite [FeS<sub>2</sub>], with lesser amounts of arsenopyrite [FeAsS], sphalerite [(Zn,Fe)S], chalcopyrite [CuFeS<sub>2</sub>] and galena [PbS]. Numerous secondary phases were also identified which will become more soluble under more reducing sediment conditions, including:

- Fe oxyhydroxides present as isolated particles (Figure 3-9);
- Fe oxyhydroxides present as alteration rims on sulphide grains (Figure 3-10);
- Fe-arsenate (FeAsO<sub>4</sub>) as oxidation rims on arsenopyrite (Figure 3-11); and

- Jarosite-type minerals (*e.g.*, jarosite and plumbojarosite).

The principal secondary phase is Fe oxyhydroxide, which is present in all samples as isolated particles and rims (Figures 3-9 and 3-10). Numerous microbeam analyses indicate that the Fe oxyhydroxides are highly variable in composition and mostly amorphous. Many of the Fe oxyhydroxide particles and rims contain trace amounts of Cu and (or) Zn, and some have detectable As. Although Fe oxyhydroxides are observed in all samples, they are most abundant in the beach and shallow-water tailings. Such observations are consistent with the likelihood of increased sulphide oxidation in the periodically exposed tailings in the shallow zones of the pond. Numerous grains of pyrite have well-developed oxidation rims and, unusually, the rims also occur on chalcopyrite and sphalerite. Arsenopyrite grains also show well developed alteration rims of ferric arsenate (Figure 3-11).

The prevalence of redox-sensitive secondary phases in the tailings deposits, and the abundance of associated trace metals (Cu, Zn, As and Pb), preclude fertilization as a viable form of bioremediation for the tailings pond. Specifically, the environmental risks associated with fertilizer amendments outweigh the potential benefits with respect to water management. Such conclusions also relate to other case studies which have shown long-term degradation to water quality associated with the remobilization of arsenic (Martin et al., 2004) and copper (Martin et al., 2003) under conditions of enhanced algal productivity.

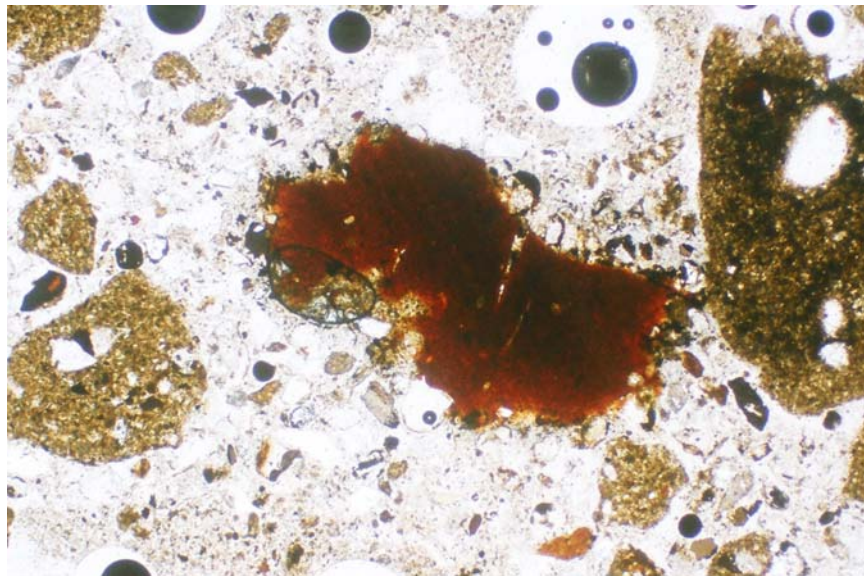


**Figure 3-9:** Sample 006 in plain transmitted light, width of field 2.6 mm, showing a large particle of reddish, heterogeneous Fe oxyhydroxide.



**Figure 3-10:** Sample 006 in plain reflected light, width of field 0.625 mm, showing Fe-oxyhydroxide rims on pyrite. The adjacent white prismatic grain southeast of the altered pyrite is arsenopyrite.

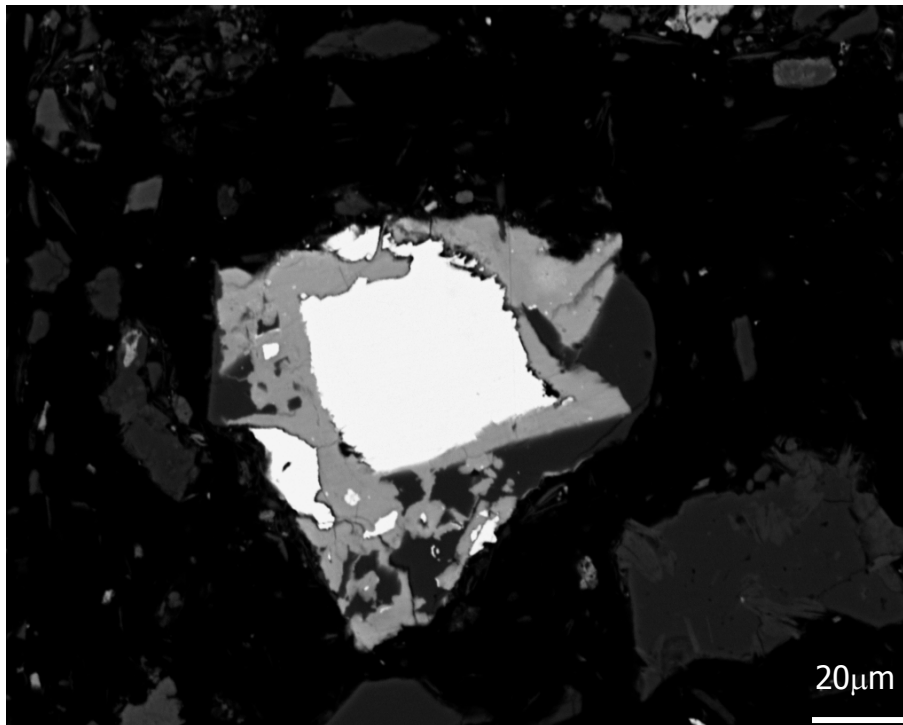


**Figure 3-11:** Backscattered-electron image of sample 005 showing a grain of arsenopyrite with a readily visible alteration rim (Fe arsenate).

### 3.2 Brown McDade Pit Lake

The Brown-McDade pit lake has been described previously in Lorax (2004) and at that time, Zn and nitrate were the parameters of greatest concern for pit lake water quality. Although there is no direct discharge from the Brown-McDade pit lake, pit water has been pumped out of the facility episodically to maintain the lake level below an adit on the west high wall which drains into the Pony Creek watershed. Given that the pit lake elevation is in non-steady-state and either requires ongoing dewatering or spillover through the adit into the Pony Creek watershed, remediation strategies have been considered to improve water quality towards minimizing the potential for environmental impact. Specifically, the potential for bioremediation of the Brown-McDade pit lake is assessed below.

The pit lake is small, occupying only the lowest 8 meters of the pit; its length is on the order of 100 m while its width is perhaps a few tens of meters. The pit lake lies in a north-south orientation and three sampling stations have been established over the past few years ranging in depth from 4 to 8 m (Figure 3-12). Station SP1 at the southern-most end of the pit lake is the deepest site and is used here to characterize the pit lake water column characteristics.

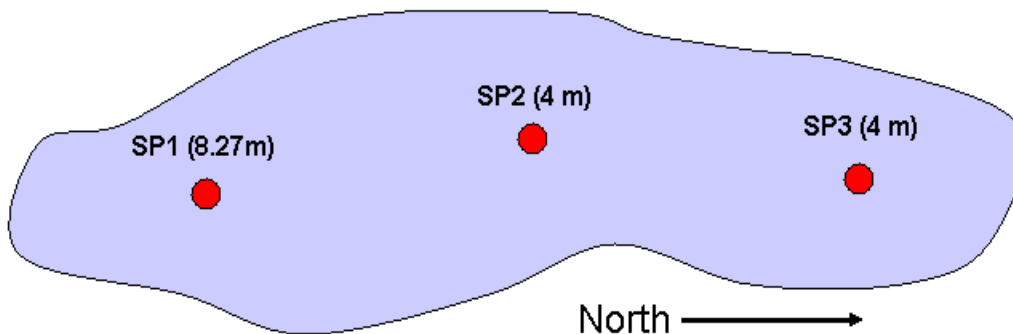


**Figure 3-12: Station Locations and approximate water depth within the Brown-McDade Pit Lake.**

Station SP1 was sampled on three occasions at different depths: February, 2004 at 1, 4 and 8 m depth; March 2005 at 1.5 and 4 m depth; and, in August 2005 at 3 and 6.5 m depth.

The pit lake appears to remain salt-stratified as identified in the original Lorax (2004) report as can be seen in the calcium and sulphate data (Figure 3-13). The most recent sampling (August, 2005) hints at the possible loss of some salt from the system; however, salinity gradients are still visible and largely unaffected through the monitoring period (Figure 3-13).

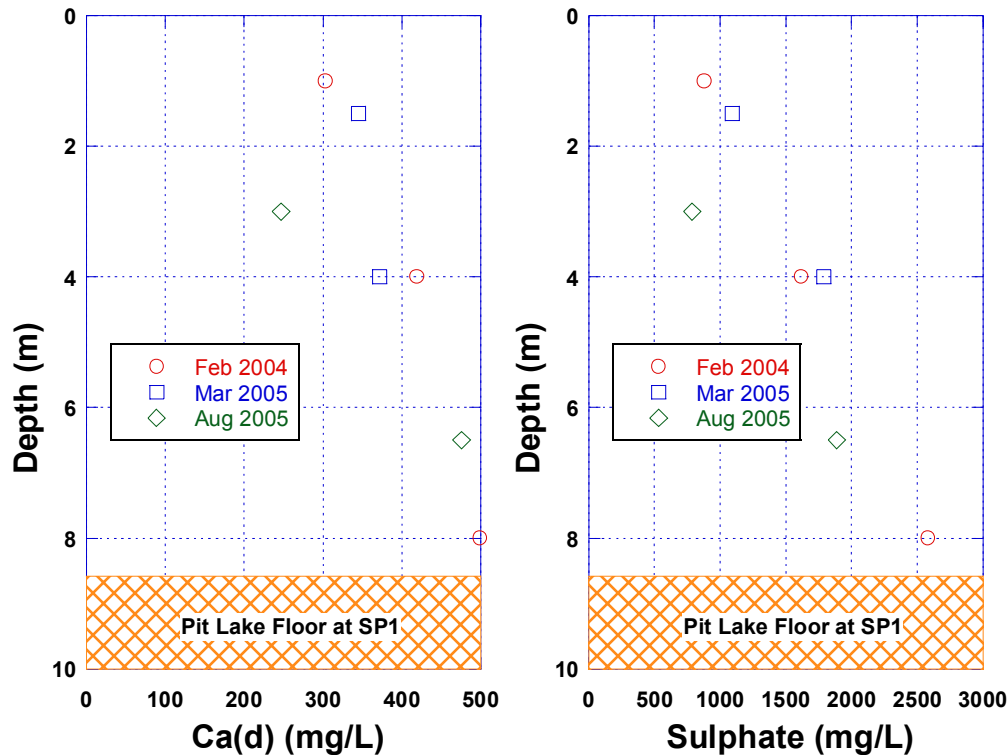


**Figure 3-13: Dissolved Ca and Sulphate in the Brown-McDade pit lake during three separate surveys at Station SP1.**

The redox conditions within the pit lake are also similar to those seen in 2004 with oxic conditions persisting in the surface layer and sub-oxic (but not anoxic) conditions dominant at depth. Evidence for this structure can be seen in the redox-sensitive parameters Mn and nitrate (Figure 3-14), which are secondary oxidants in the oxidation of reduced phases (*i.e.*, organic matter or sulphide minerals). These parameters exhibit antithetic behaviour consistent with their redox behaviour. Specifically, dissolved Mn (II) is reductively remobilized at depth (to concentrations as high as 15 mg/L) whereas nitrate is consumed in pit bottom waters. While nitrate is persistent (and thermodynamically favoured) in oxygenated surface waters, it is reduced through either denitrification or ammonification in the suboxic waters (Figure 3-14). Although ammonia has not been measured in the pit lake, it is likely that it exists in the pit waters at depth where it will remain stable under sub-oxic conditions.

Zinc and cadmium distributions are presented in Figure 3-15 and illustrate the congruent behaviour of these two elements with higher concentrations at depth underlying lower (but elevated nonetheless) concentrations in surface waters. Such behaviour is anticipated as both elements share many geochemical characteristics. In particular, both elements can often be associated with pH neutral drainage from sulphide oxidation in addition to forming solid-solutions with carbonate minerals. Both elements are elevated to levels that warrant considerations of mitigation.

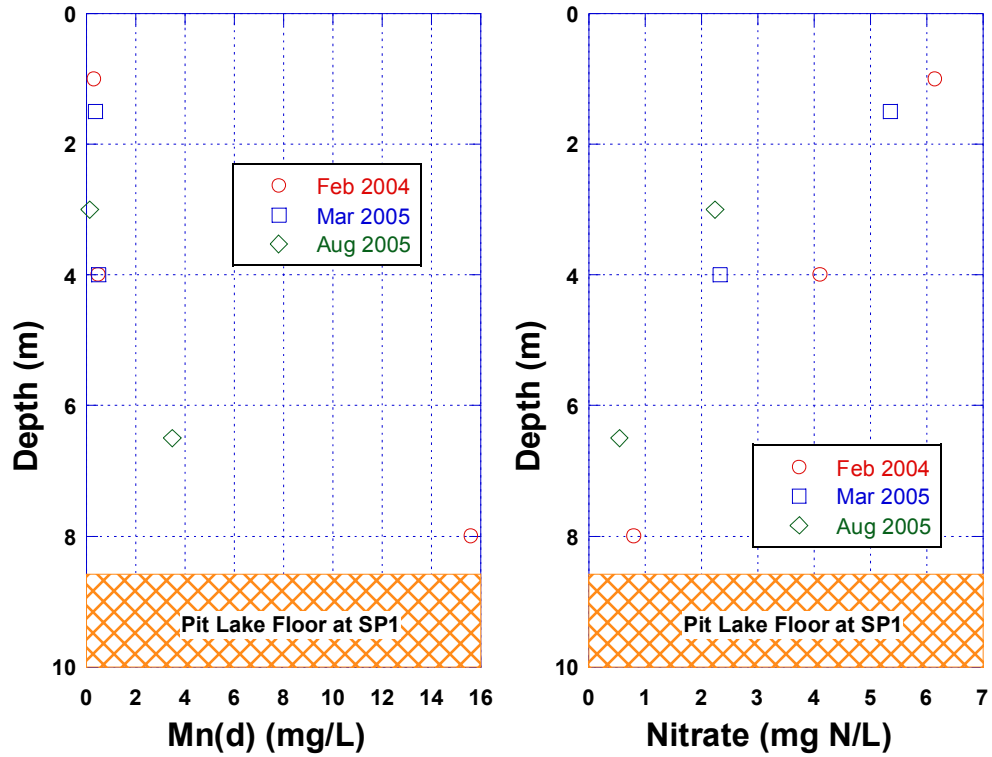


Figure 3-14: Dissolved Mn and Nitrate in the Brown-McDade pit lake during three separate surveys at Station SP1.

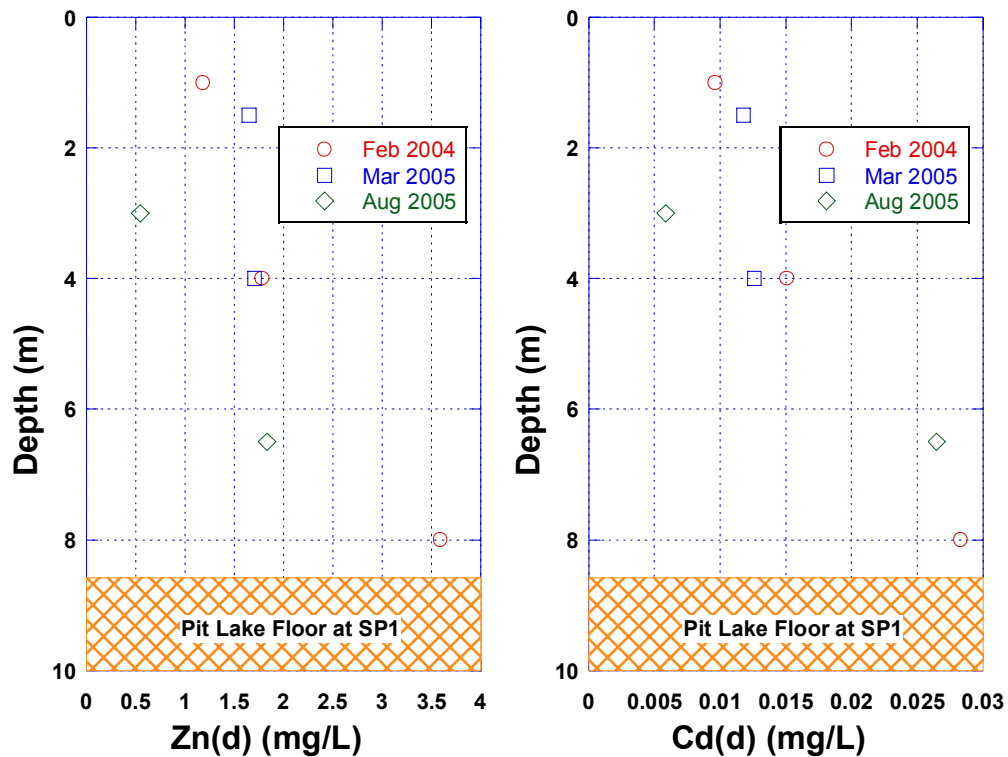


Figure 3-15: Dissolved Zn and Cd in the Brown-McDade pit lake during three separate surveys at Station SP1.

Zinc, cadmium, nitrate and sulphate are all amenable to mitigation through bioremediation through lake fertilization. Zinc and cadmium are subject to direct and indirect uptake by algal cells and both precipitate rapidly in the presence of dissolved sulphide generated as a byproduct of sulphate reduction. Sulphate reduction can be enhanced through the breakdown of organic matter produced through lake fertilization. Nitrate (and ammonia if it exists) can serve as nitrogen sources for algal growth thereby reducing their concentrations as a part of the same remediation program. Sulphate exists in excess, and like nitrate, will be consumed through its use as a secondary oxidant in the decomposition of organic matter. The byproduct of the reduction of sulphate is free sulphide, a species responsible for removing the metals Zn and Cd through precipitation of insoluble sulphide minerals.

The pit lake already displays evidence of limited algal growth in the forms of what appear to be algal mats in the shallow areas of the pit lake (Figure 3-16) suggesting that some limited source of phosphorus (the limiting nutrient) exists in this system. By inference, the system should be well-poised for elevated primary productivity with the addition of a phosphorus-rich nutrient mix.



**Figure 3-16: Southern-most shore of the Brown-McDade pit lake showing the presence of an algal mat blanketing the shallow lake floor.**

An important consideration in assessing the potential benefits of fertilization is the amenability of the surface waters to accepting and assimilating phosphorus without loss through inorganic precipitation. The primary sink in the Brown-McDade pit lake is the concentration of Ca, which, if in excess, may form an apatite-like precipitate with phosphate. Calcium concentrations in the pit lake surface waters currently reside in the 200 to 300 mg/L range. While this concentration is sufficient to cause some phosphate loss to the sediments, it is not so high as to negate fertilization as an effective mitigation strategy. Indeed, algal growth has been stimulated in systems hosting higher calcium concentrations than this pit lake.

One final consideration for bioremediation of the Brown-McDade pit lake has to do with the potential for mobility of As. Unlike the tailings pond, the pit lake does not host arsenic in any substantive fashion. Accordingly, the sensitivity to reductive dissolution and release from the solid phase does not exist in this facility. In essence, the Brown-McDade pit lake is an ideal candidate for bioremediation.

## ***4. Conclusions and Recommendations***

---

## **4. Conclusions and Recommendations**

---

The Mount Nansen gold mine was operated between the years of 1997 and 1999. Oxide and sulphide ore were mined from the Brown-McDade Pit, producing approximately 250,000 tonnes of arsenic- and cyanide-bearing tailings which were stored in an impoundment within the Dome Creek watershed down-gradient of the mill. Since closure, residual CN (and break-down products), and solid-phase arsenic exist in the tailings pond while elevated Zn concentrations exist in the pit lake. The following section summarizes the findings of the analysis of the existing data for both of these facilities and presents an assessment of treatment considerations particularly as it pertains to bioremediation.

### **4.1 Tailings Pond**

The Mount Nansen tailings pond has received CIP tailings from oxide and sulphide zones primarily from within the Brown-McDade pit. Accordingly, the tailings host residual mill byproducts including cyanide, thiocyanate, ammonia, nitrate and nitrite as well as a suite of ancillary parameters.

Most of the original tailings porewater constituents trapped during operations appear to have dissipated through a variety of loss mechanisms in the intervening years (*e.g.*, cyanide through flushing and ongoing oxidation/hydrolysis); however, some parameters such as ammonia and thiocyanate have persisted given the nature of their respective microbial degradation pathways. Specifically, thiocyanate has been persisted given its resistance to microbial assimilation in the presence of ammonia; ammonia appears to have persisted in part due to its formation from the breakdown of cyanide, as well as due to the ineffective volatilization of ammonia at pH = 8.

With the exception of episodic effluent criteria exceedences for cyanide, all parameters appear to have remained below their respective discharge limits. Late fall/winter concentrations for several parameters including ammonia, thiocyanate and several ancillary parameters appear to have increased markedly; however, it is suspected that this behaviour is an artifact of the draining of tailings porewaters into a small tailings pond volume (due to pump down). These elevated concentrations should not be of concern as the small tailings pond volume will be very susceptible to dilution in the spring; freshet waters should rapidly diminish these concentrations by the time discharge is required in the spring.

There are very active nitrogen cycling and removal mechanisms at work in the tailings pond, which likely include: denitrification, nitrification, ammonia volatilization,

ammonia sorption to particles, and discharge to Dome Creek. In regard to direct discharge of effluent to Dome Creek, dilution of effluent for 2005 discharges prior to the confluence with Victoria Creek are approximately 20% for the seepage pond discharge alone and 10% for the discharge of seepage + tailings pond effluent together. Considerably more dilution occurs at the confluence with Victoria Creek where seepage and seepage + pond dilutions are 50-fold and 25-fold, respectively.

Much of the Tailings have been subjected to many wetting/drying cycles; evidence of oxidation rims through mineralogical examination suggests that sulphide oxidation is presently occurring but that excess carbonate minerals commixed with the sulphides are responsible for maintaining high pH and preventing the onset to acidic conditions. It is currently unclear whether the increasing arsenic concentration is seasonal; however, it is suspected that concentrations within the tailings pond result from a combination of: 1) ongoing arsenopyrite oxidation under pH neutral conditions; 2) and possible reductive release of As from Fe-oxyhydroxides under ice cover when oxygen is prevented from entering the tailings pond waters.

Given that the parameters of concern are largely involved in the nitrogen cycles within the tailings pond, it is tempting to suggest that bioremediation is a viable option for lowering ammonia, cyanide and thiocyanate concentrations below their present values. However, mineralogical examination of tailings and authigenic mineral phases within the tailings pond suggests that if bioremediation were to occur, a significant risk would exist for the marked remobilization of As (and Cu) to the pond waters. It is primarily for this reason that bioremediation is not recommended for the Mount Nansen tailings pond. Instead, it is suggested that since the concentrations are currently compliant and active consumption, dilution and discharge mechanisms continue to reduce the inventories of these species within the facility, that no action be taken. Tailings pond water should be allowed to improve on its own. This “wait and see” approach is supported by the large assimilative capacities afforded by the receiving environment, particularly in Victoria Creek.

## **4.2 Pit Lake**

During the final stages of the operations in the Brown McDade pit, mining proceeded into the sulphide zone where it exposed bedrock with a high potential to generate acid rock drainage (ARD). Accordingly, the initial filling stage of the pit, ARD from the lower part of the pit generated high concentrations of sulphate and trace metals in the shallow pit lake. An independent source of alkalinity appears to maintain the pit lake at neutral pH.

Once the pit lake began to fill and the exposed sulphides were submerged, release from lower pit walls ceased and comparatively fresh water created the upper layer of the lake. After the initial formation of the lake, little mixing occurred between the bottom water and the comparatively fresh water surface layer above. While this behaviour seems unusual in such a shallow pit lake, the persistence of lake stratification is strong evidence for the lack of substantive mixing. The small pit lake surface area, in concert with protective high walls, most likely accounts for the persistence of stratification. This salt-stratification will likely degrade with time through small-scale eddy diffusion to the extent that the lake will eventually mix more substantively in the future.

The concentration profiles of  $\text{NO}_3^-$  and Mn in the water column suggests that the redox state in the bottom layer is currently sub-oxic and gradually evolving to more strongly reducing conditions. These data support the notion that the lake is oligotrophic and incapable of producing seasonal episodes of anoxia, making it an ideal candidate for bioremediation.

Except for Mn, Zn and Cd, which are highest in concentrations in the bottom layer, dissolved metal concentrations are comparable to those in the overlying water layer(s). The top layer is characterized by a much lower solute concentration than the bottom layer and in addition to sulphate, calcium and magnesium appear to dominate its chemical composition. Redox conditions are oxidizing in surface waters and sub-oxic at depth. In the absence of remediation, it is anticipated that lake surface water concentrations will not differ markedly from that currently seen in surface the layer.

The pit lake appears to host significant potential for bioremediation; there is evidence of algal mats currently existing in the pit lake shallows. Furthermore, the primary parameters of concern (Zn, nitrate, Cd and sulphate) are all candidates for bioremediation through whole-lake fertilization.

A viable bioremediation strategy would involve addition of P alone (or in concert with nitrogen) to surface water in frequent, low doses. Provided primary productivity could be raised to eutrophic or hyper-eutrophic levels, Zn (and Cd) would be taken up by algal assimilation, whereas nitrate would be consumed as a nutrient. Zn, Cd and sulphate would be consumed if the deeper layers can be driven to anoxia and sulphate reduction. There is no arsenic liability in the pit lake; thus, the primary limitation to productivity and successful remediation is the presence of Ca in surface waters, which could remove some fraction of the phosphorus as an inorganic precipitate; frequent, low doses of phosphorus will aid in its efficient uptake by phytoplankton.

### **4.3 Recommendations**

*Do not fertilize tailings pond* – the liability associated with arsenic remobilization in concert with the already low concentration of total and WAD cyanide and the marked dilution capacity of Dome and Victoria Creeks suggest that bioremediation is not an option for the tailings pond. Rather, the pond should be allowed to recover naturally as residual contaminated porewaters are flushed from the system.

*Fertilize pit lake* – The Brown-McDade pit lake hosts no liability for bioremediation and is an ideal candidate given the suite of problematic parameters. Fertilization would utilize a regiment of frequent, low-dose phosphorus additions so as to minimize the risk of phosphate loss from the system either through inorganic precipitation or through discharge to the receiving environment. The nutrient addition should be either a pure phosphorus amendment or a mixed nutrient with nitrogen.

*Static tests should be performed on the tailings* – Given the presence of sulphide minerals in the tailings pond and high dissolution rates of carbonate minerals, it is recommended that a suite of static tests be run on the tailings within the facility to ensure that the tailings will remain pH neutral in perpetuity. This is particularly important in light of the fact that pond is alternately wetted and dried seasonally and that much of the neutralizing potential is being flushed out of the system in the form of carbonate alkalinity.

## ***References***

---

## References

---

- Balistrieri L. S. and Murray J. W. (1992) The biogeochemical cycling of trace metals in the water column of Lake Sammamish, Washington: response to seasonally anoxic conditions. *Limnol. Oceanogr.* **37**(3), 529-548.
- Calvert S. E. (1987) Oceanographic controls on the accumulation of organic matter in marine sediments. In *Marine Petroleum Source Rocks*, Vol. 26 (ed. J. Brooks and A. J. Fleet), pp. 137-151. Geological Society of London Special Publication.
- Conor Pacific Environmental Technologies Inc., 2000. *Mount Nansen Minesite, Historical Review, Site Assessment and Field Sampling Program.*
- Davison W. (1993) Iron and manganese in lakes. *Earth Sci. Rev.* **34**, 119-163.
- Dodds W. K. and Prisco J. C. (1990) A comparison of methods for assessment of nutrient deficiency of phytoplankton in a large oligotrophic lake. *Can. J. Fish. Aquat. Sci.* **47**, 2328-2338.
- Donat, J. R. and Bruland, K. W. (1995). Trace Elements in the Oceans, CRC Press. Chapter **11**: 247-281.
- Ebbs, S. (2004). "Biological degradation of cyanide compounds." *Environ. Biotech.* **15**: 231-236.
- Emerson, S., Jacobs, L. and Tebo, B. (1983). The behaviour of trace metals in marine anoxic waters: solubilities at the oxygen-hydrogen sulphide interface. *Trace Metals in Sea Water*. C. S. W. e. al: 579-608.
- Forsberg C. (1989) Importance of sediments in understanding nutrient cycling in lakes. *Hydrobiologia* **176/177**, 263-277.
- Froelich P. N., Klinkhammer G. P., Bender M. L., Luedtke N. A., Heath G. R., Cullen D., Dauphin P., Hammond D., Hartman B., and Maynard V. (1979) Early oxidation of organic matter in pelagic sediments of the eastern equatorial Atlantic: suboxic diagenesis. *Geochim. Cosmochim. Acta* **43**, 1075-1090.
- Fukushima T., Aizaki M., and Muraoka K. (1989) Characteristics of settling matter and its role in nutrient cycles in a deep oligotrophic lake. *Hydrobiol.* **176/177**, 279-295.
- Green W. J., Ferdelman T. G., and Canfield D. E. (1989) Metal dynamics in Lake Vanda (Wright Valley, Antarctica). *Chem. Geol.* **76**, 85-94.

- Hamilton-Taylor J. and Davison W. (1995) Redox-driven cycling of trace elements in lakes. In *Physics and Chemistry of Lakes* (ed. A. Lerman, J. A. Gat, and D. M. Imboden), pp. 217-263. Springer-Verlag.
- Hamilton-Taylor J. and Willis M. (1990) A quantitative assessment of the sources and general dynamics of trace metals in a soft-water lake. *Limnol. Oceanogr.* **35**, 840-851.
- Higgs and Associates Ltd., 1994. *Initial Environmental Evaluation, Mt. Nansen Development*, Volume 1 and 2.
- Huerta-Diaz, M. A. and Morse, J. W. (1990). "A quantitative method for determination of trace metal concentrations in sedimentary pyrite." *Mar. Chem.* **29**(2-3): 119-144.
- Jacobs, L. and Emerson, S. (1982). "Trace metal solubility in an anoxic fjord." *Earth Planet. Sci. Lett.* **60**: 237-252.
- Kwon, H. K., Woo, S. H. and Park, J. M. (2002). "Thiocyanate degradation by *Acremonium strictum* and inhibition by secondary toxicants." *Biotechnol. Lett.* **24**: 1347-1351.
- Ludzack and Shaffer (1960). Activated sludge treatment of cyanide, cyanate and thiocyanate. 15<sup>th</sup> Industrial Waste Conference, Perdue University, Lafayette, Ind.
- Lorax (2004). Preliminary Assessment of Pit Lake Chemistry and Dynamics: The Brown-McDade Pit Lake, Mount Nansen Mine
- Martin A. J., Jambor J. L., Pedersen T. F., and Crusius J. (2003) Post-depositional mobility of Cu in a metal-mining polish pond (East Lake, Canada). *Env. Sci. Tech.* **37**(21), 4925-4933.
- Martin A. J. and Pedersen T. F. (2004) Alteration to lake trophic status as a means to control arsenic mobility in a mine-impacted lake. *Wat. Res.* **38**, 4415-4423.
- Mackin J. E. and Swider K. T. (1989) Organic matter decomposition pathways and oxygen consumption in coastal marine sediments. *Jour. Mar. Res.* **47**, 681-716.
- McKee, J. D., Wilson, T. P., Long, D. T. and Owen, R. M. (1989). "Pore water profiles and early diagenesis of Mn, Cu and Pb in sediments from large lakes." *J. Great Lakes Res.* **15**: 68-83.
- Morel, F. M. M. and Hudson, R. J. M. (1985). The geobiological cycle of trace elements in aquatic systems: Redfield revisited. *Chemical Processes in Lakes*. W. Stumm, Wiley-Interscience.: 251-282.
- Morfett, K., Davison, W. and Hamilton-Taylor, J. (1988). "Trace metal dynamics in a seasonally anoxic lake." *Environ. Geol. Wat. Sci.* **11**: 107-114.

Perry K. A. and Pedersen T. F. (1993) Sulphur speciation and pyrite formation in meromictic ex-fjords. *Geochim. Cosmochim. Acta* **57**, 4405-4418.

Reynolds, G. L. and Hamilton-Taylor, J. (1992). "The role of planktonic algae in the cycling of Zn and Cu in a productive soft-water lake." *Limnol. Oceanogr.* **37**: 1759-1769.

Schindler D. W., Turner M. A., and Hesslein R. H. (1985) Acidification and alkalization of lakes by experimental addition of nitrogen compounds. *Biogeochemistry* **1**, 117-133.

Tessier A., Rapin F., and Carignan R. (1985) Trace metals in oxic lake sediments: possible adsorption onto iron oxyhydroxides. *Geochimica et Cosmochimica Acta* **49**, 183-194.

Westerlund, S. F. G., Anderson, L. G., Hall, P. O. J., Iverfeldt, A., Loeff, M. M. R. V. D. and Sundby, B. (1986). "Benthic fluxes of cadmium, copper, nickel, zinc and lead in the coastal environment." *Geochim. Cosmochim. Acta* **50**: 1289-1296.

# ***Appendix A***

---

## **MINERALOGY OF TAILINGS FROM THE MOUNT NANSEN SITE, YUKON**

# **MINERALOGY OF TAILINGS FROM THE MOUNT NANSEN SITE, YUKON**

Prepared for: **Energy Mines and Resources,  
Yukon Government**  
Whitehorse, Yukon

**November 2005**



J.L. Jambor  
Leslie Investments Ltd  
Research and Consulting  
316 Rosehill Wynd  
Tsawwassen, B.C. V4M 3L9  
Ph: (604) 948-1368  
E-mail: [JLJambor@aol.com](mailto:JLJambor@aol.com)

## EXECUTIVE SUMMARY

Six samples of tailings from the former Mount Nansen mine, Yukon, were mineralogically examined primarily to determine whether mineral species susceptible to destabilization under reducing conditions are present. The principal candidates that would be amenable to such reductive effects in the tailings setting are ferric iron oxyhydroxides, which are well-known sorbers of heavy metals and semi-metals such as Cu, Zn, and As.

All six of the tailings samples are quartz-rich, and five of the samples also contain major amounts of carbonate minerals. Pyrite [FeS<sub>2</sub>] is by far the predominant sulfide mineral and locally occurs in percentage amounts. Arsenopyrite [FeAsS] and sphalerite [(Zn,Fe)S] are present in small amounts in all samples and are the principal primary sources of As and Zn, respectively. Chalcopyrite [CuFeS<sub>2</sub>] and galena [PbS] occur locally in minute amounts and are the main primary sources of Cu and Pb, respectively.

The principal secondary phase is Fe oxyhydroxide; other secondary minerals detected to occur at least locally include gypsum [CaSO<sub>4</sub>·2H<sub>2</sub>O], jarosite [KFe<sub>3</sub>(SO<sub>4</sub>)<sub>2</sub>(OH)<sub>6</sub>], plumbojarosite [PbFe<sub>6</sub>(SO<sub>4</sub>)<sub>4</sub>(OH)<sub>12</sub>], covellite [CuS], and Fe arsenate that forms oxidation rims on arsenopyrite. Although the Fe oxyhydroxides have been observed in all samples, they are most abundant in the beach and shallow-water tailings. Numerous microbeam analyses indicate that the Fe oxyhydroxides are highly variable in composition, but Cu, Zn, and As are commonly detectable in their energy-dispersion spectra. Large particles of Fe oxyhydroxide are especially abundant in the tailings sample from the north beach. The oxyhydroxide from this site is typically highly heterogeneous on a micrometres scale and likely contains a Ca-dominant carbonate phase as well as appreciable amounts of non-sulfide Cu. Reductive dissolution of the ferric Fe oxyhydroxides and other secondary minerals would result in the release of Cu, Zn, Pb, and As.

# CONTENTS

<b>INTRODUCTION</b> .....	3
<b>SAMPLES AND METHODS</b> .....	3
<b>RESULTS</b> .....	4
<i>Sample 004A</i> .....	5
<i>Sample 004B</i> .....	13
<i>Sample 005</i> .....	20
<i>Sample 006</i> .....	28
<i>Sample 007</i> .....	38
<i>Sample 008</i> .....	41
<i>Sample 009</i> .....	45
<b>CONCLUSIONS</b> .....	46
<b>APPENDIX</b> .....	54

## INTRODUCTION

The Mount Nansen former Au–Ag mine is about 60 km west of Carmacks, Yukon. Modest tonnages (<1 Mt) of ore were milled on-site during highly sporadic production from 1968 to 1999. The site was abandoned by private interests in 1999 and is currently under government maintenance. Part of the ongoing rehabilitation program presumably involves revegetation, and Lorax Environmental Services has expressed a concern that fertilization may lead to increased algal growth in the tailings-storage facility; the increased organic content in turn may result in the development of reducing conditions at the tailings – water interface. Previous observations at other tailings sites have indicated that remobilization of sorbed trace elements such as As and Cu have occurred in the reduced conditions that followed fertilization. Therefore, the objective of the mineralogical study reported here was “to identify any problematic phases which may become destabilized under more reducing sedimentary conditions” (written communication, Lorax Environmental Services, Sept. 15, 2005).

## SAMPLES AND METHODS

Six samples of Mount Nansen tailings in plastic bags were received by LRC on September 21, 2005. Data for the collection sites are given in Table 1. None of the samples was dry, and some consisted of a mixture of solids and free-flowing aqueous fluid. All of the samples were removed from their bags and were placed in, or on, plastic receptacles, and were allowed to dry at room temperature. The drying process took almost a week to complete because of the large amount of fluid in some of the samples. Monitoring during the drying period did not reveal colour changes attributable to further oxidation, and only on sample 004 was a minute amount of

Table 1. Collection sites of the tailings samples

Sample	GIS Lat	Long	Depth, m
004	62°02.534'	137°07.066'	beach, North end
005	62°02.527'	137°07.034'	0.84
006	62°02.527'	137°07.061'	0.3
007	62°02.509'	137°06.951'	1.68
008	62°02.531'	137°06.939'	2.13
009	62°02.536'	137°06.852'	beach, South end

surficial precipitate observed to have formed. The precipitate occurred as a peppering of sub-millimeter white to colourless blebs; a small intact piece of bleb-bearing sample was removed for subsequent further examination.

Each of the dried samples was only weakly cemented and could be pulverized using only forefinger pressure. However, the finest grained samples (004, 007, and 008) required more finger pressure than samples 009 and an apparently coarser fraction within 004. Sample 004 was therefore crudely split into a coarse fraction (004B) and the remnant bulk sample (004A); the 004B sample was obtained simply by hand-picking of some of the coarser grained pieces.

Each of the samples was hand-pulverized as indicated above, and was split to yield a sample for mineralogical examination. Each of the mineralogical samples was further split, with one portion submitted to Vancouver Petrographics for the preparation of optical sections, and the other retained for possible X-ray diffractometry. The optical sections were prepared as polished thin-sections on 26 × 46 mm glass slides. To minimize the dissolution of possible water-soluble minerals, it was specified by LRC that no water be used during section preparation.

The optical sections were received on October 31, 2005, and were examined in both transmitted and reflected light. Areas deemed to merit further study by microbeam methods were marked on the sections, and a photomicrograph was taken to aid in locating the relevant grains within each marked area. Scanning electron microscopy and energy-dispersion spectroscopic analyses (SEM–EDS) were done at 20 kV with a Philips XL-30 instrument and a coupled Princeton Gamma Tech IMIX-4 analyzer, at the Department of Earth and Ocean Sciences, University of British Columbia (UBC). X-ray diffractometry was done with a Siemens rotating-anode instrument at UBC; details of the Rietveld refinements that were done to obtain the quantitative mineralogy of two of the samples are given in Appendix 1.

## **RESULTS**

Megascopic comparison of the pulverulent mineralogical samples revealed that there is little colour variation among the group. All have a slightly brownish or tan tint rather than being neutral grey; within this limited variation, sample 004B is the most ochreous, and samples 007 and 008 can be described as the lightest in colour and the least discolored.

### ***Sample 004A***

The as-received 004 material consisted of damp solids unaccompanied by a liquid phase. Although the sample was megascopically appraised to contain some of the coarsest grains in the six-sample suite, a portion of the sample consists of fine-grained, clay-size material that presumably occurred as a layer or layers in the cored interval. The overall appearance is brownish ochreous, with the clay-like material slightly lighter.

The optical section is megascopically light brown, but a few large particles or aggregates are distinctly reddish brown. No sulfides are visible.

The section viewed microscopically in transmitted light is extremely fine-grained, with maximum particle sizes only about 60  $\mu\text{m}$  across. The non-opaque assemblage is quartz- and carbonate-dominant; an acid (25% HCl) test of the non-mounted fraction gave an instantaneous vigorous effervescence, indicating the presence of abundant calcite [ $\text{CaCO}_3$ ] or dolomite [ $\text{CaMg}(\text{CO}_3)_2$ ]. Otherwise, only small amounts of mica (muscovite and biotite) were readily identifiable optically, but X-ray diffractometry was performed on companion sample 004B to obtain a better resolution of the fine-grained matrix minerals and the total mineral assemblage. The megascopic distinctly reddish brown particles are fragments of Fe oxyhydroxide that are highly heterogeneous because of intergrowths and occluded tailings particles.

Although sulfides were not observed megascopically, their apparent absence arises solely because of the small size of the grains. One grain of pyrite in the section is 65  $\mu\text{m}$  across; otherwise, however, the largest grains are only  $\sim 30$   $\mu\text{m}$  across, and most are  $< 15$   $\mu\text{m}$ . Only one grain of pyrite was observed to have a rim of secondary Fe oxyhydroxide. Despite its fine grain size, pyrite is relatively abundant insofar as an order-of-magnitude estimation of its content is  $\sim 1\%$ . Only a trace amount of galena [ $\text{PbS}$ ], and possibly sphalerite [ $(\text{Zn},\text{Fe})\text{S}$ ], was observed.

Several of the oxyhydroxide fragments were examined by EDS analysis because Fe oxyhydroxides are known well to be scavengers of trace elements, including those of the heavy metals and semi-metals. A large particle of sulfide-free Fe oxyhydroxide is shown in Figure 1, and two EDS spectra of different spots on the particle are given in Figure 2. Both spectra show that, in addition to the expected high content of Fe, the particle is rich in Ca. The relatively low Si and S contents indicate that the Ca is not attributable to the presence of a Ca silicate or a Ca sulfate (such as gypsum,  $\text{CaSO}_4 \cdot 2\text{H}_2\text{O}$ ); thus, it is likely that the Ca occurs as calcite, or was derived from an additive such as lime [ $\text{CaO}$ ] or its reaction product, portlandite [ $\text{Ca}(\text{OH})_2$ ].

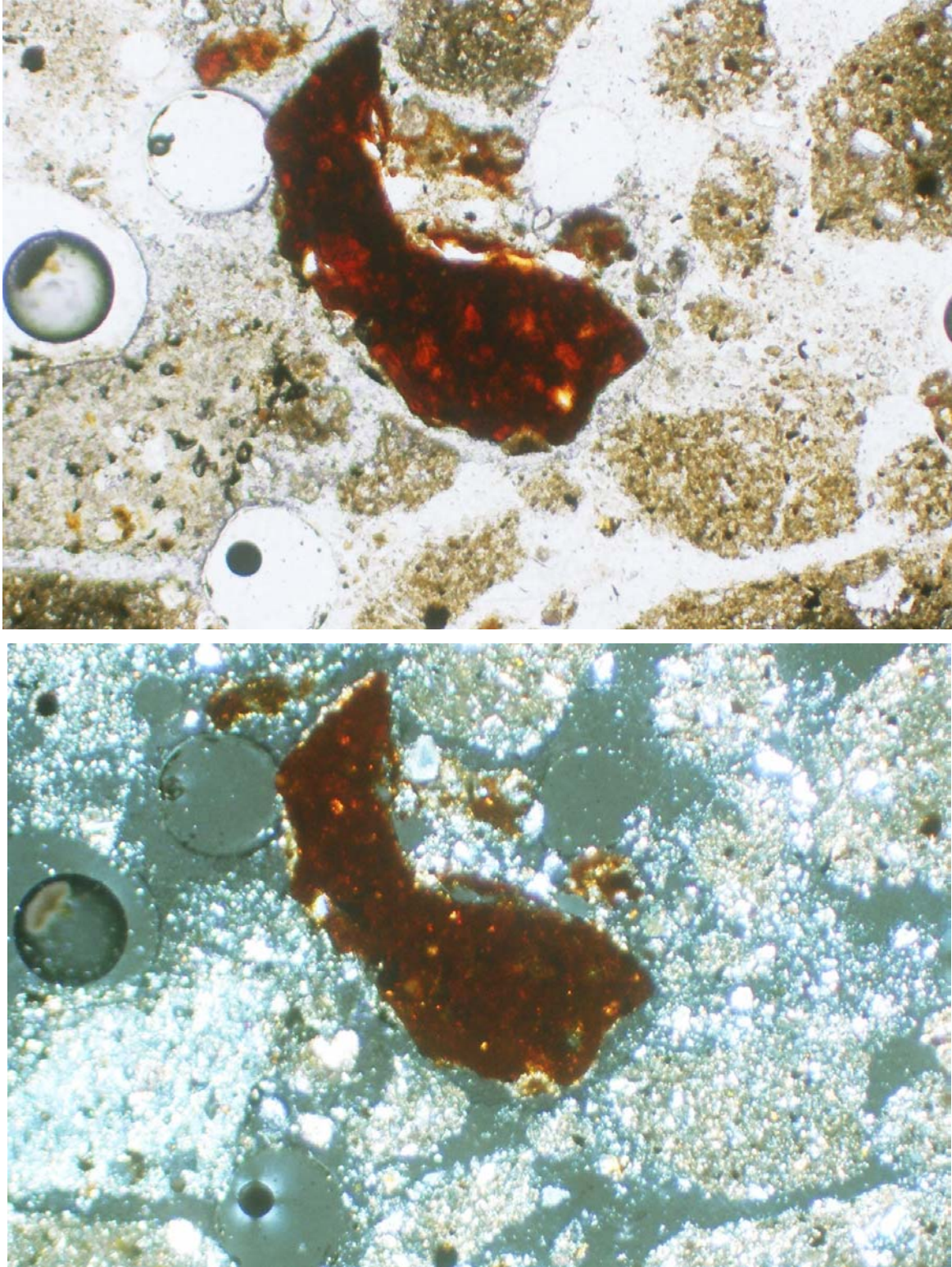


**Figure 1.** Sample 004A in plain transmitted light (top) and the same field with reflected light, polarizers almost crossed and internal reflection (bottom), width of field 1.3 mm, showing a large particle of heterogeneous, reddish Fe oxyhydroxide for which EDS spectra are given in Figure 2. The lower photo shows the fine-grained character of the sample, which consists predominantly of quartz.

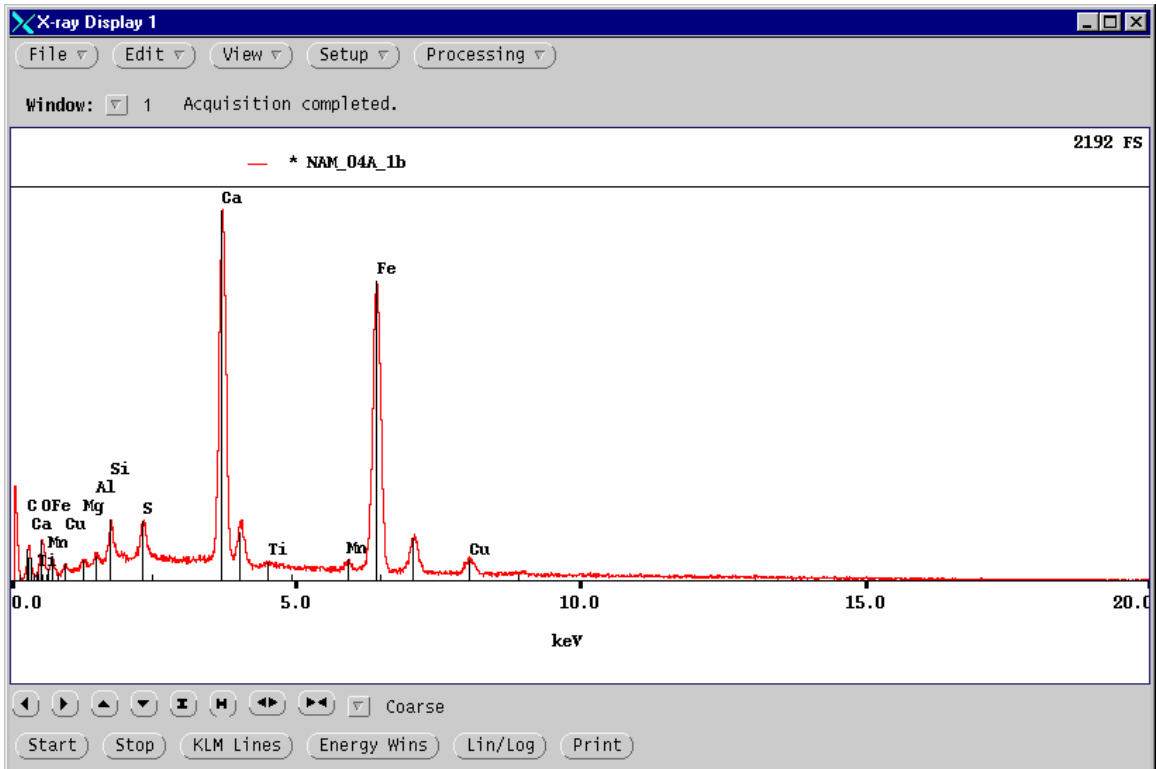
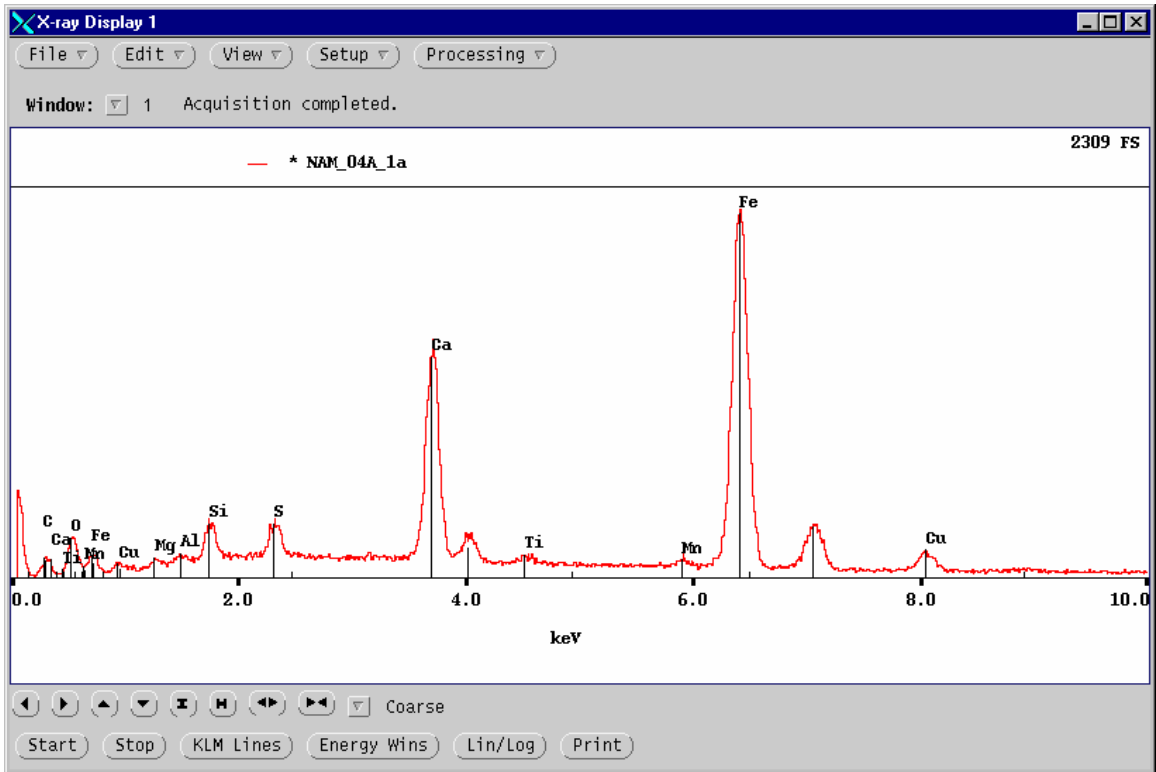


**Figure 2.** EDS spectra of different spots on the Fe oxyhydroxide of Figure 1. The high Ca content is a reflection of the heterogeneity of the particle.

The X-ray data for sample 004B indicate that calcite is abundant whereas the other minerals are not detectable. A significant feature of the two spectra is that, from an environmental perspective, Cu is present in relatively large amounts.

Several other particles of Fe oxyhydroxide in different areas of the section were similarly examined. Figure 3 illustrates a well-defined oxyhydroxide particle whose spectrum is not shown but is similar to those in Figure 2. Figure 4 shows two Fe-rich areas and Figure 5 gives the corresponding EDS spectra. Likewise, Figures 6 and 7 show two oxyhydroxide particles and their respective spectra. All of the oxyhydroxide particles show a consistent presence of Cu. Trace amounts of Zn erratically accompany the Cu (Figs. 5, 7), and one particle contains detectable As (Fig. 7).

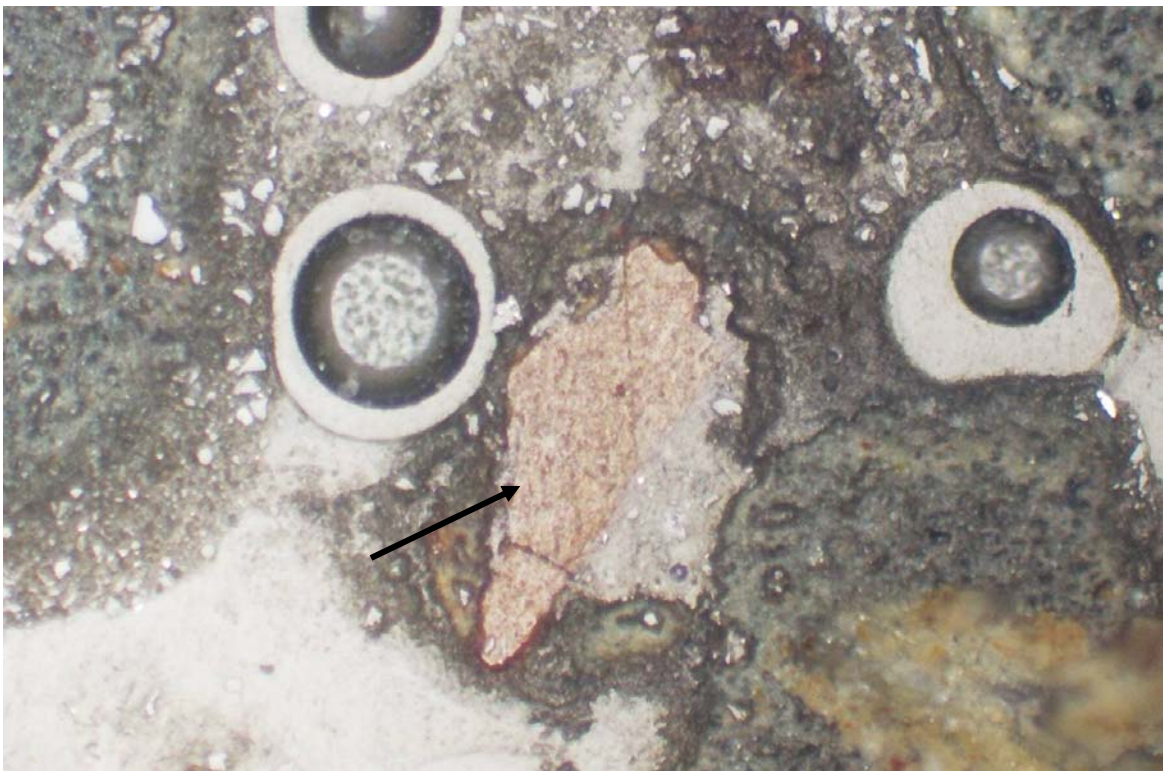


**Figure 3.** Sample 004A in plain reflected light, width of field 0.625 mm, showing at the arrow a large particle of Fe oxyhydroxide (the circular objects are bubbles in the section). Most of the fine-grained, grey grains with moderate reflectance are quartz, but on the extreme right at mid-height is a white grain of pyrite. Despite the apparently greater homogeneity of the Fe oxyhydroxide relative to that in Figure 1, EDS spectra gave a high Ca content like that in Figure 2.

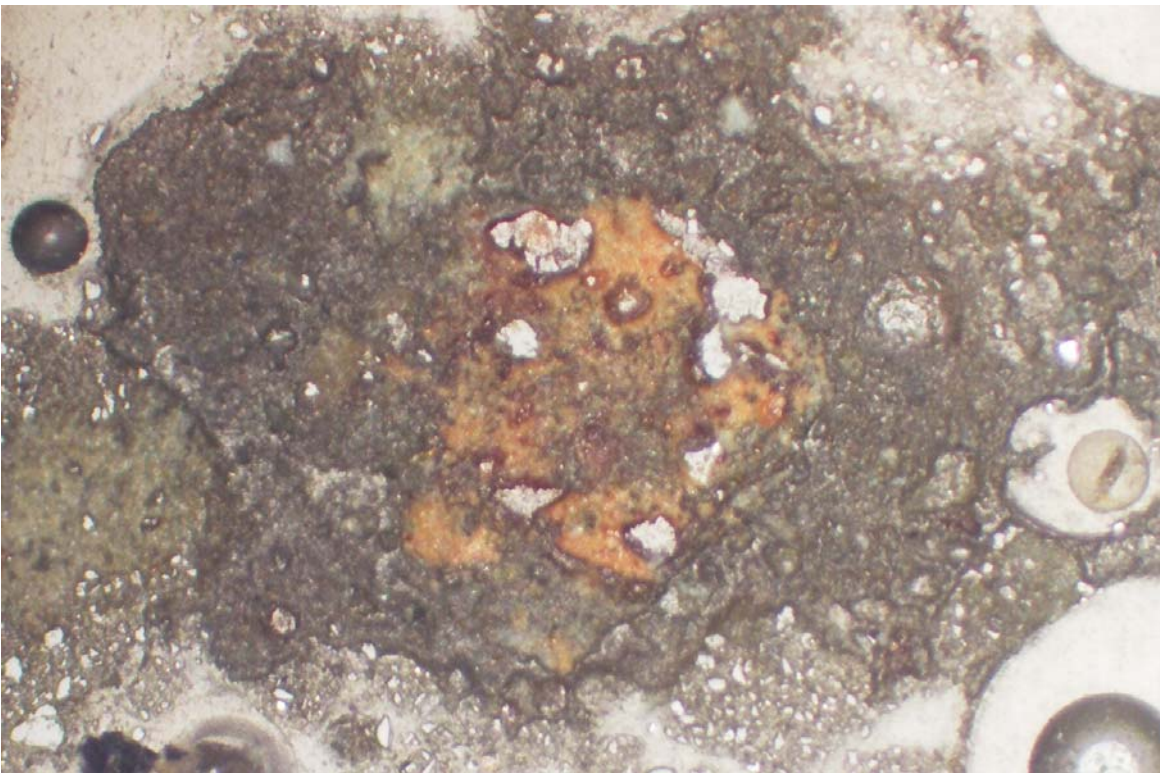
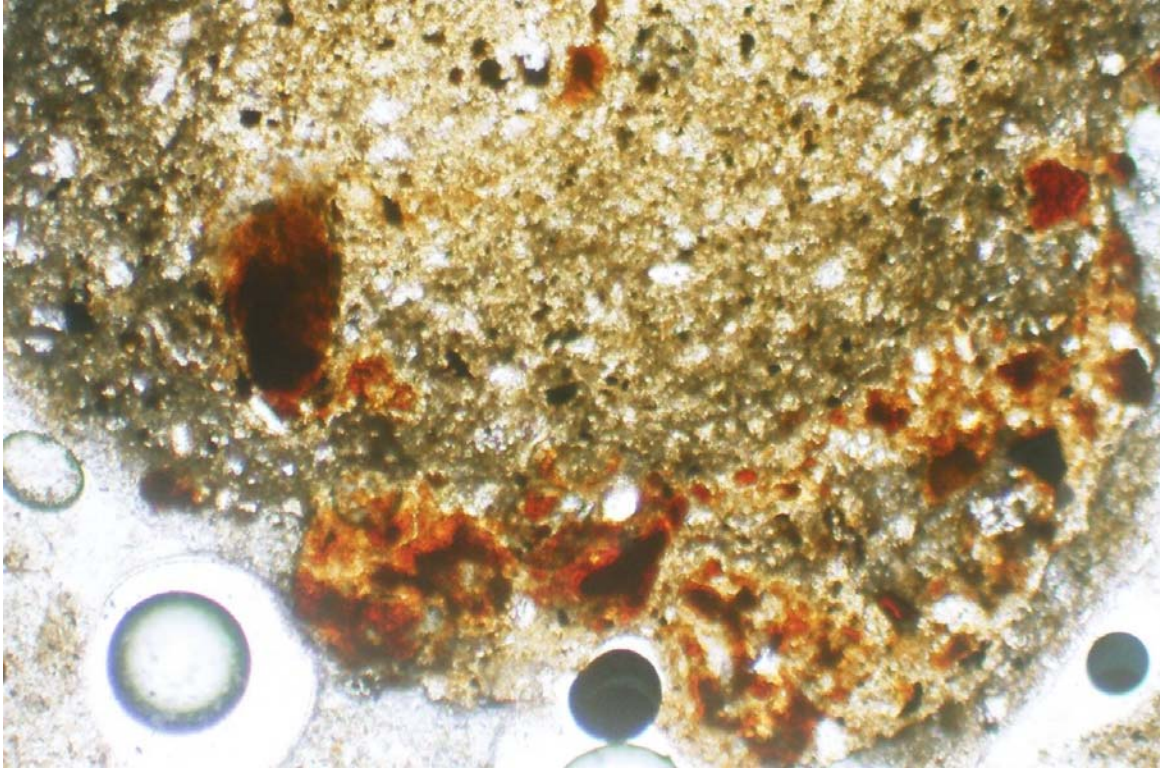


**Figure 4.** Sample 004A in plain transmitted light (top) and another area in plain reflected light (bottom), width of field 1.3 mm. The EDS spectra for the reddish Fe oxyhydroxide in the upper photo and in the lower photo are at the top and bottom, respectively, of Figure 5.

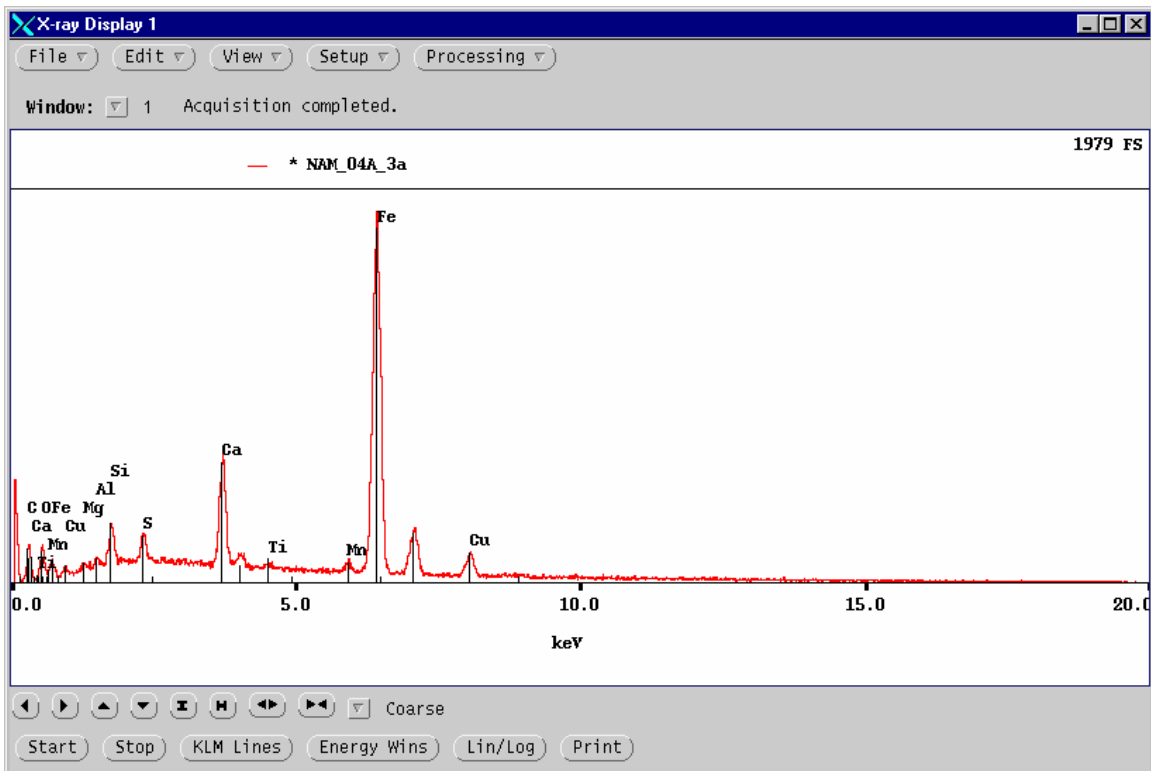
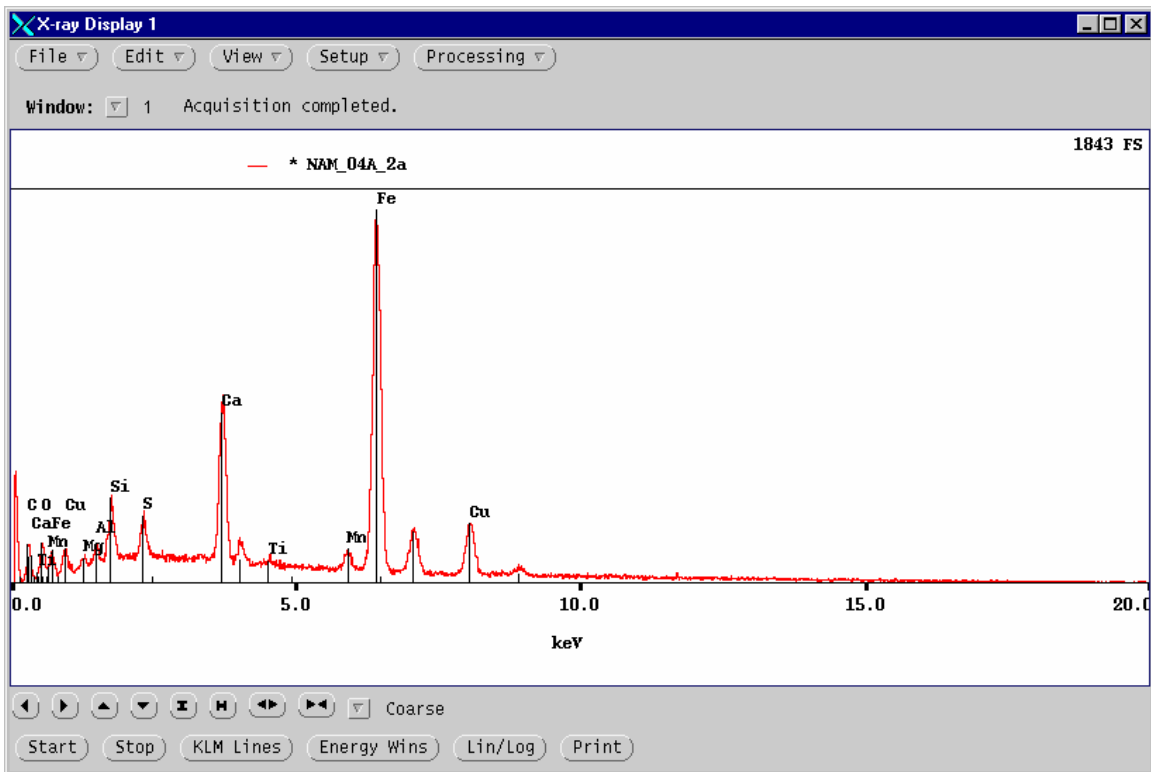


**Figure 5.** EDS spectra for the Fe-oxyhydroxide particles in Figure 4. The upper spectrum is for the large particle at mid-height on the left in the upper photo of Figure 4, but similar spectra were obtained from the adjacent particles. The bottom spectrum is for the large oxyhydroxide particle at the centre of the lower photo of Figure 4. The small unlabelled peak to the right of the Cu peak in the upper spectrum is for Zn.

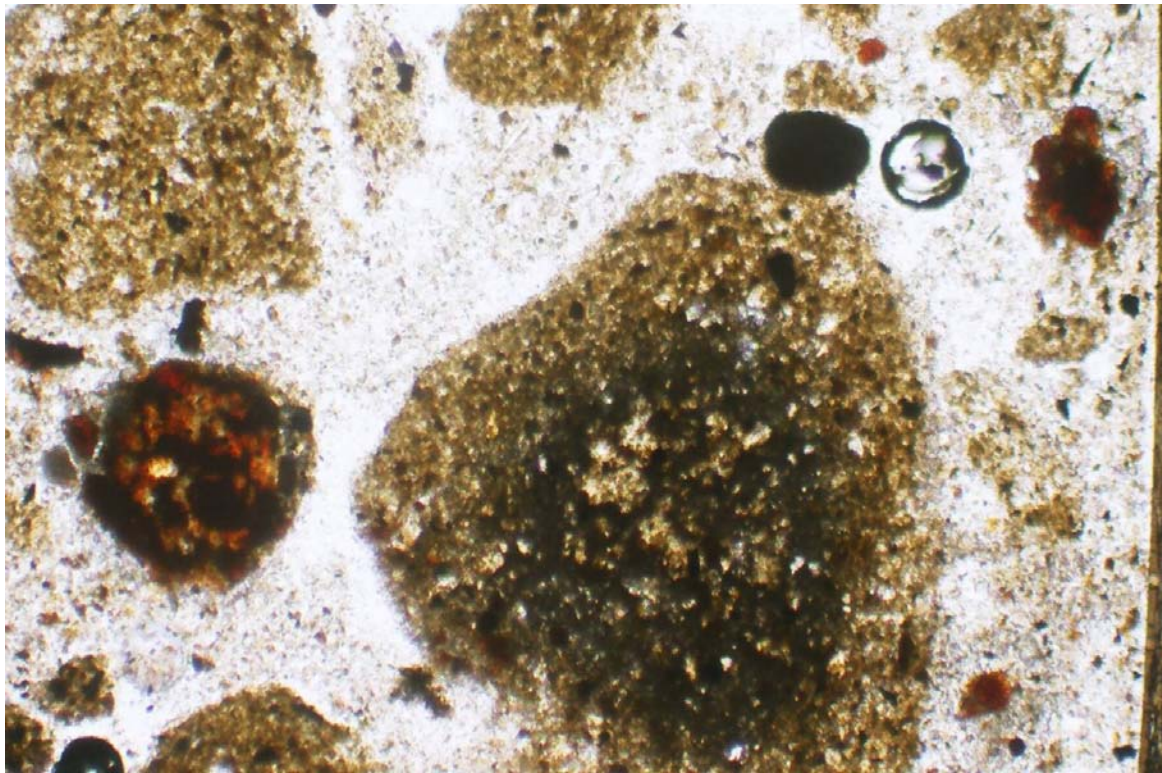
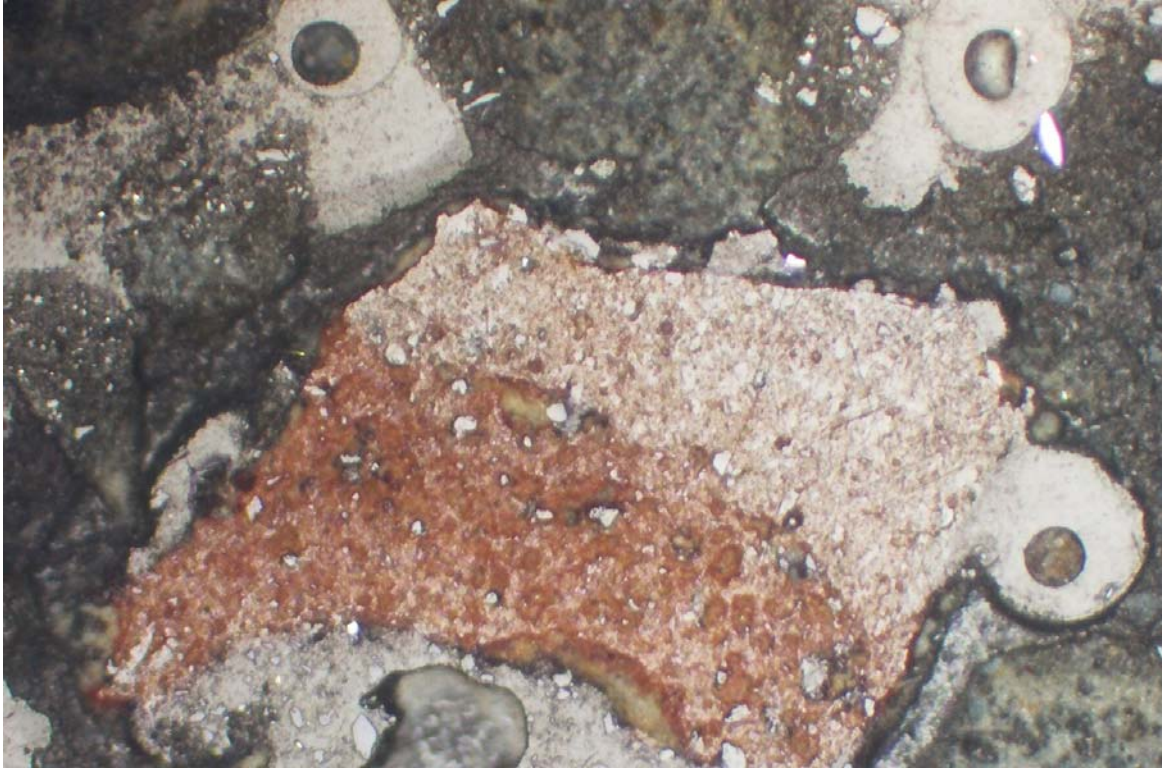


**Figure 6.** Sample 004A in plain reflected light (top) and in plain transmitted light (bottom), width of field 1.3 mm. The upper photo shows a large fragment of banded (layered) Fe oxyhydroxide. The lower photo shows the turbid, fine-grained character of the tailings, and on the left, a circular particle of reddish Fe oxyhydroxide. Spectra for the oxyhydroxide particles are in Figure 7.

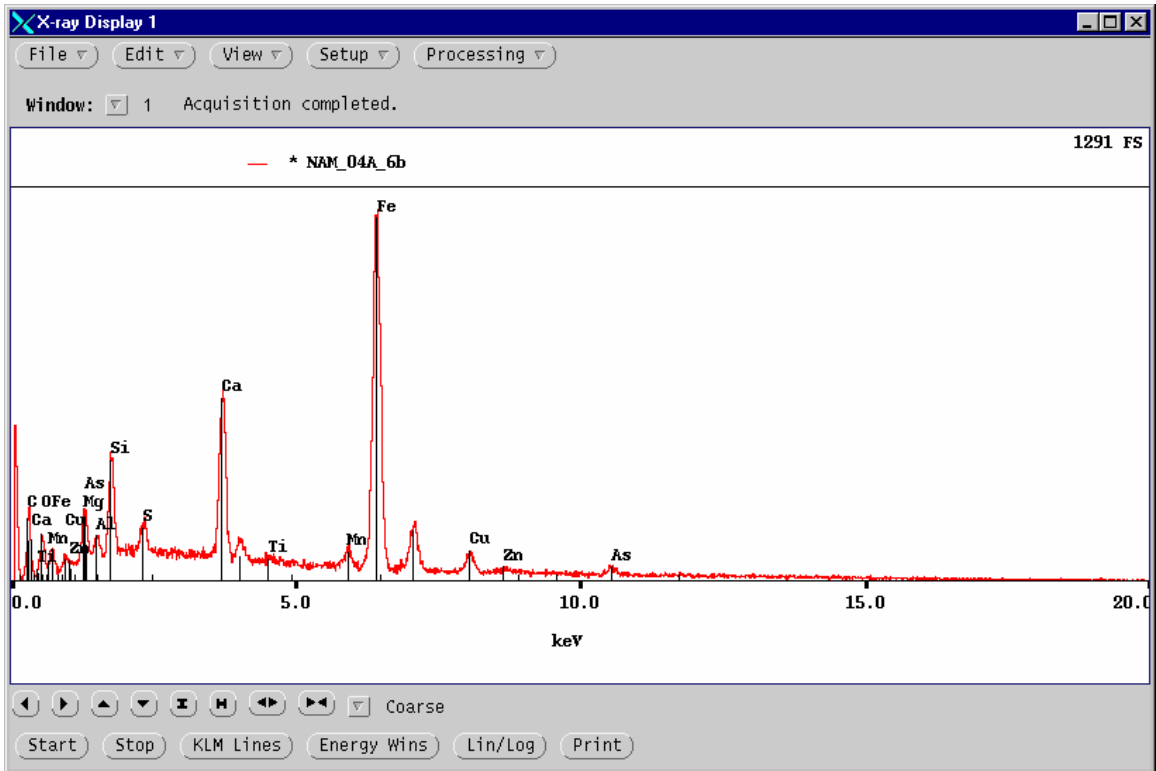
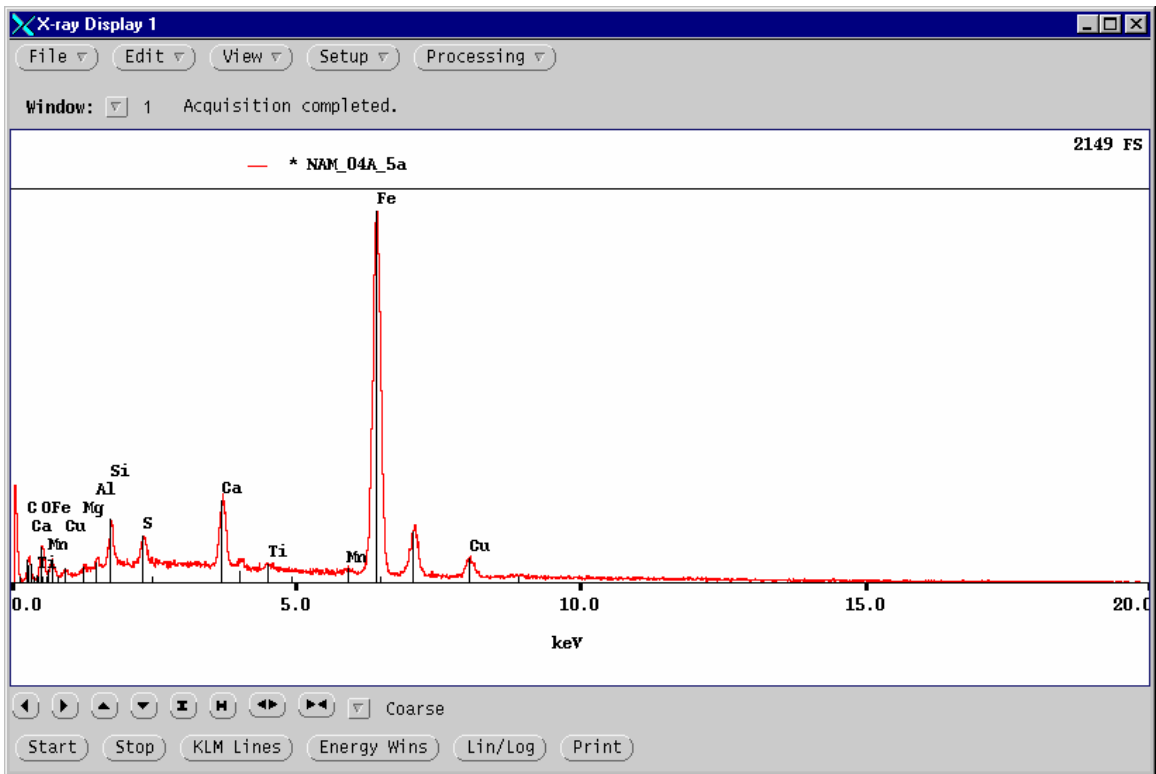


Figure 7. EDS spectra of the Fe oxyhydroxides in the upper and lower photos, respectively, of Figure 6.

### ***Sample 004B***

Sample 004B is representative of the coarser portion of sample 004. The polished thin-section megascopically contains more reddish Fe oxyhydroxide than does 004A, and a few of the oxyhydroxide particles are almost black. Transmitted-light microscopy revealed that, aside from fragments of Fe oxyhydroxide, the largest particles are quartz. Quartz and a carbonate mineral or minerals make up the bulk of the sample. The carbonate mineral does not occur as coarse grains, and most is present as matrix-like fines with muscovite. Gypsum is common both as single grains and as aggregates that cement the tailings. SEM–EDS examination of the surficial blebs on the saved intact specimen of 004 indicated that those too are gypsum.

Reflected-light microscopy showed that many of the pyrite grains in 004B are up to 50  $\mu\text{m}$  across, but the overall sulfide-mineral content is nonetheless similar to that of 004A. Several of the pyrite grains have well-developed alteration rims of Fe oxyhydroxide (Figs. 8, 10, 15). A few grains of arsenopyrite [FeAsS] and sphalerite, and one of secondary covellite [CuS], are present; however, despite the relatively high Cu content of the Fe oxyhydroxides, no chalcopyrite [CuFeS<sub>2</sub>] was observed in 004A or 004B.

The sample was chosen for a quantitative mineralogical determination because it was considered to provide the best opportunity to establish the identity of the Fe oxyhydroxides. The results (Appendix 1) indicate that the carbonate mineral is calcite and that goethite [ $\alpha$ -FeO(OH)] is below the detection limit. A specific search was made for ferrihydrite [nominally 5Fe<sub>2</sub>O<sub>3</sub>·9H<sub>2</sub>O] but it was not detectable. Although the bulk of the Fe oxyhydroxide may therefore be presumed to be amorphous, the presence of at least some ferrihydrite cannot be discounted; the mineral has extremely poor X-ray diffraction qualities and would be difficult to detect because of that property when combined with a relatively low percentage in a complex bulk assemblage. A noteworthy feature is that a small amount (0.6 wt%) of jarosite [KFe<sub>3</sub>(SO<sub>4</sub>)<sub>2</sub>(OH)<sub>6</sub>] was determined to be present in the sample.

The character of the alteration rims on pyrite, and the results of EDS analyses of the rims and of the fragmental-type Fe oxyhydroxides are given in Figure 8 to 13. The results show the same pattern that was detected on 004A. The fragmental oxyhydroxide is typically Ca- and Cu-rich; however, the Ca but not the Cu contents decrease as the oxyhydroxide becomes increasingly opaque, thus indicating that the Cu is associated with the oxyhydroxide rather than the Ca-rich phase.

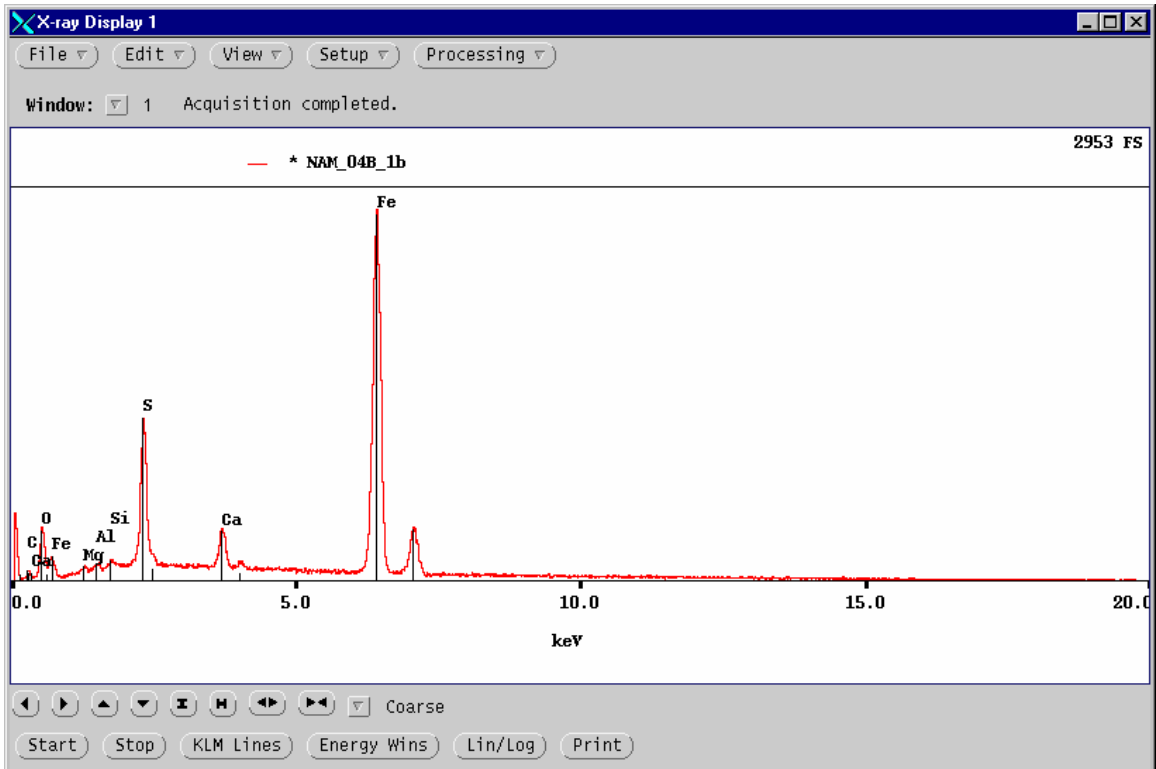


**Figure 8.** Sample 004B in plain reflected light (top), width of field 0.625 mm, showing two grains of pyrite with grey alteration rims of Fe oxyhydroxide. The EDS spectrum is for the oxyhydroxide associated with the grain at the lower right; a spectrum for the rim on the elongate grain near the centre gave similar results, but with a trace amount of Cu.

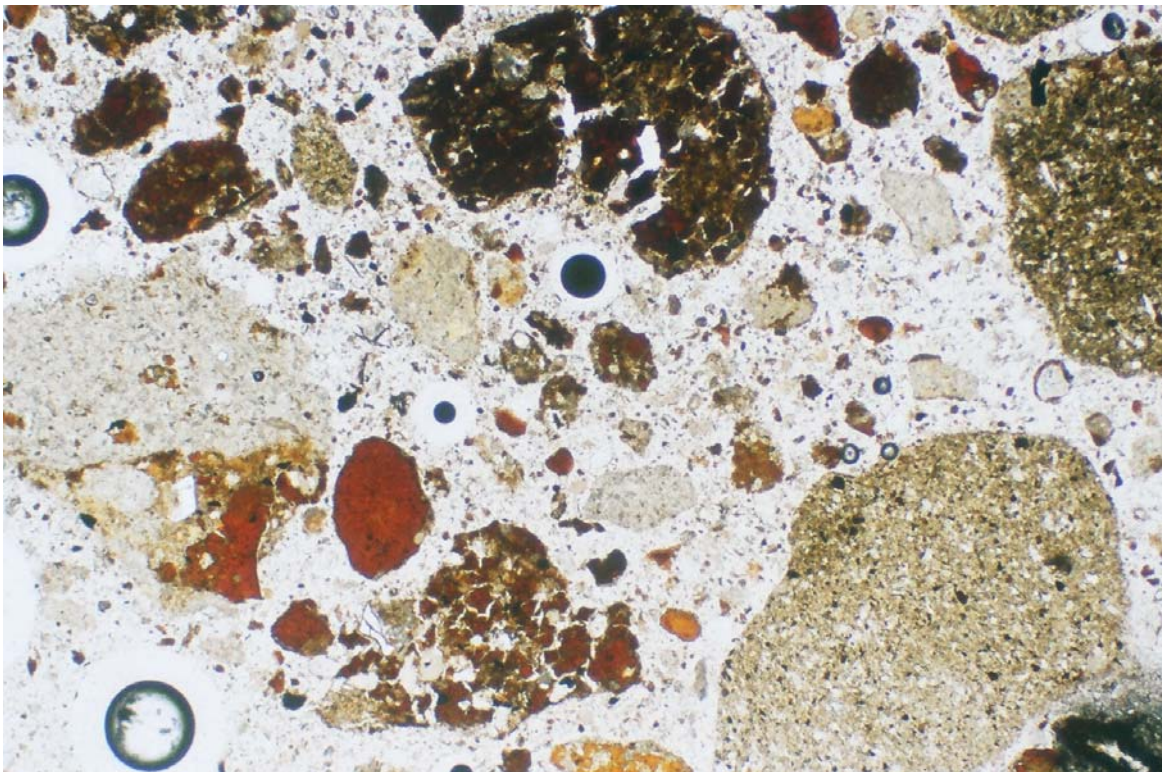
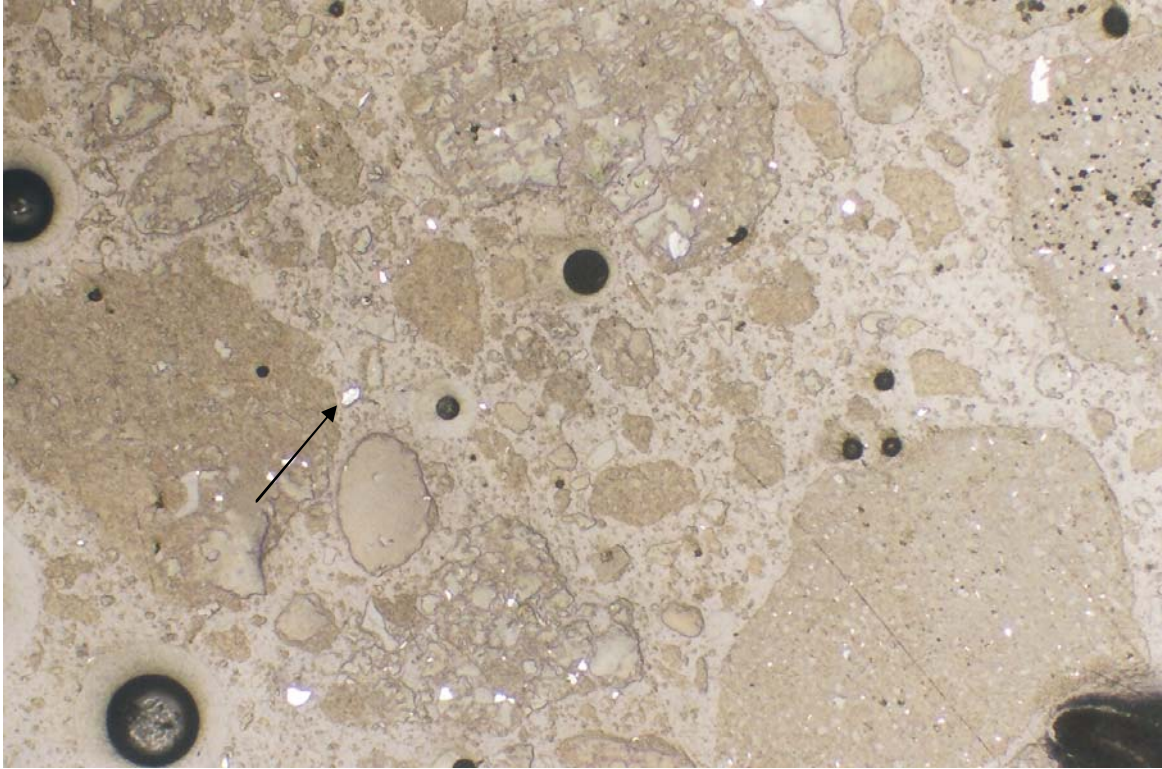


**Figure 9.** An overview of part of sample 004B in plain reflected light (top), and the same field in plain transmitted light (bottom), width of field 2.6 mm. The white grains in the upper photo are pyrite, and the reddish to almost opaque particles in the lower photo are Fe oxyhydroxide. The arrow points to the altered pyrite grain shown in Figure 10.

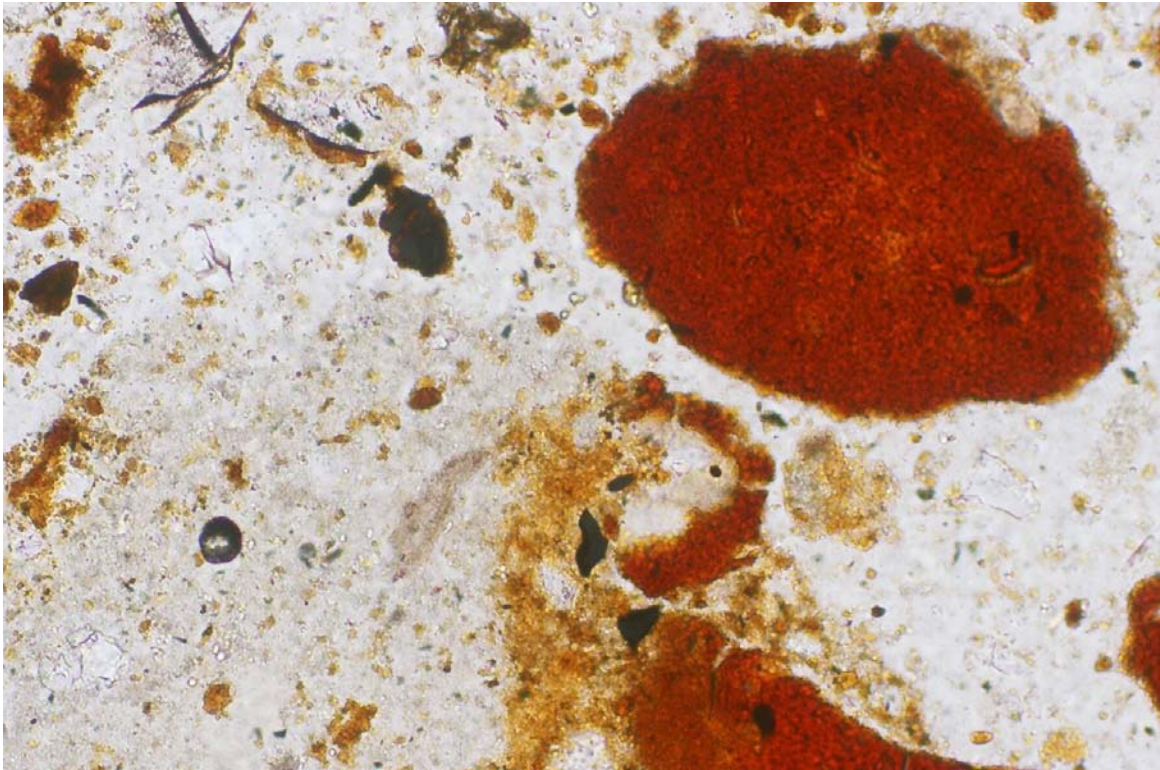


**Figure 10.** An enlarged part of Figure 9, in plain reflected light (top) and in plain transmitted light (bottom), width of field 0.625 mm. The white grains are pyrite, and the reddish material is Fe oxyhydroxide. EDS spectra for both are in Figure 11.

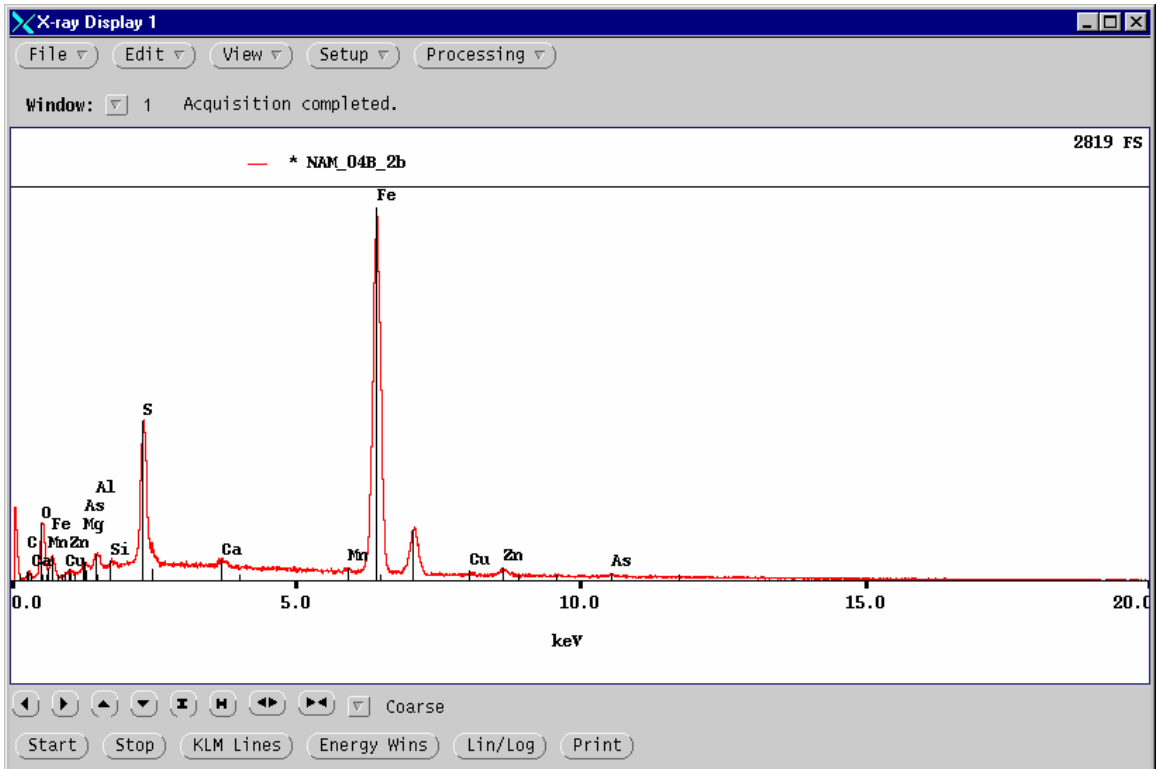
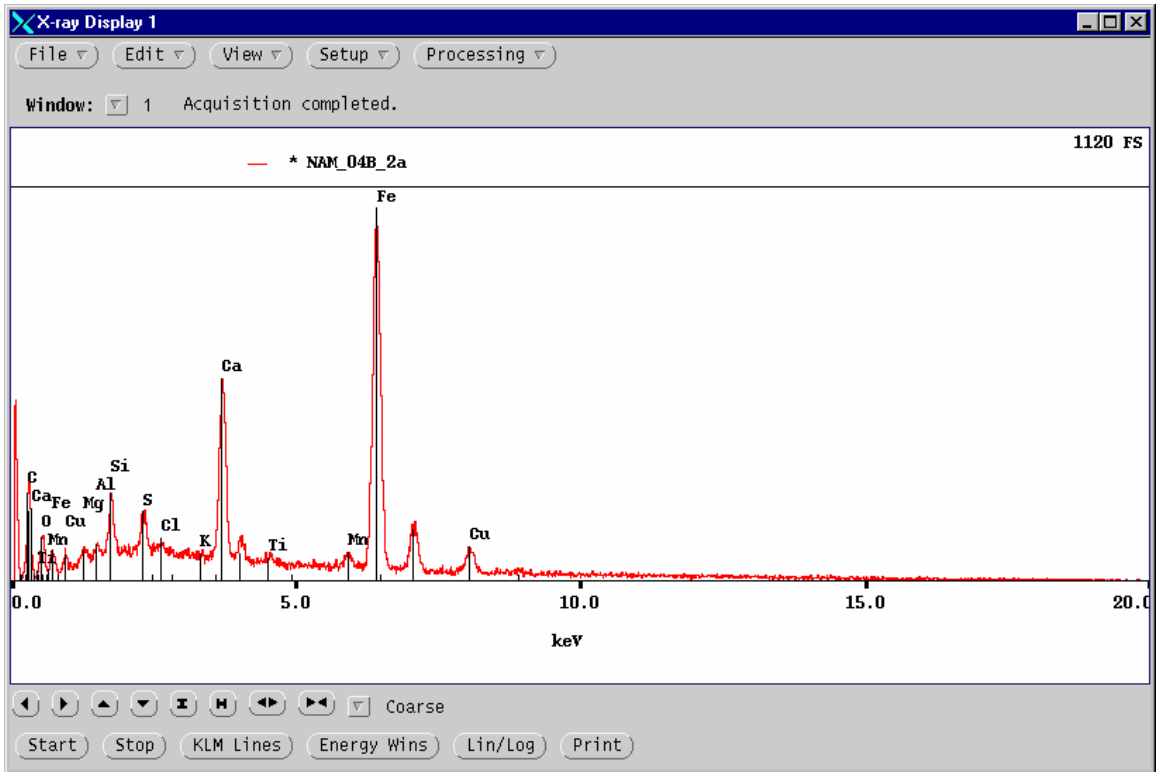


**Figure 11.** EDS spectra for (top) the large, oval Fe oxyhydroxide at the upper right of Figure 10, and (bottom) for the Fe-oxyhydroxide alteration of pyrite. The spectrum of the fragmental oxyhydroxide is Ca- and Cu-rich whereas the alteration associated with pyrite contains trace amounts of Zn and As.

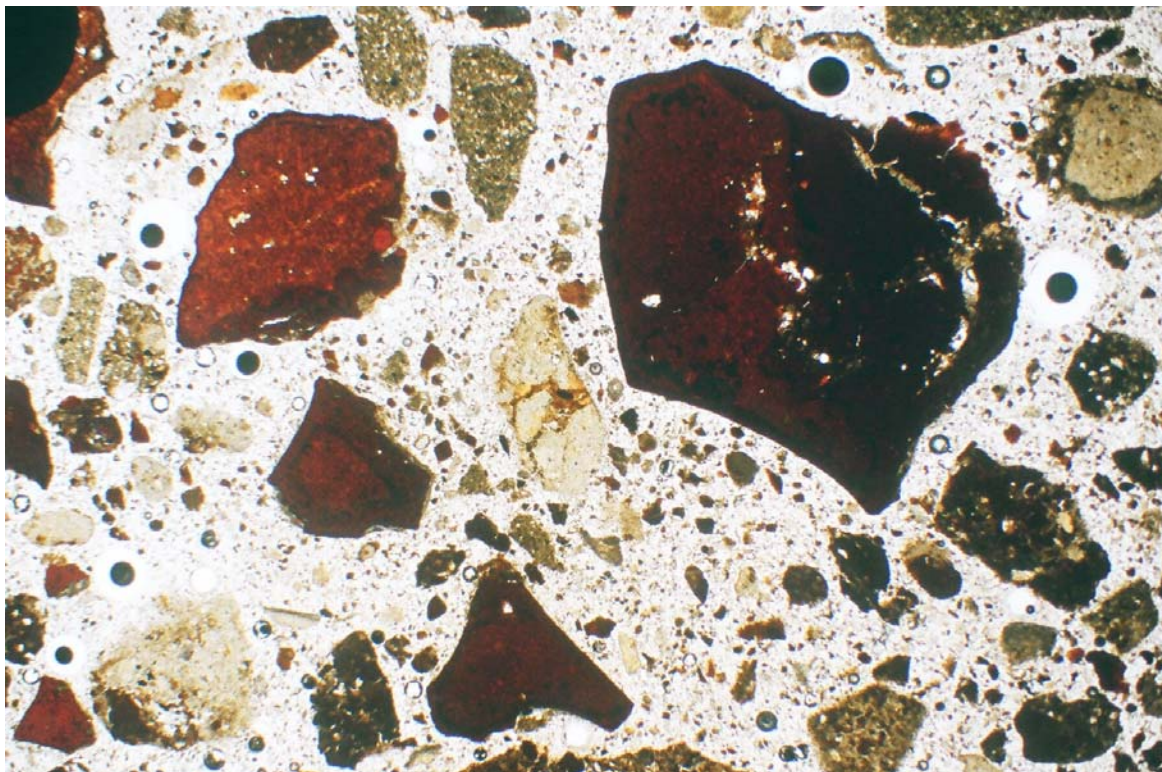
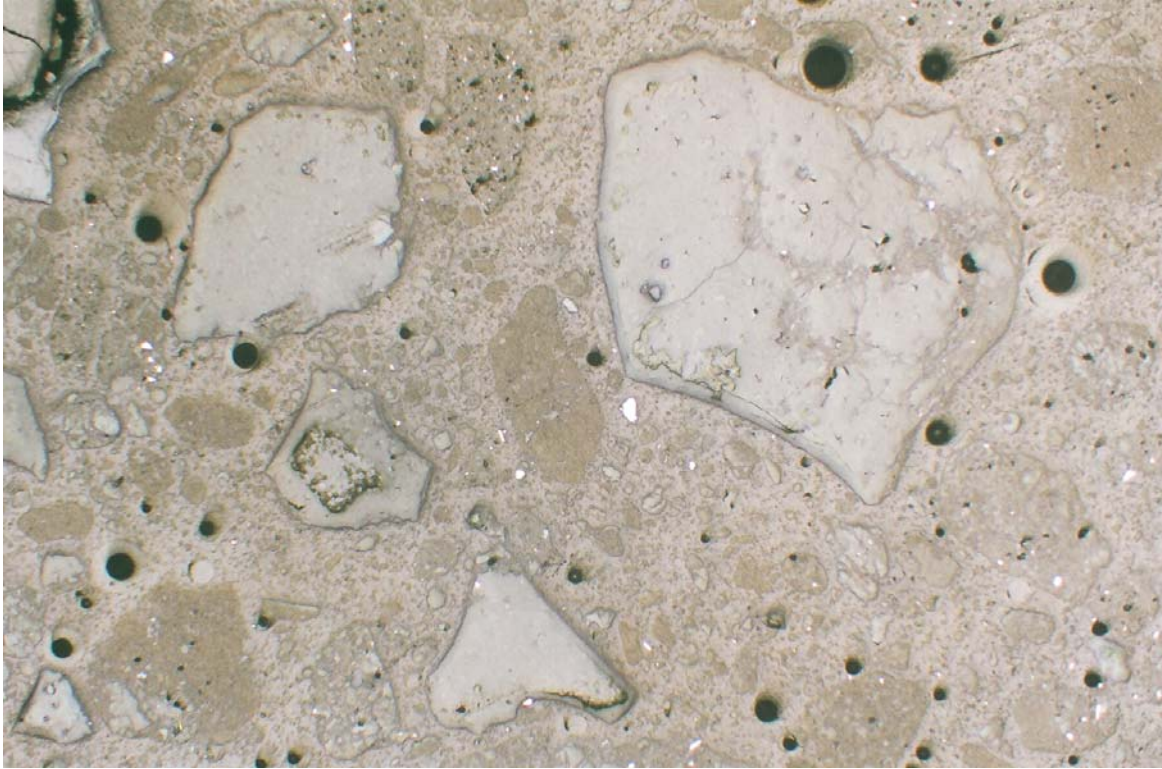


**Figure 12.** Overview of an area rich in Fe oxyhydroxides in 004B. The upper photo is with plain reflected light, and the lower one is of the same field in plain transmitted light, width of field 5.2 mm. EDS spectra of the largest particle on the left show the typically high Ca and Cu contents whereas the more opaque large particle on the right is much lower in Ca but not Cu.

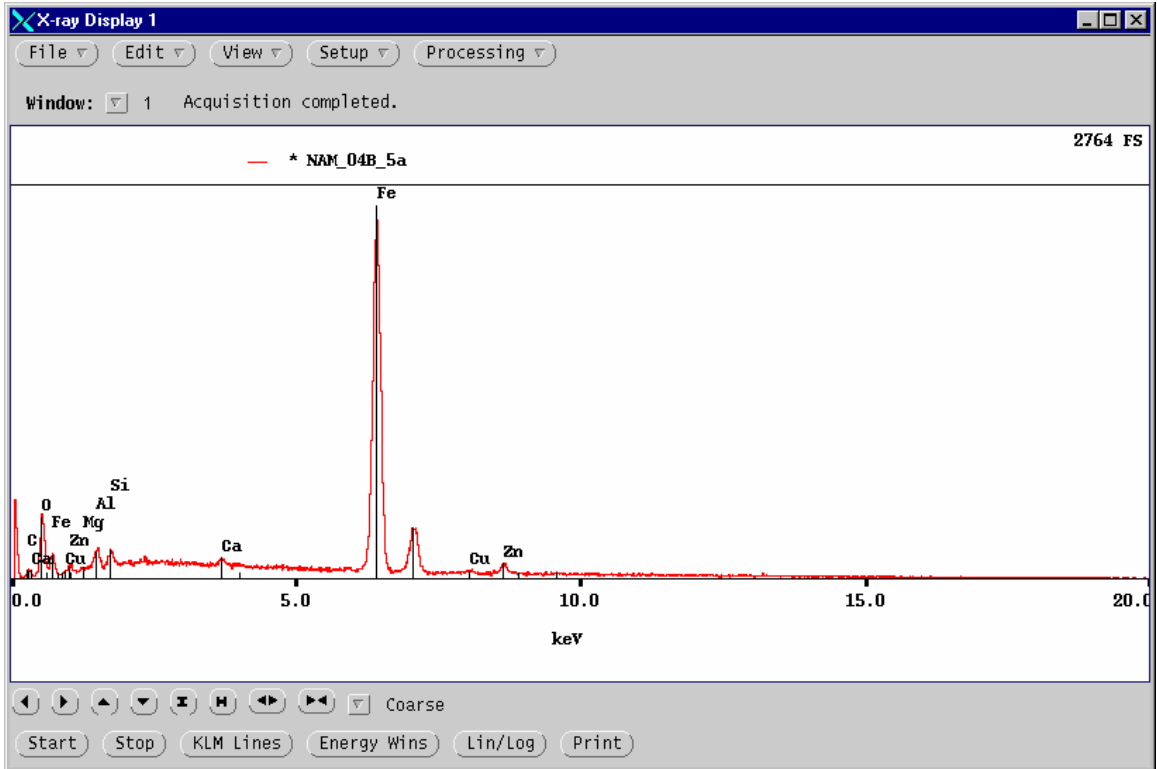


**Figure 13.** Sample 004B in plain reflected light (top), width of field 0.625 mm. The EDS spectrum is for the broad Fe-oxyhydroxide rim around a core of residual pyrite at the lower left. The upper right quadrant of the photo is fully occupied by a fragment of Fe oxyhydroxide which has the typical high Ca and Cu contents.

### ***Sample 005***

The as-received sample was wet and clay-like; its plasticity was pronounced, and the bag had to be slit open because much of the material adhered to the plastic and could not be easily extruded. Despite the wetness of the material, liquid was not present as an isolated phase. The solids were a light grayish brown, but a few ochreous spots, to a maximum of 1½ to 2 mm in diameter, were observed.

The polished thin-section megascopically has a less oxidized appearance than sample 004 insofar as only two or three reddish Fe-oxyhydroxide particles are distinct. Reflected-light microscopy revealed that the section is more sulfide-rich than 004, and the pyrite content was estimated to be ~3%. Pyrite grain sizes are typically <50 µm across. Several grains of sphalerite and of arsenopyrite are present. As well, a few grains of chalcopyrite, trace amounts of galena and secondary covellite (the largest grain of the latter is ~7 × 20 µm), and one particle of polycrystalline marcasite [FeS<sub>2</sub>] about 30 µm across, were observed. One of the grains of sphalerite has a narrow rim of covellite. Pyrite forms >95% of the total sulfide content, and the relative abundance of the others was estimated to be sphalerite > arsenopyrite > chalcopyrite > covellite.

The non-sulfide assemblage, as in 004, consists largely of quartz and carbonates. The overall appearance in transmitted light is brownish (Fig. 14), but large fragmental Fe oxyhydroxides of the type observed in 004 are rare. Two grains of carbon, the larger one 30 × 200 µm, were noted (Fig. 15); the grains are not intergrown with other minerals or attached to them, and possibly the carbon is of anthropogenic origin.

A few of the pyrite and arsenopyrite grains have narrow oxidation rims, and a well-developed rim on an arsenopyrite grain is shown in Figure 16. The EDS spectrum (Fig. 17) indicates that the rim is a Fe arsenate. An unidentified rim on galena (Fig. 18) is apparently a Cu–Zn sulfate. EDS spectra of the large particles of Fe oxyhydroxide (Figs. 19, 21) indicate that they are As-bearing but, unlike in sample 004, they do not have detectable amounts of Cu (Figs. 20, 22).

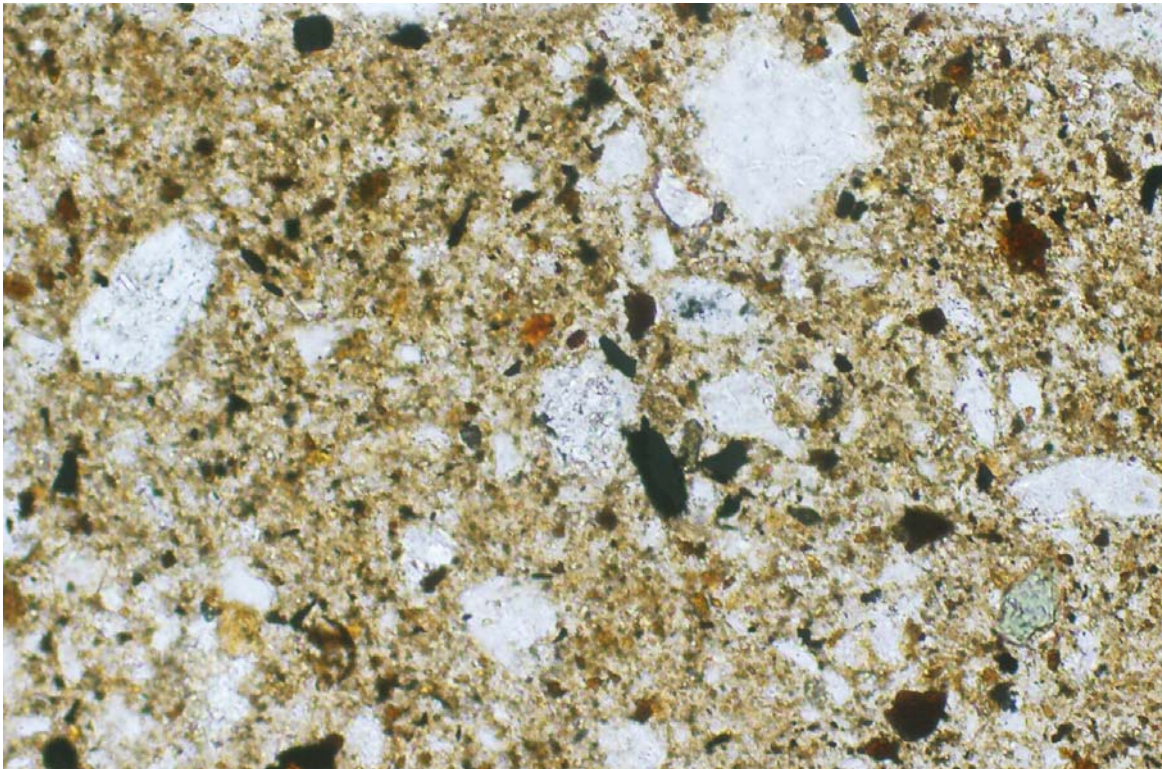


**Figure 14.** Sample 005 in plain reflected light (top), and the same field in plain transmitted light (bottom) and with polarizers crossed (next page), width of field 0.625 mm. The white grains in the upper photo are pyrite, and the clear grains in the lower photo are mainly quartz.

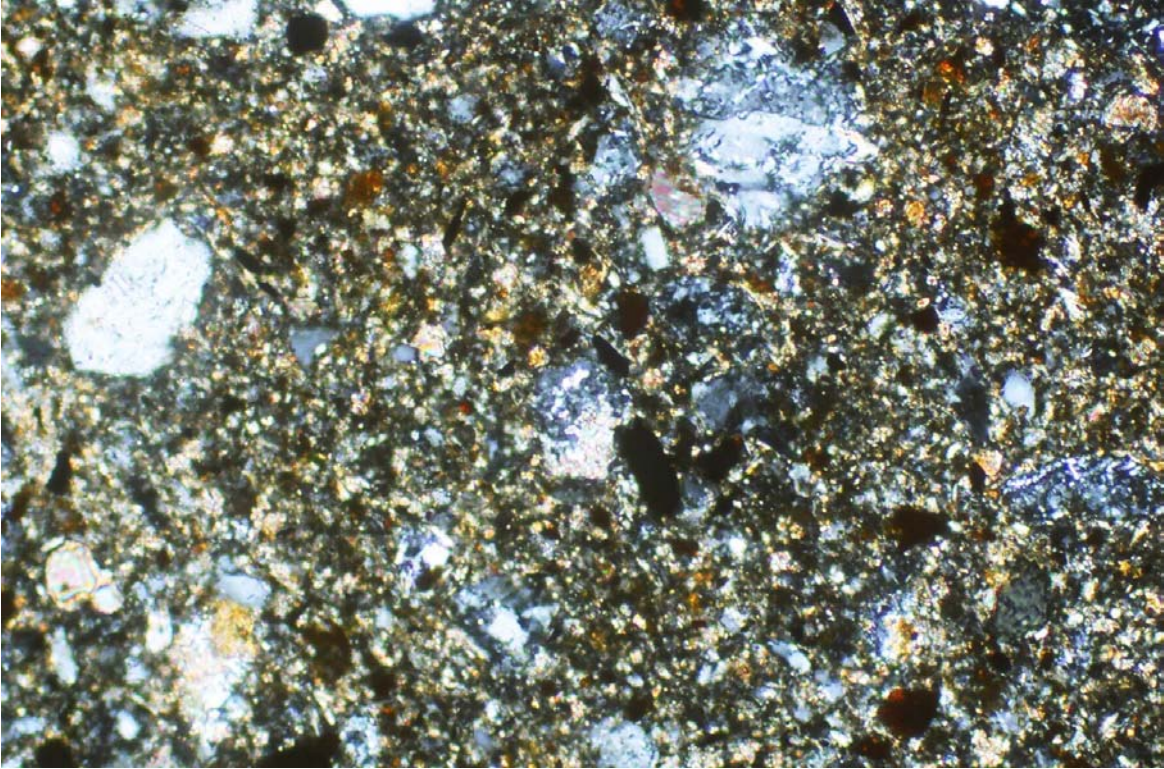


**Figure 14** (cont'd). The same field as on the preceding page, but with polarizers crossed. The white to grey grains are mainly quartz, and the coloured grains are mainly carbonate minerals.



**Figure 15.** Sample 005 in plain reflected light, width of field 0.625 mm. The white grains are mainly pyrite, and the elongate brownish grain above centre is carbon.

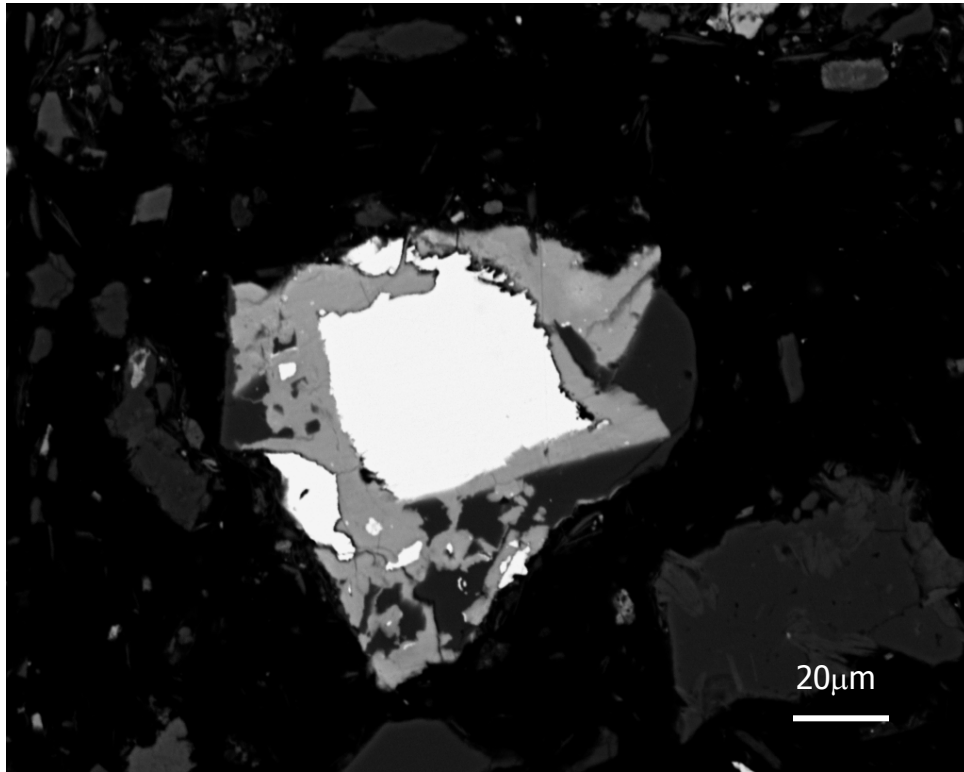


**Figure 16.** Sample 005 in plain reflected light (top), width of field 0.625 mm. Near the centre is a grain of arsenopyrite with a barely perceptible alteration rim that is readily evident in the backscattered-electron image.

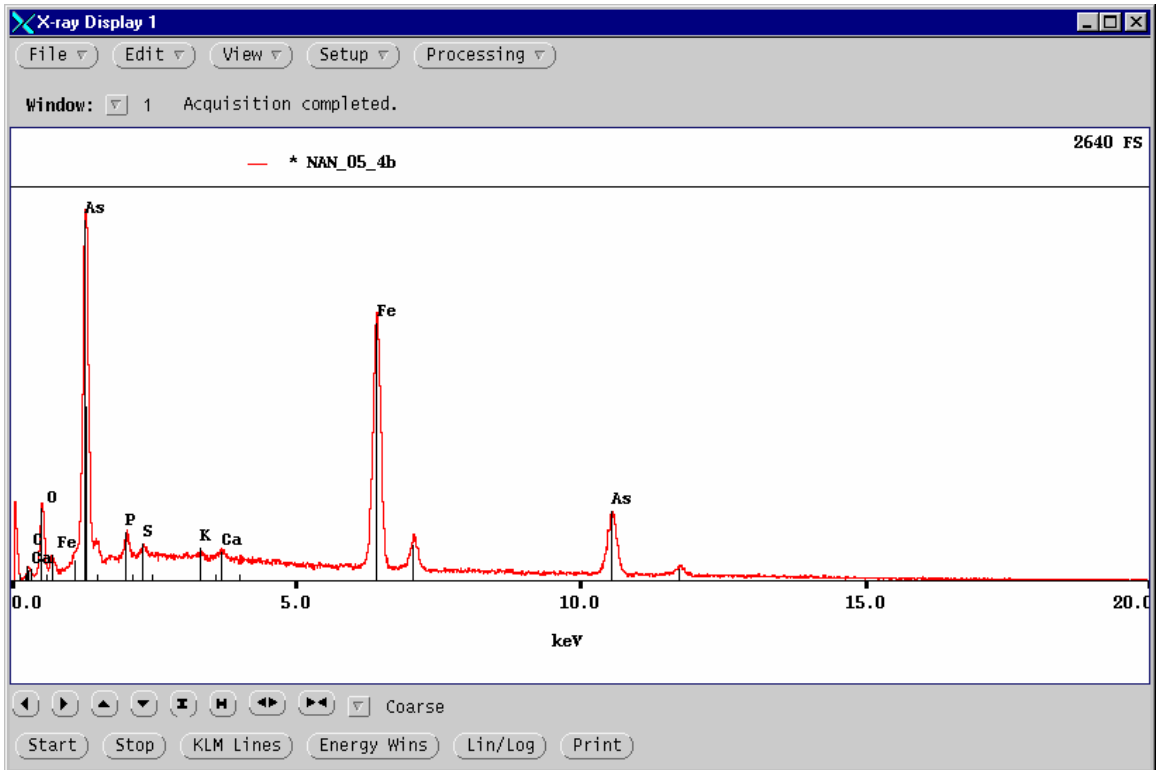


**Figure 17.** EDS spectrum of the rim on the arsenopyrite grain of Figure 16. The spectrum indicates that the rim is a Fe arsenate.



**Figure 18.** Sample 005 in plain reflected light, width of field 0.625 mm. To the right of centre is a roughly rectangular bluish grain with a core of galena (white). An EDS spectrum of the outermost rim indicates that the rim is probably a Cu–Zn sulfate.

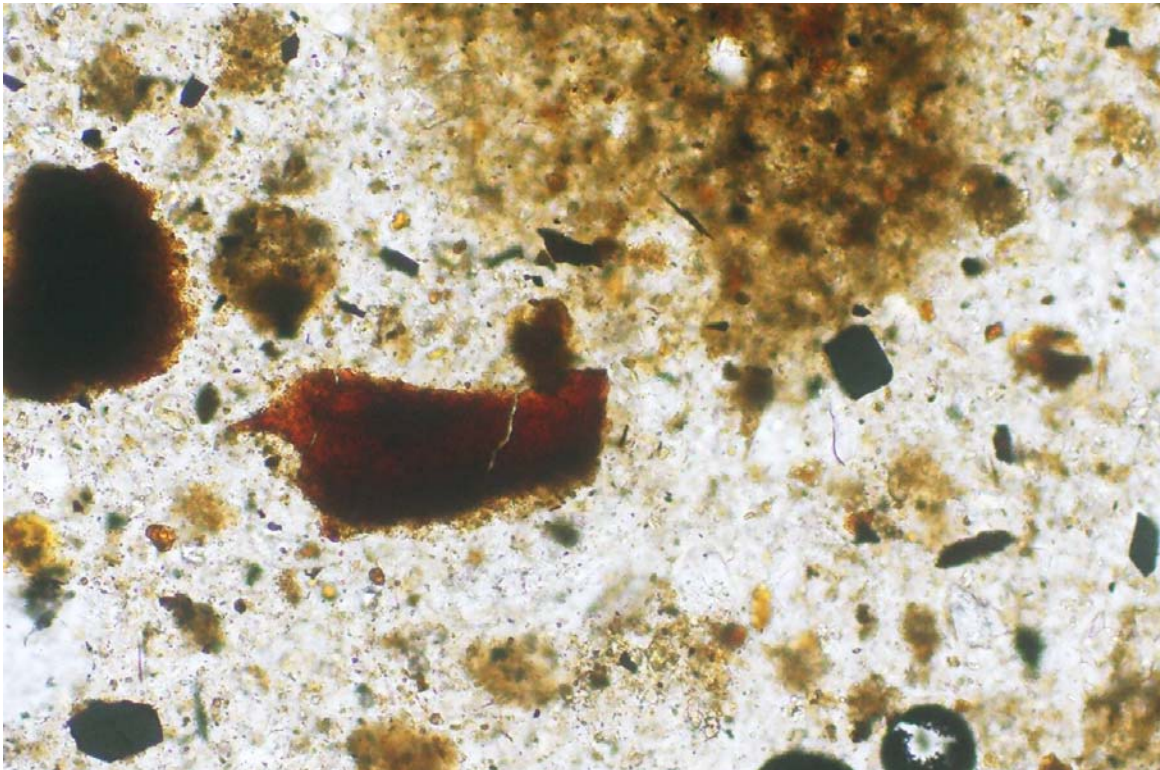


**Figure 19.** Sample 005 in plain reflected light (top) and in plain transmitted light (bottom), width of field 0.625 mm. The white grains are pyrite, and the arrow points to a grain of sphalerite, beneath which is a large particle of As-bearing Fe oxyhydroxide (Fig. 20).

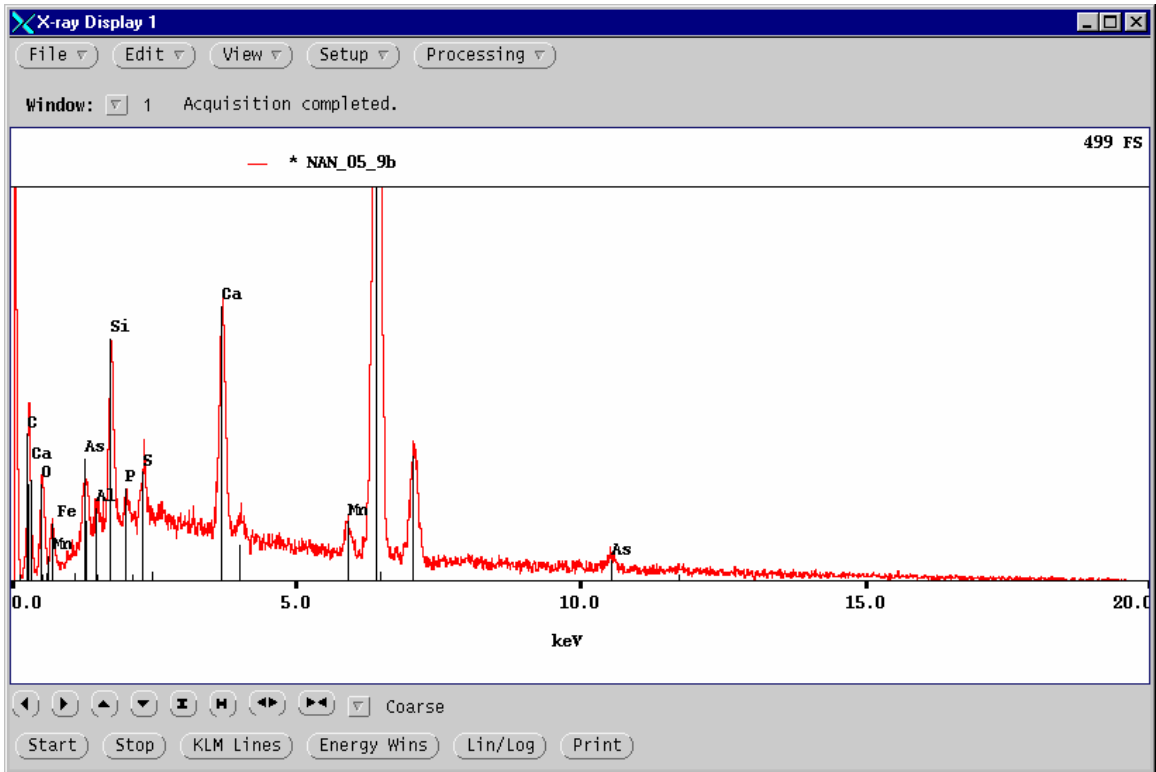


**Figure 20.** Expanded-scale EDS spectrum of the large particle of As-bearing Fe oxyhydroxide shown in Figure 19.



**Figure 21.** Sample 005 in plain reflected light, width of field 0.625 mm. The white grains are pyrite. The upper arrow points to a reddish particle of As-bearing Fe oxyhydroxide (Fig. 22). The lower arrow points to a large grain of dolomite; the small adjoining, roughly oval, grey grain on the right is sphalerite.

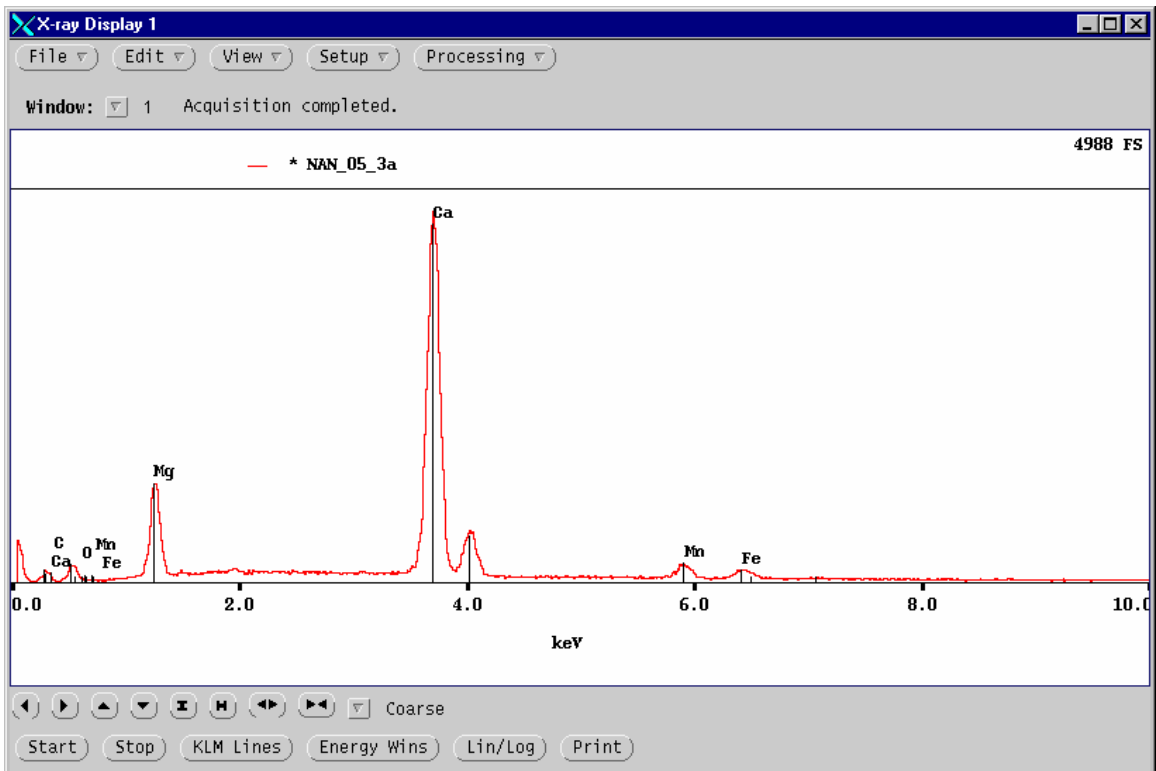
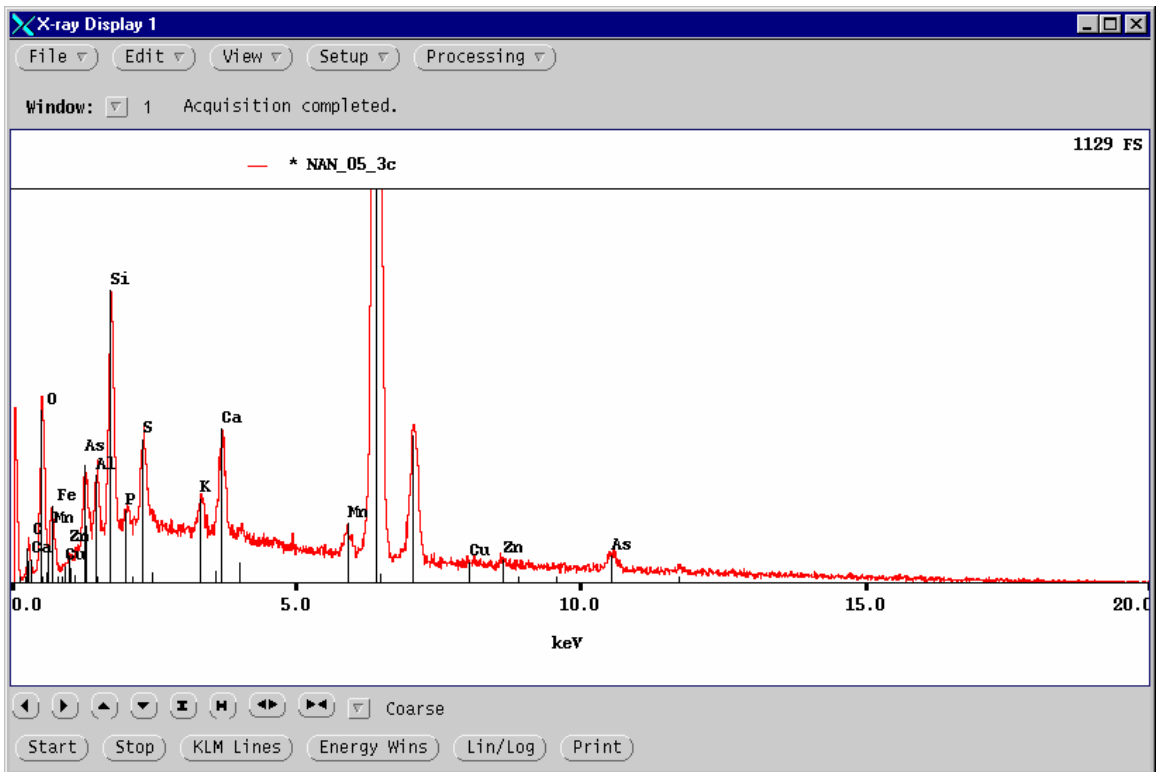


**Figure 22.** EDS spectra of the Fe oxyhydroxide (top) and dolomite (bottom) of Figure 21. The upper spectrum is at an expanded scale to illustrate the presence of As.

### ***Sample 006***

The as-received sample was similar in colour to that of 005 but was noted to be slightly coarser grained. About a quarter of the material was observed to be finer grained than the main mass, and only within this finer portion were there sparse spots of ochreous material, each only about 1 mm in diameter. Abundant excess fluid was present, requiring that the sample be ejected into a plastic vessel rather than onto a sheet.

The polished thin-section is megascopically light brown, like that of 005. Only three distinctly reddish particles of presumed Fe oxyhydroxide are present. Very fine-grained sulfides are dispersed throughout the section.

Microscopy in transmitted light revealed that only one of the reddish particles observed megascopically is solid Fe oxyhydroxide, and the others are polishing artifacts. The non-opaque assemblage consists principally of quartz and carbonates. Many of the quartz particles are fine-grained chert-like mosaic intergrowths rather than single grains, but both types are abundant. A few of the carbonate grains are coarse-grained and homogeneous; the rains are variously calcite of end-member composition, and ferroan dolomite. Chlorite and muscovite are present as fine-grained intergrowths with quartz; the chlorite also occurs sparingly as lath-like intergrowths and is more abundant than in sample 005. A few grains of epidote, amphibole, and biotite were observed.

The sulfides are megascopically visible because the grain size of pyrite is commonly up to 100  $\mu\text{m}$  across, and many grains range from 50 to 90  $\mu\text{m}$ . Fewer grains of pyrite than in 005 are present, but the overall content is about the same because of the larger size of the grains in 006. Chalcopyrite, arsenopyrite, and sphalerite occur sparingly. Oxidation rims on pyrite are more common and are broader than in 005 (Fig. 23), and a distinct feature is that several of the Fe-oxyhydroxide particles appear to be pseudomorphs after pyrite.

Numerous EDS spectra were obtained for the alteration rims and for isolated Fe-oxyhydroxide particles (Figs. 25-32). Many of the particles and rims contain trace amounts of Cu and (or) Zn, and some have detectable As. One of the particles has a composition corresponding to that of plumbojarosite  $[\text{PbFe}_6(\text{SO}_4)_4(\text{OH})_{12}]$ ; Fig. 31].



**Figure 23.** Sample 006 in plain reflected light, width of field 0.625 mm, showing Fe-oxyhydroxide rims on pyrite. The adjacent white prismatic grain southeast of the altered pyrite in the upper photo is arsenopyrite, as is the elongate white grain in the lower photo.

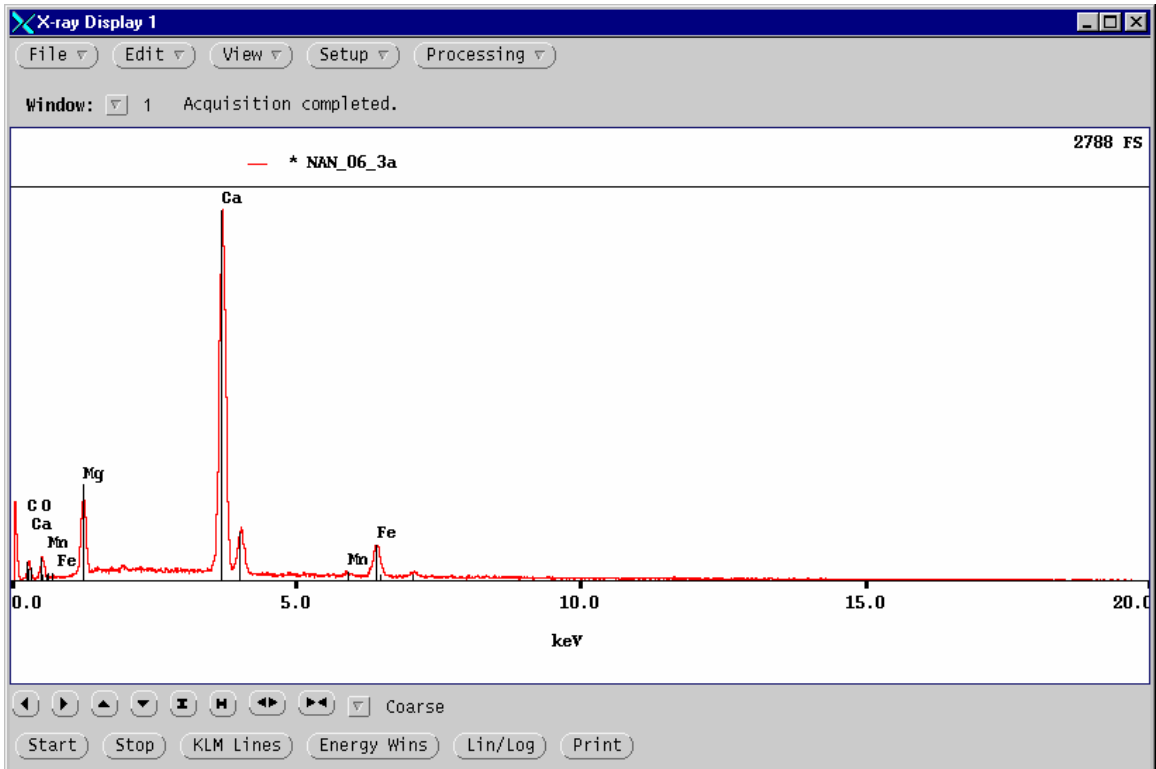
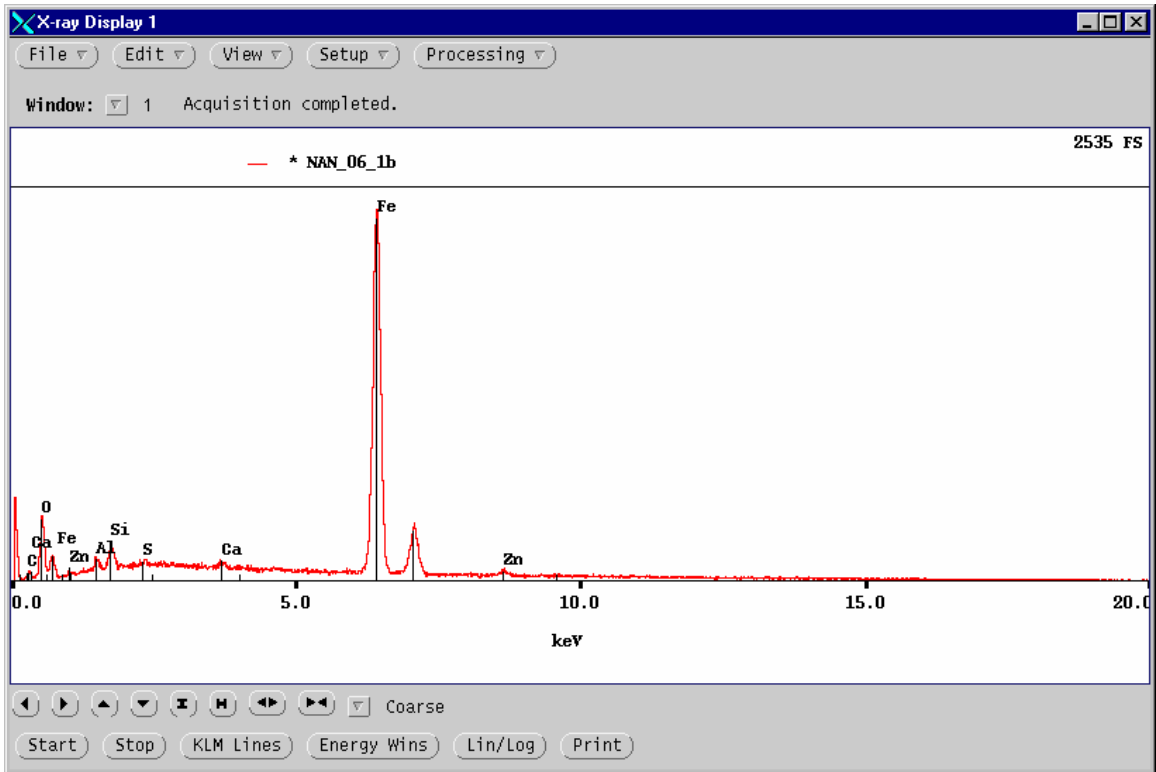


**Figure 24.** EDS spectrum of the Fe-oxyhydroxide rim on pyrite in the upper photo of Figure 23. The rim on the grain in the lower photo gave a similar spectral result. The lower spectrum is of the large dolomite grain showing cleavage traces at the northeastern corner of the lower photo in Figure 23.



**Figure 25.** Sample 006 in plain reflected light, width of field 0.625 mm, showing Fe-oxyhydroxide alteration of pyrite. An EDS spectrum of the oxyhydroxide in the upper photo showed the presence of trace Zn, but no heavy metals were detected in the oxyhydroxide in the lower photo.

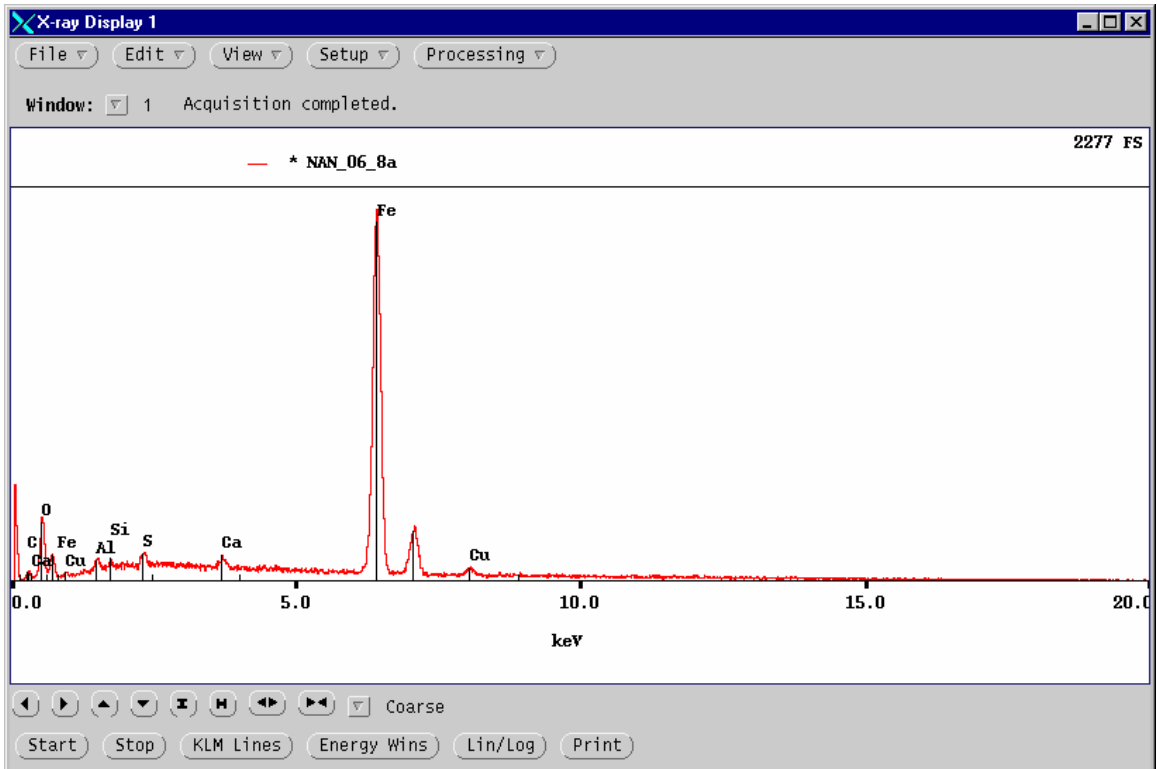


**Figure 26.** Sample 006 in plain reflected light, width of field 0.625 mm, showing a Fe-oxyhydroxide rim on pyrite, and the EDS spectrum for the rim.

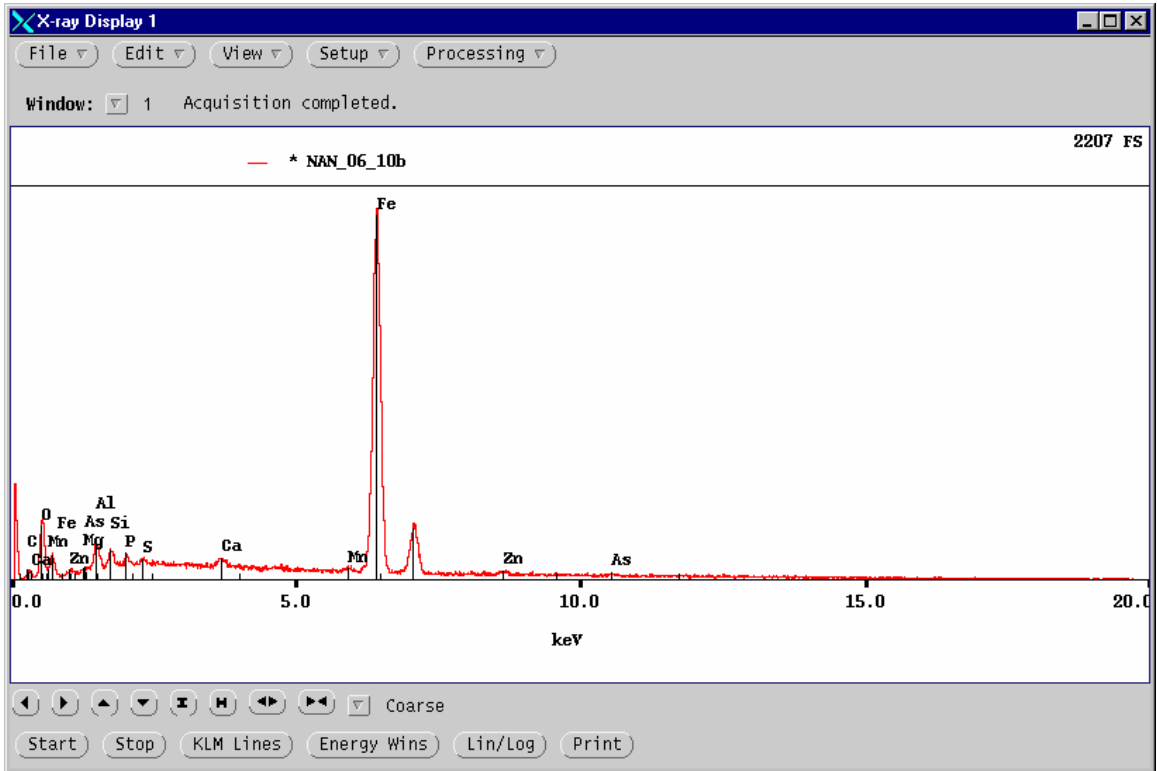


**Figure 27.** Sample 006 in plain reflected light, width of field 0.625 mm, showing residual pyrite and secondary covellite (blue) enclosed within an outer rim of Fe oxyhydroxide, for which the EDS spectrum is shown (trace Zn only). The large grey particle at the far left, mid-height, is also relatively pure Fe oxyhydroxide, but it contains a trace amount of As.

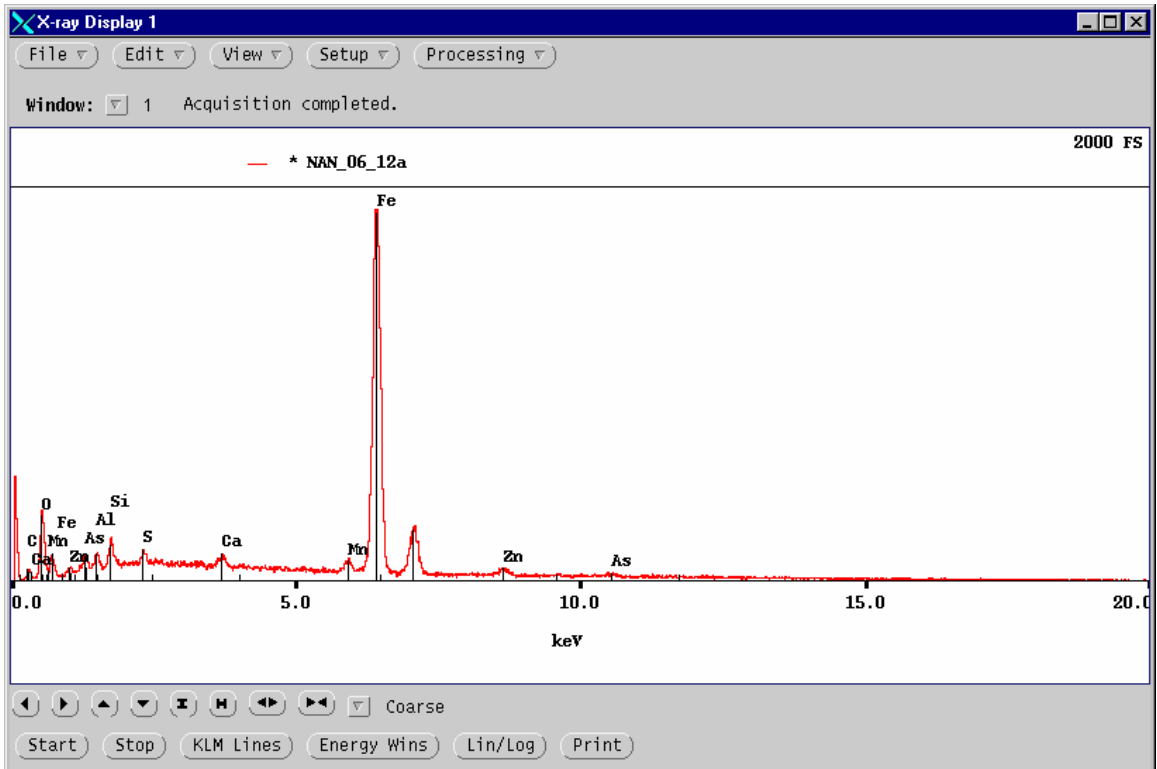


**Figure 28.** Sample 006 in plain reflected light, width of field 0.625 mm, showing residual pyrite within Fe oxyhydroxide that the EDS spectrum indicates to be Zn- and As-bearing.

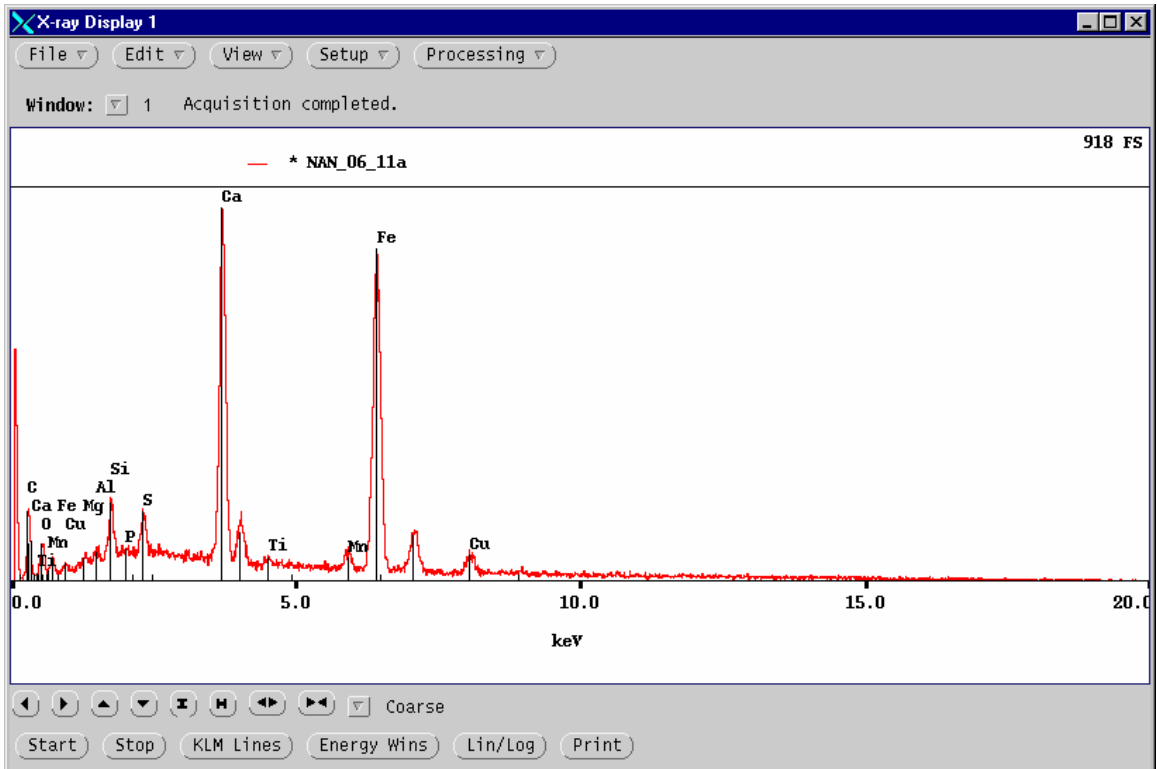
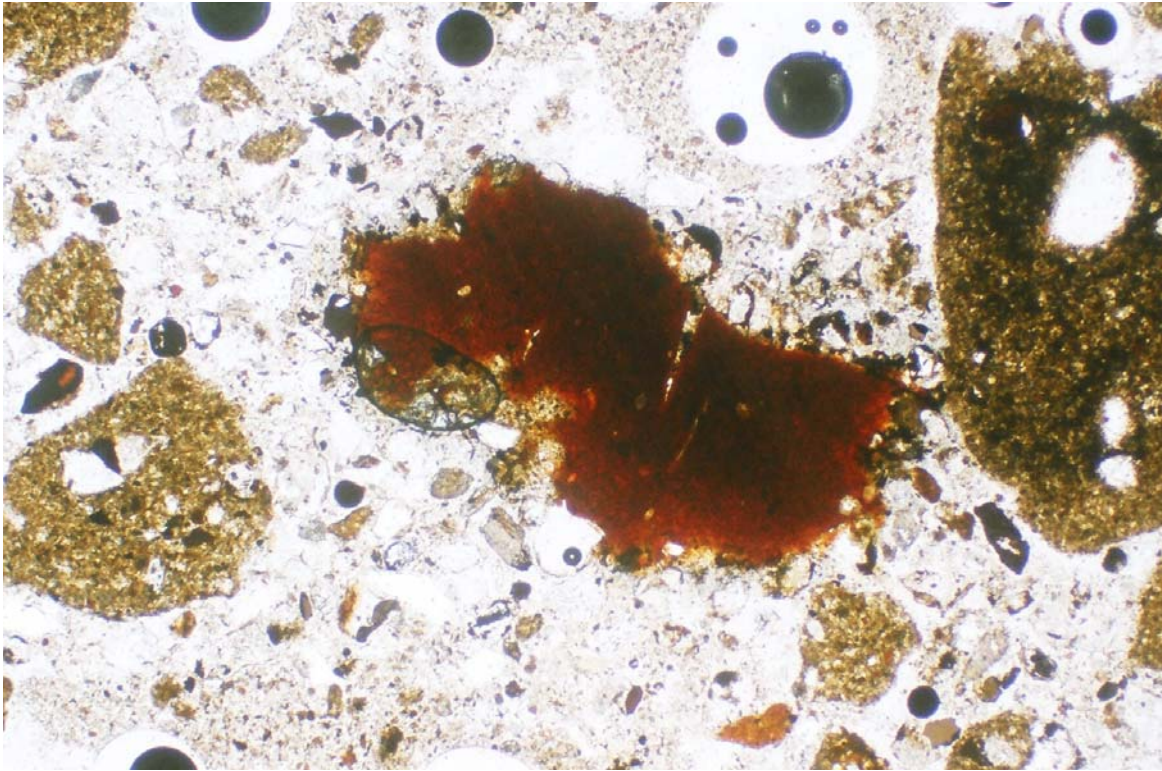


**Figure 29.** Sample 006 in plain transmitted light, width of field 2.6 mm, showing a large particle of reddish, heterogeneous Fe oxyhydroxide. The spectrum of the particle is similar to those obtained for Ca–Cu-rich particles in sample 004.

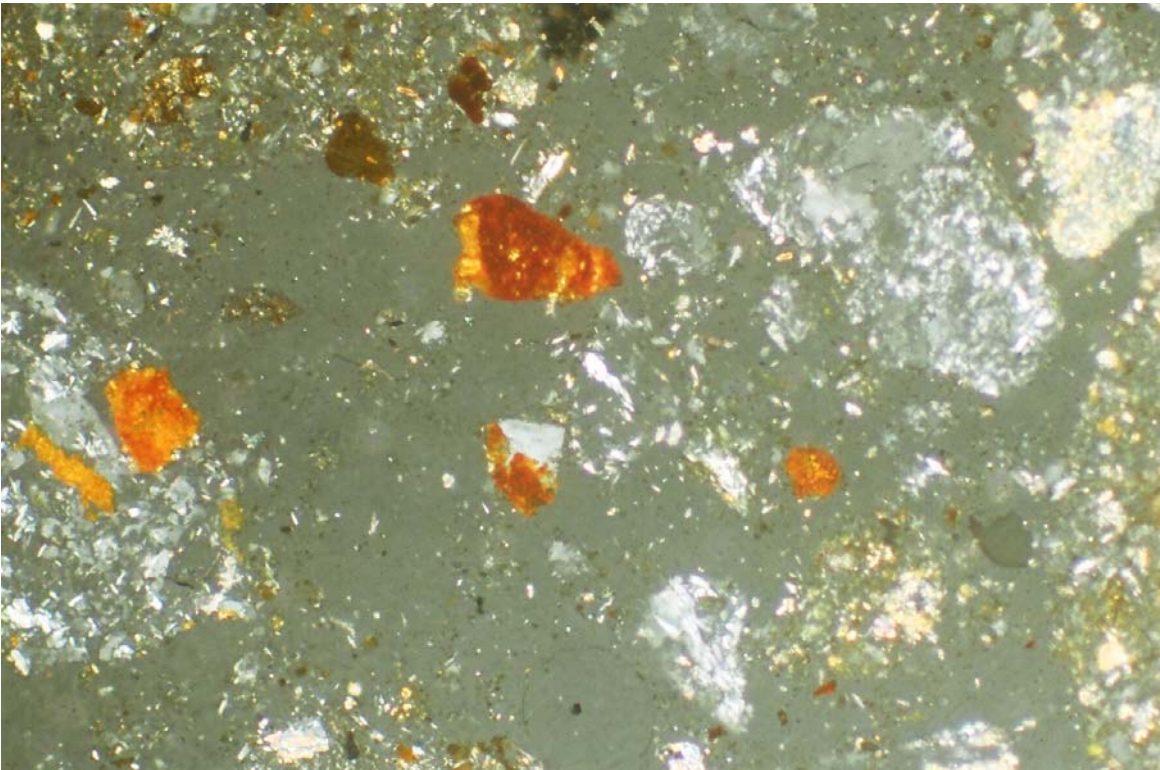


**Figure 30.** Sample 006 in plain reflected light (top), and with almost crossed polarizers and internal reflection (bottom), width of field 0.625 mm. The reddish Fe-oxyhydroxide particle above centre contains only a trace of Zn, but the left portion of the particle also contains plumbojarosite (Fig. 31).

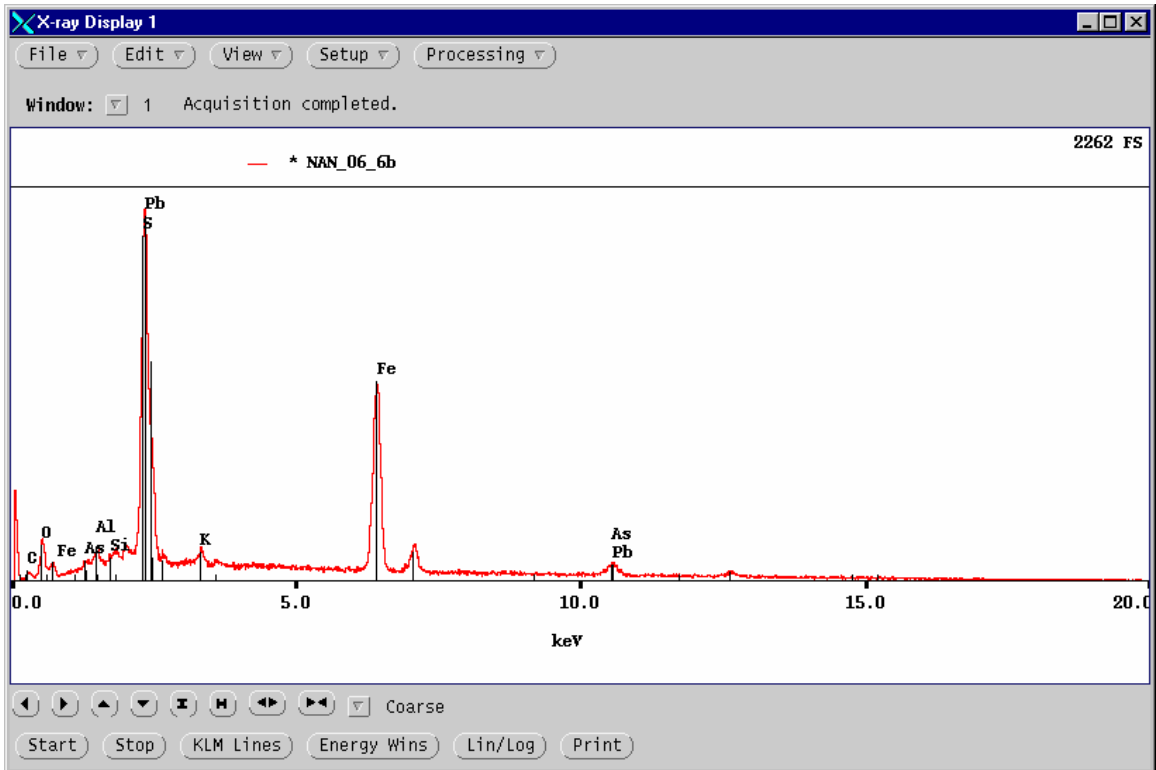


**Figure 31.** EDS spectrum of the plumbojarosite of Figure 30. The mineral is present as an intergrowth of micrometres-scale rhombic crystals.



**Figure 32.** Sample 006 in plain reflected light, width of field 0.625 mm. The Fe-oxyhydroxide particle at the northwestern corner contains traces of various elements, but no heavy metals. The zoned oxyhydroxide in the southeastern quadrant, likely a pseudomorph after pyrite, is similarly relatively pure.

### ***Sample 007***

The as-received material was fine-grained, with a plastic-like consistency, and was the lightest in colour among the sample suite. No sign of oxidation was evident. The bagged material also contained abundant aqueous fluid.

Despite the light colour of the as-received material, the megascopically viewed polished thin-section is slightly darker than that of 006. However, no reddish (ochreous) areas are evident in 007. Only a few specks of sulfide minerals are visible.

Transmitted-light microscopy confirmed that the large particles of Fe oxyhydroxide that are present in all of the preceding samples are absent in 007. The tailings are microscopically turbid (Fig. 33), but thin edges of the section indicate the typical quartz–carbonate predominance; chlorite and muscovite appear to be abundant as laths that form a fine-grained matrix.

The unmounted powder was tested with 25% HCl and gave an instantaneous vigorous effervescence. However, a test of the polished thin-section with alizarin solution did not give a reaction for calcite, thus suggesting that the carbonate mineral is dolomite. To confirm the carbonate-mineral identification and to determine whether the bulk non-opaque assemblage is similar to that of sample 004B, an X-ray diffractogram was obtained. The results (Appendix 1) confirm that the carbonate mineral, unlike that in 004B, is dolomite rather than calcite. The presence of jarosite was detected, but the X-ray peak heights indicate that the amount is no more than a trace.

Reflected-light microscopy revealed that the pyrite content and grain sizes are like those of sample 004A, *i.e.*, only rarely are pyrite grains more than 50  $\mu\text{m}$  in diameter. Several grains of arsenopyrite and sphalerite were observed. Two minute grains of covellite, the larger one only  $\sim 10$   $\mu\text{m}$  across, are present, but no chalcopyrite was seen. One grain has the properties and a composition corresponding to those of the sulfosalt mineral jamesonite [ $\text{Pb}_4\text{FeSb}_6\text{S}_{14}$ ; Fig. 34]. Small particles of Fe oxyhydroxides, about the same size as pyrite, are disseminated in the section, but only one grain of pyrite was detected to have an oxidation rim, and the rim is only  $\sim 1$   $\mu\text{m}$  wide. Thus, 007 is among the least oxidized of the samples in the suite.

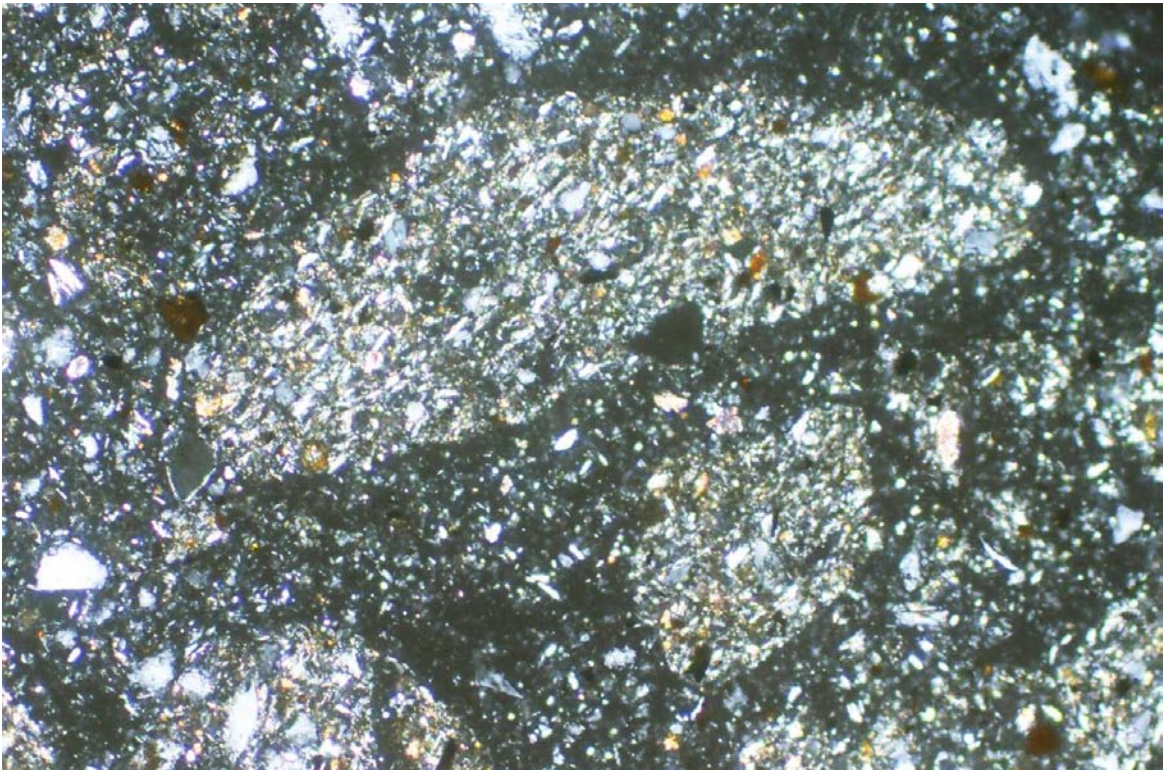
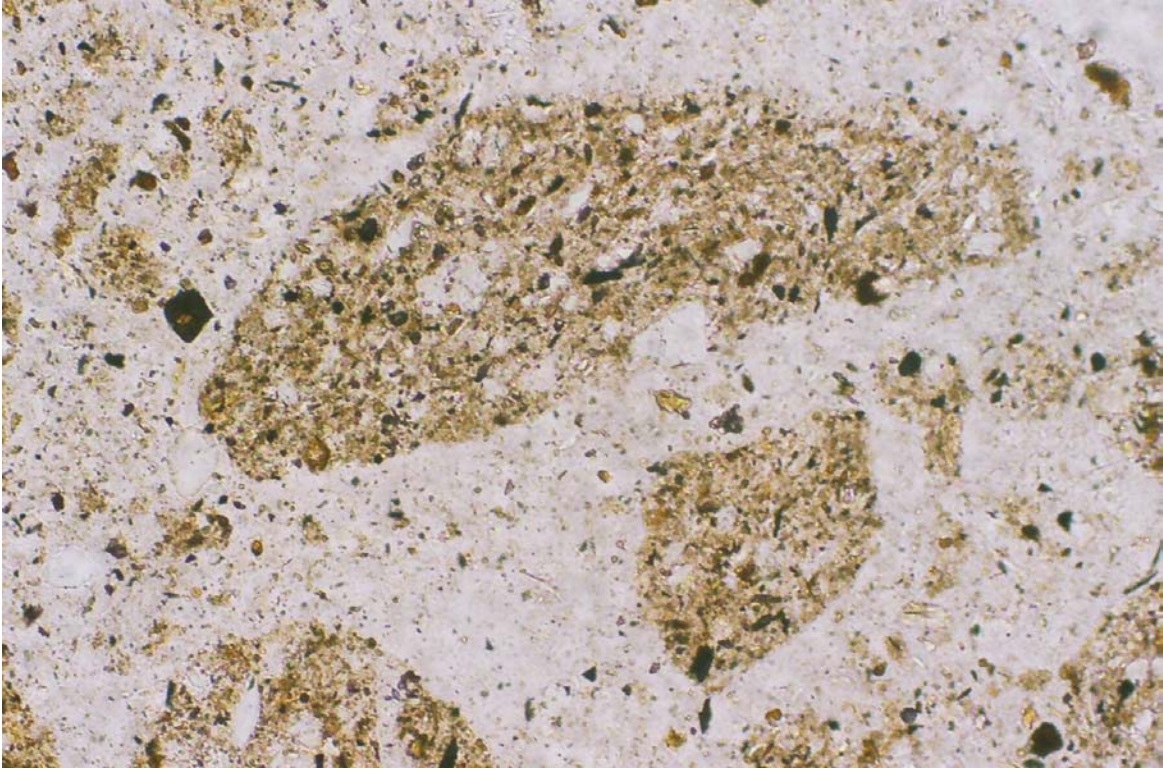


**Figure 33.** Sample 007 in plain transmitted light (top) and with polarizers crossed (bottom), width of field 0.625 mm, showing the brownish and turbid character, and the extremely fine grain size of the tailings.

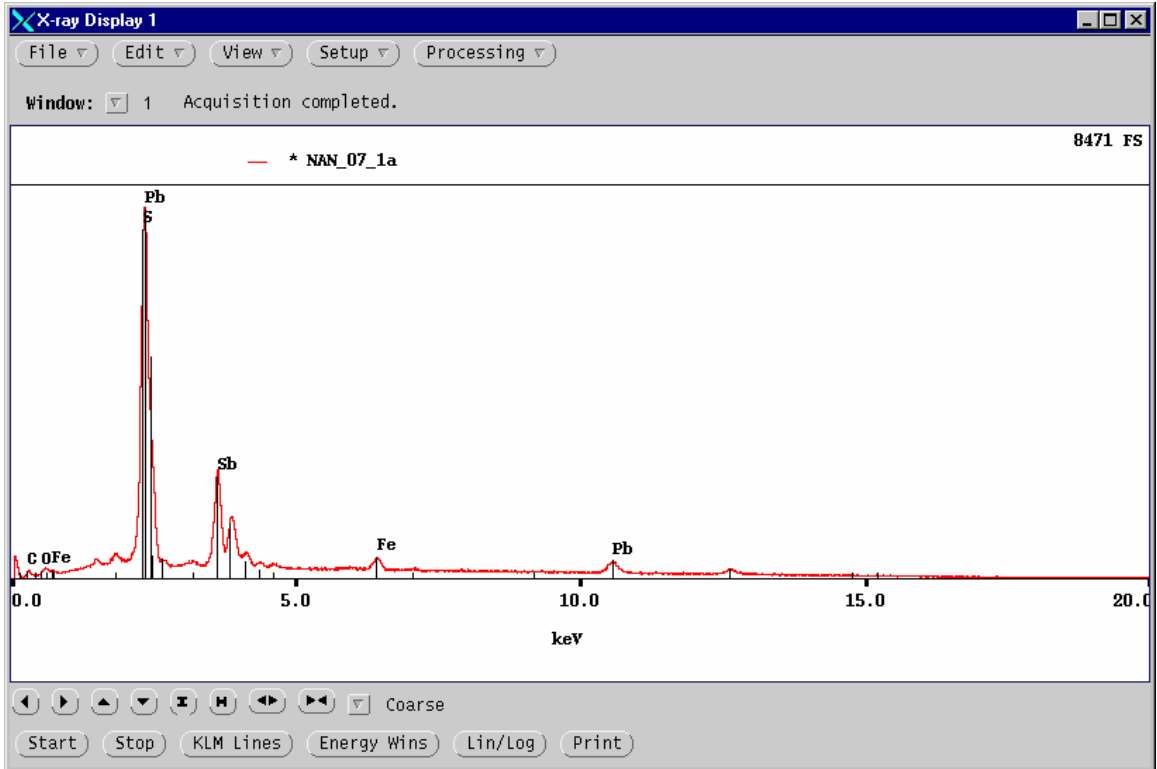


**Figure 34.** Sample 007 in plain reflected light, width of field 0.625 mm. The bright white grains are pyrite, and at the centre is an elongate grain interpreted to be jamesonite, for which the EDS spectrum is shown.

### ***Sample 008***

The as-received material was very fine-grained, with a plastic-like behaviour, and contained a small amount of free-flow liquid. The sample was slightly more brownish than 007, and ochreous streaks were visible (Fig. 35).

The polished thin-section is megascopically similar in colour to that of 007, but no sulfides are visible. Microscopy in transmitted light revealed that 007 and 008 are similarly turbid and fine-grained, and in 008 the upper range of grain sizes is 15 – 25  $\mu\text{m}$  for >90% of the material. The X-ray diffractogram of 008 indicates that the principal mineral assemblage is like that of 007, but 008 has more gypsum and contains both dolomite and calcite (Appendix 1). As in 007, a small amount of jarosite was detected in 008.

Reflected-light microscopy revealed the pyrite to be extremely fine-grained; most of the largest grains are only 10 – 15  $\mu\text{m}$  across, and only a few grains are in the upper part of that range. The typical sulfide assemblage of pyrite with accessory sphalerite and arsenopyrite is present, but no chalcopyrite was observed. Total sulfide content is estimated to be <1%. No alteration rims of Fe oxyhydroxide on sulfides, and no large particles of Fe oxyhydroxide were seen; however, an apparent pseudomorph after pyrite is shown in Figure 35, and numerous small particles of oxyhydroxide are disseminated throughout the section (Figs. 35, 37). EDS spectra of the specific oxyhydroxide particles indicated in Figure 35 and 37 contain detectable amounts of As and Zn or Cu (Figs. 36, 38).

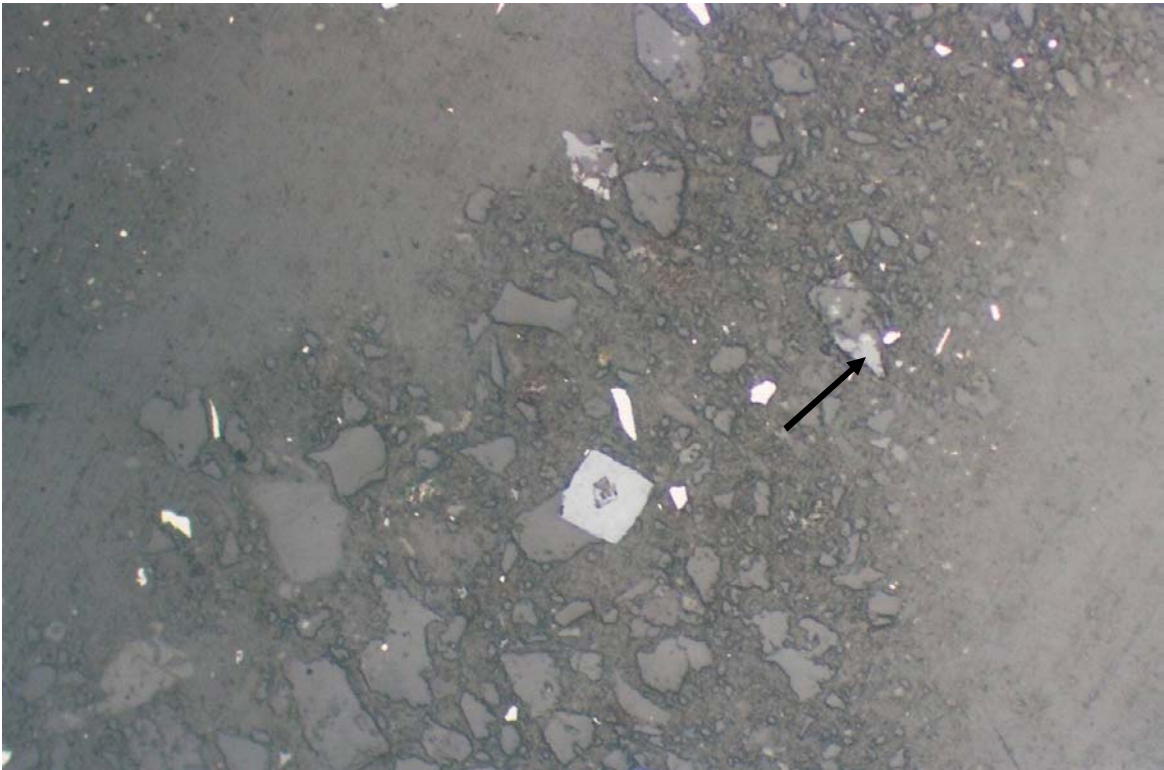


**Figure 35.** Sample 008. The upper photo, width of field 6 cm, is of the as-received tailings, whose wetness and plasticity are evident from the appearance of the extruded masses. The locally ochreous character can be seen in the uppermost mass. The lower photo is in plain reflected light, width of field 0.625 mm. EDS spectra of the cube-shaped and adjacent (at arrow) Fe oxyhydroxides are in Figure 36.

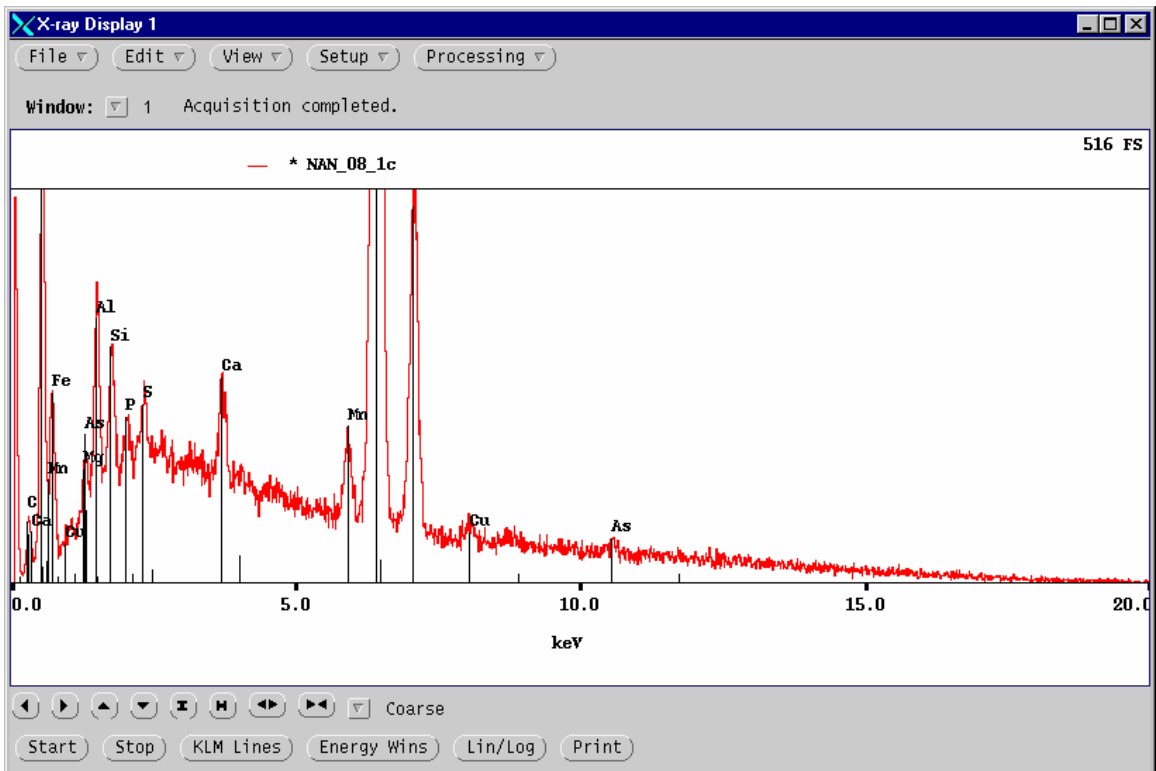
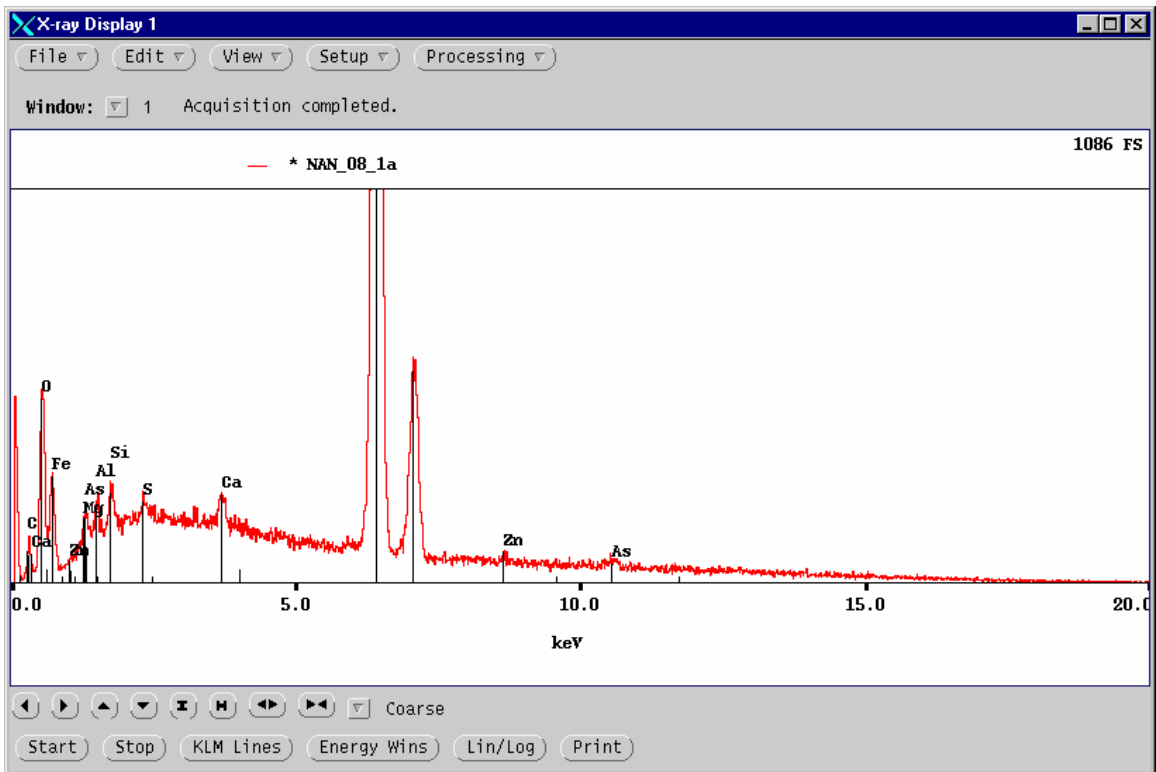


**Figure 36.** Expanded-scale EDS spectra of the cube-shaped (upper spectrum) and the other Fe-oxhydroxide particles shown in Figure 35. Both particles contain detectable amounts of As.

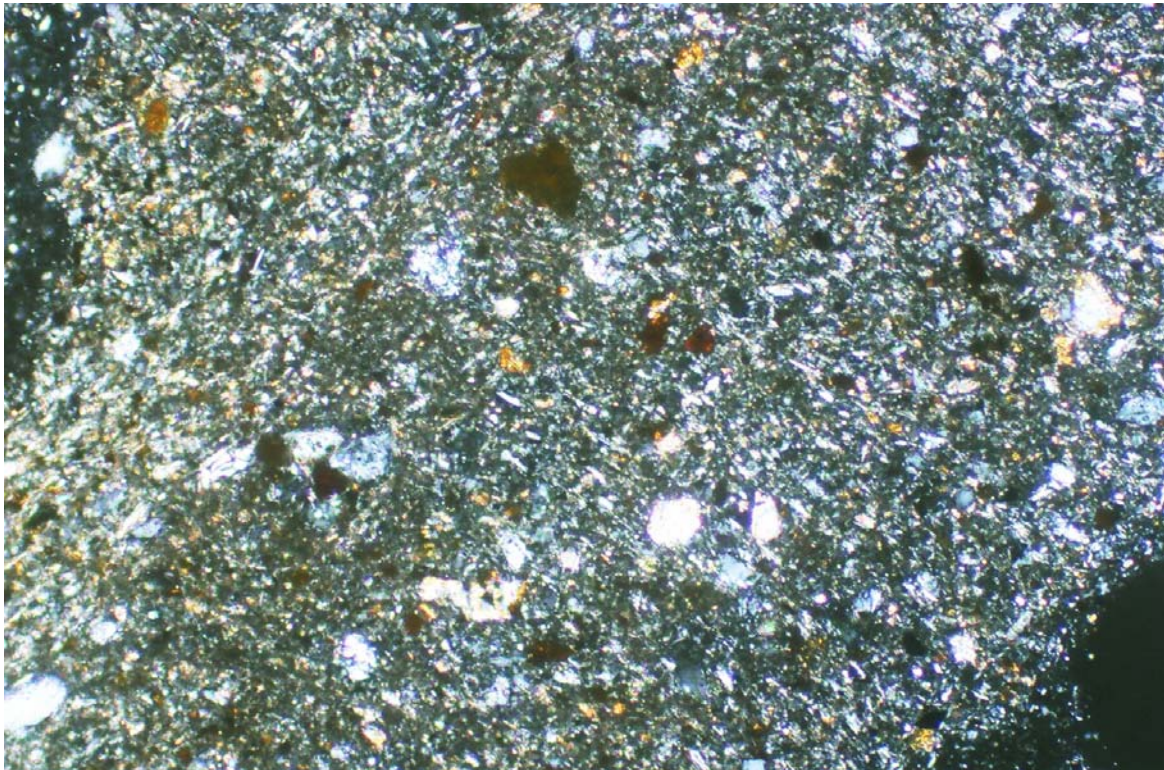
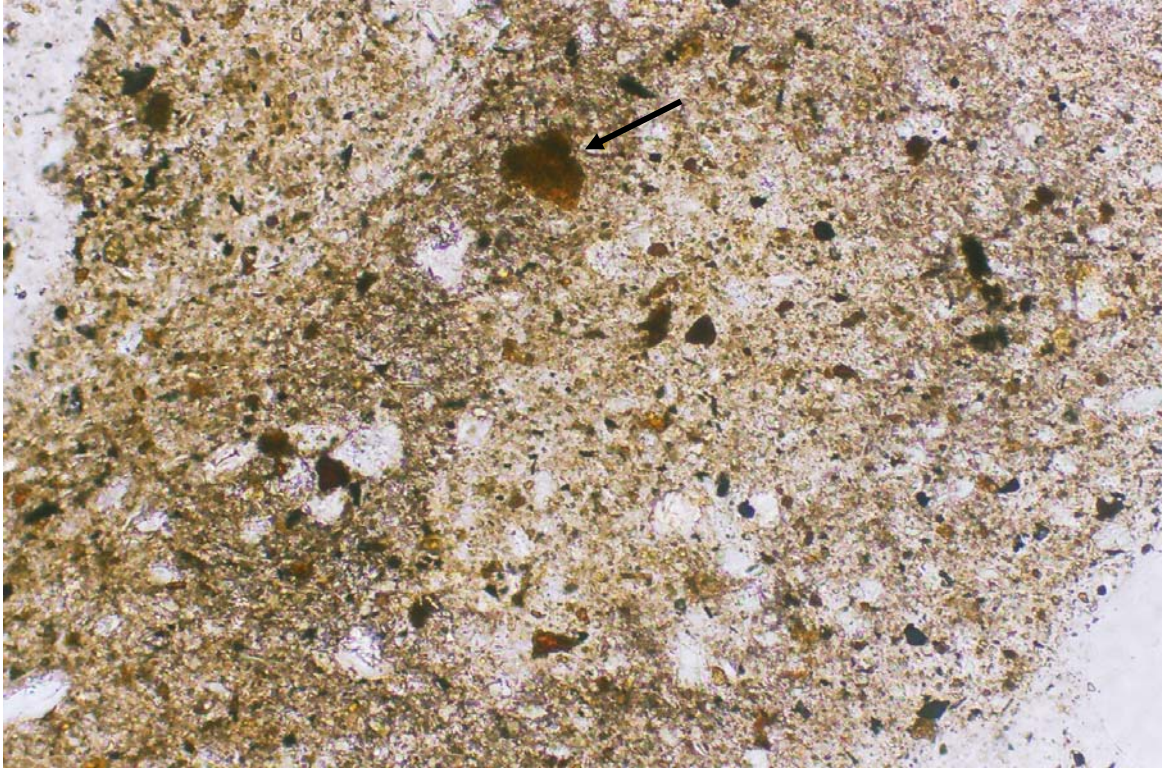


**Figure 37.** Sample 008 in plain transmitted light (top) and the same field with polarizers crossed (bottom), width of field 0.625 mm, showing the brownish, turbid, extremely fine-grained character of the tailings. The EDS spectrum for the largest Fe-oxyhydroxide particle (arrow) is in Figure 38.

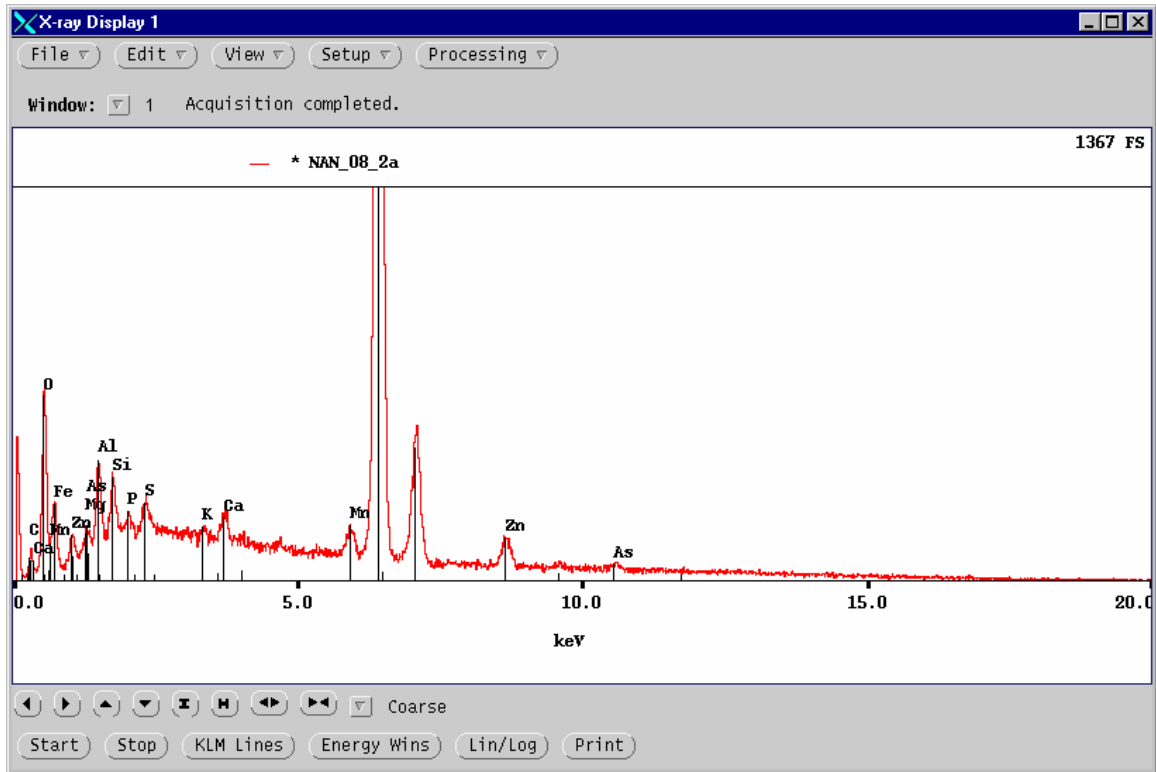


**Figure 38.** Expanded-scale EDS spectrum of the particle of Fe oxyhydroxide shown in Figure 37. The particle is Zn- and As-bearing.

### **Sample 009**

The as-received sample is slightly coarser grained than all of the preceding ones. The material was damp, with no separate aqueous phase, and the solids dried more rapidly than any of the other samples.

The polished thin-section is megascopically light brownish, more like that of 004A rather than 007 or 008. Pin-points of sulfides are abundantly dispersed throughout the section.

Reflected-light microscopy showed that 009 is the coarsest grained and most sulfide-rich sample in the tailings suite. The pyrite content is probably >5%, and individual grains are commonly up to 150  $\mu\text{m}$  across. Sphalerite, arsenopyrite, and chalcopyrite, in decreasing order of abundance, make up about 2% of the total sulfide content. Other sulfides observed in the section in trace amounts are galena, Ag-rich tetrahedrite  $[(\text{Cu},\text{Ag})_{10}(\text{Fe},\text{Zn})_2\text{Sb}_4\text{S}_{13}]$ , and covellite.

The non-opaque assemblage differs from that of the other samples. Particle sizes are up to 200  $\mu\text{m}$  across and consist predominantly of quartz as individual grains and chert-like

aggregates (Fig. 39). Gypsum is common as individual crystals and as aggregates that cement the tailings particles (Fig. 40). A distinct difference is the low carbonate content; a 25% HCl test of the powder gave such a weak reaction that it was uncertain whether the bubbles that evolved were from a carbonate mineral or entrapped air. A Rietveld analysis of the X-ray diffractometry data indicated that calcite is present, but the amount is <0.5 wt% (Appendix 1). Noteworthy features are the detection of a small amount of goethite (1.5 wt%) and of an appreciable amount of jarosite (5.1 wt%).

Numerous grains of pyrite in the section have well-developed oxidation rims and, unusually, the rims also occur on chalcopyrite and sphalerite (Figs. 41-44). Typically such rims do not form on sphalerite unless the pH is high; the presence of the rims in an oxidizing sulfide-rich environment suggests that the tailings at the site were initially more carbonate-rich and currently are in a transition stage that will progress to low-pH conditions as the small amount of remaining calcite is consumed.

EDS spectra of various Fe-oxyhydroxide particles are shown in Figures 42-45. The results are highly variable, but some of the spectra indicate the presence of Cu, Zn, or As in association with Fe oxyhydroxides. The spectra also indicate that plumbojarosite forms a portion of the secondary assemblage.

## CONCLUSIONS

The primary objective of the mineralogical study was the determination of whether minerals that may become destabilized under reducing sedimentary conditions are present. The mineralogical results indicate that a variety of secondary minerals is present and that these minerals have sequestered potentially deleterious elements such as Cu, Zn, Pb, and As. The principal hosts for these elements are Fe oxyhydroxides and jarosite-type minerals, neither of which is stable under reducing conditions.

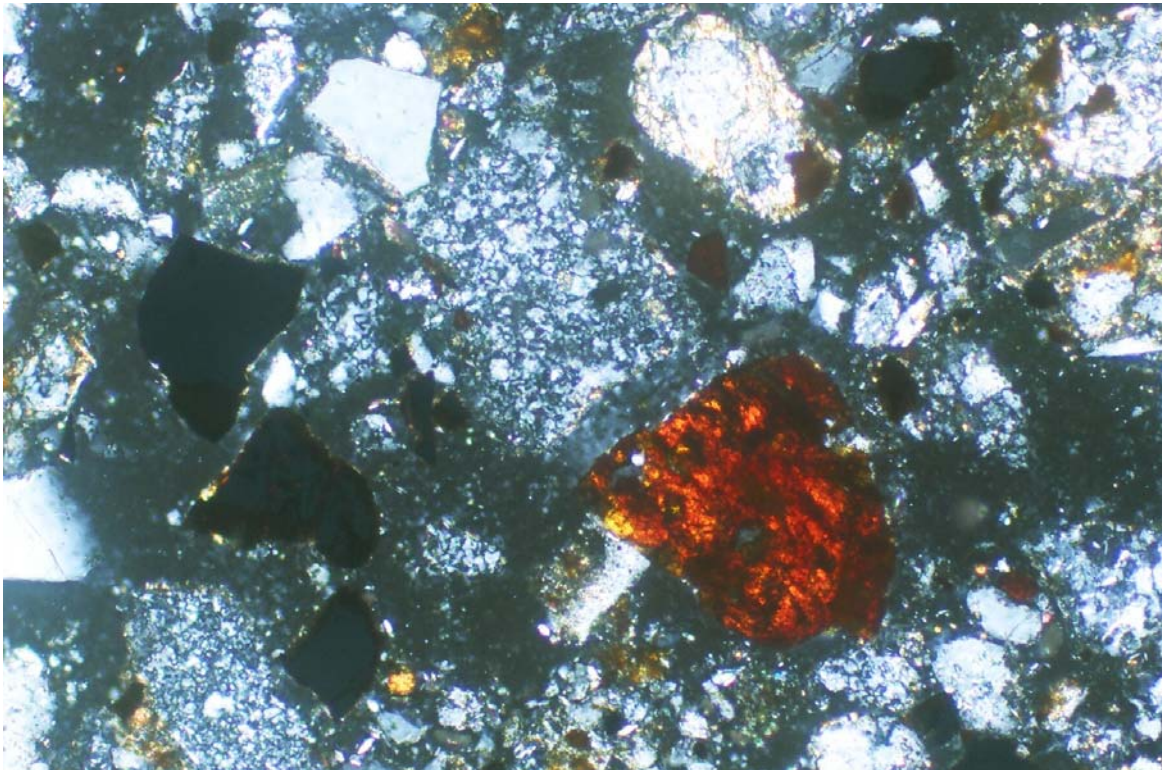
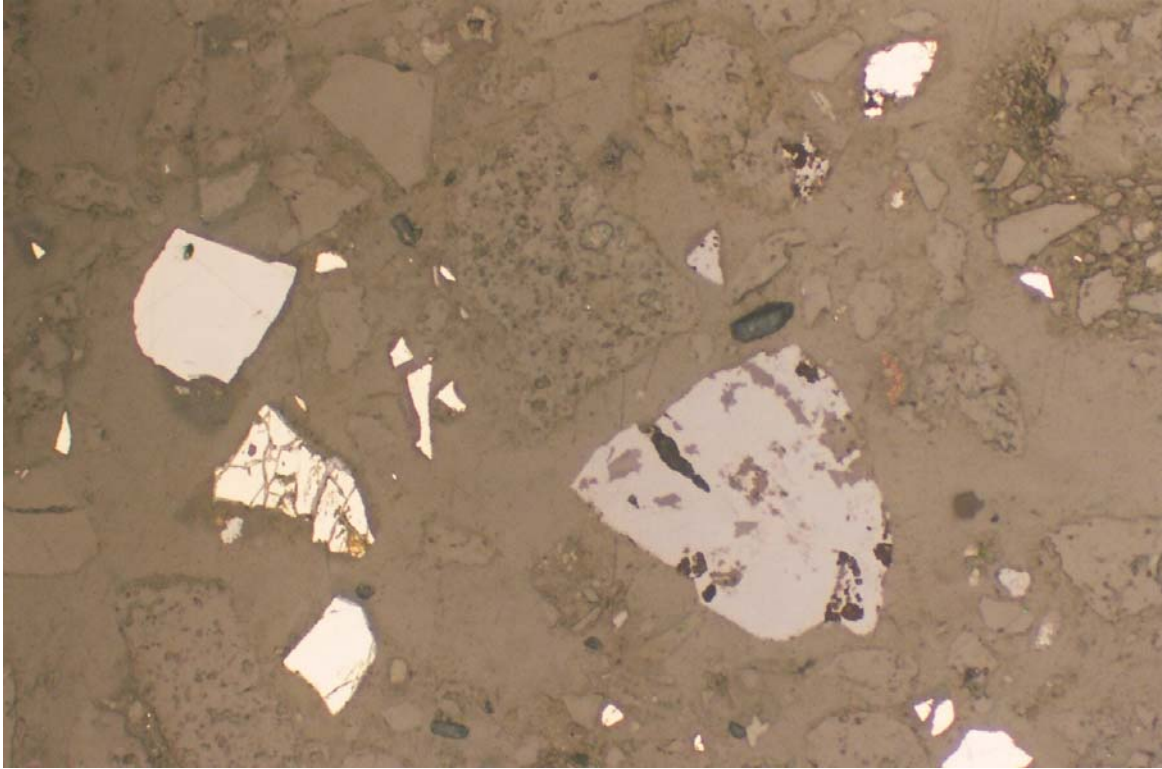


**Figure 39.** Sample 009 in plain reflected light (top) and in transmitted light with crossed polarizers (bottom), width of field 0.625 mm. The grey grain on the far left (upper photo) is tetrahedrite, and the whitish grains are pyrite. The lower photo shows a large particle of Fe oxyhydroxide for which the EDS spectrum did not show detectable heavy metals or metalloids.

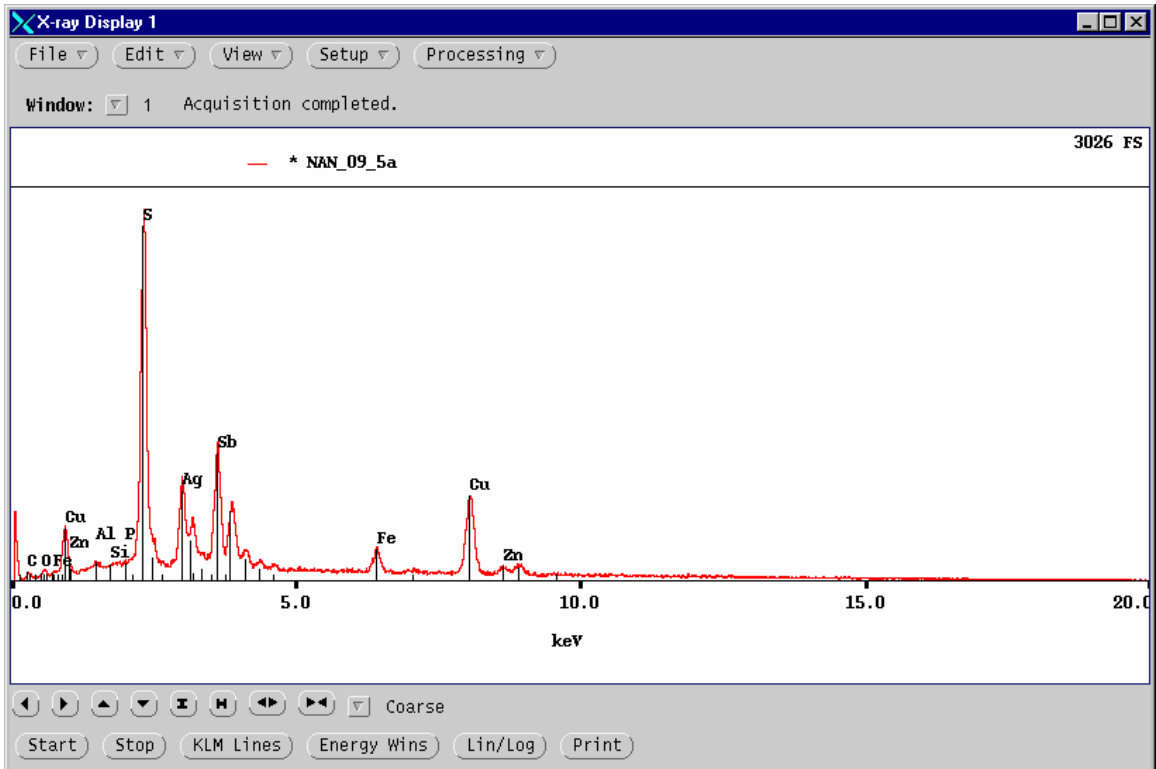


**Figure 40.** EDS spectrum of the Ag-rich tetrahedrite of Figure 39. The photomicrograph is for plain reflected light, width of field 0.625 mm. The white grains are pyrite. The darker, rough-looking, cementing mineral in the large aggregate above centre is gypsum, which also occurs as crystals in the surrounding area.

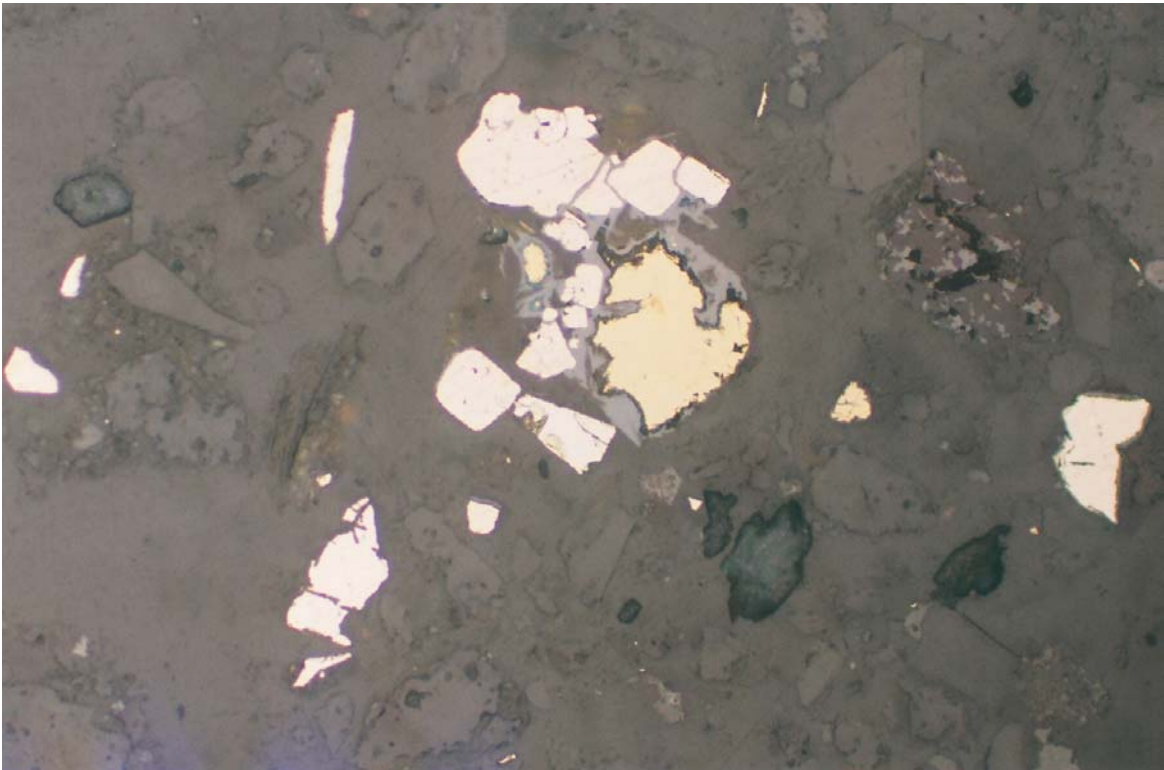


**Figure 41.** Sample 009 in plain reflected light, width of field 0.625 mm. The upper photo shows white grains of pyrite and, on the left, a weakly altered grain of yellow chalcopyrite. Numerous grains of gypsum are present on the right. In the lower photo, chalcopyrite near the centre is enclosed within Fe oxyhydroxide (Fig. 42).

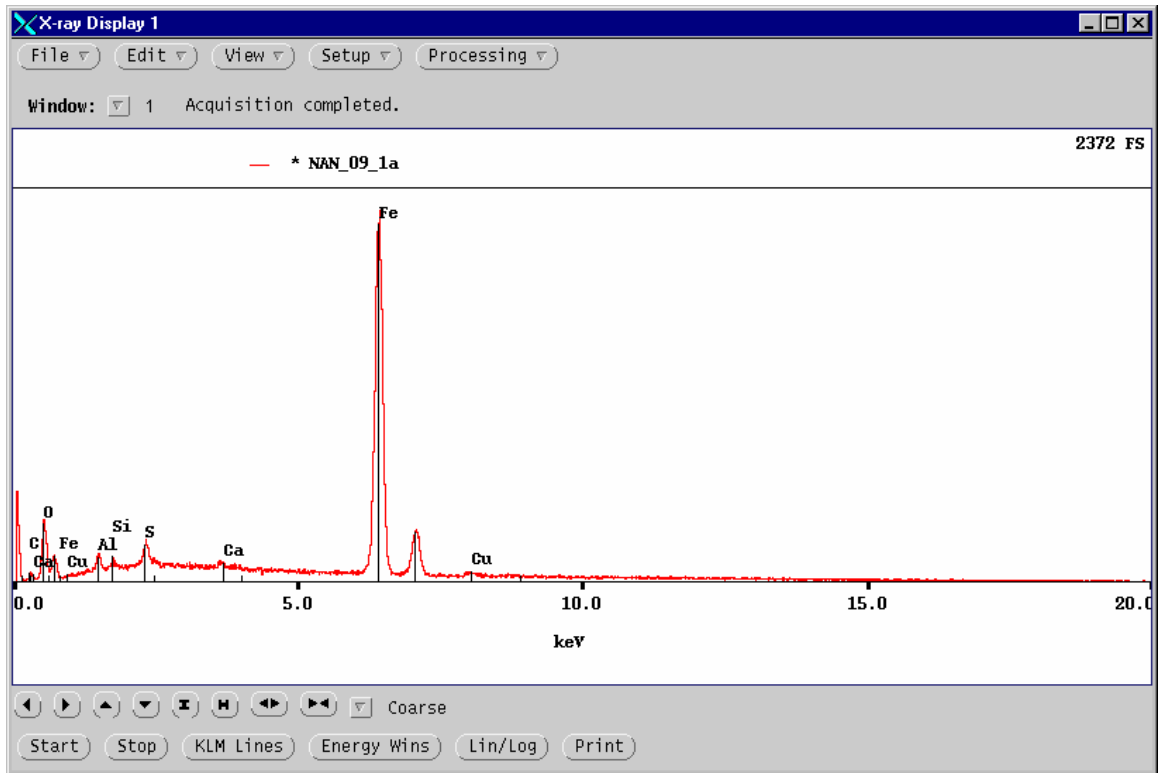


**Figure 42.**EDS spectrum of the Fe-oxyhydroxide associated with the chalcopyrite in the lower photo of Figure 41. The photomicrograph (plain reflected light, width of field 0.625 mm) shows pyrite with a well-developed oxyhydroxide rim.

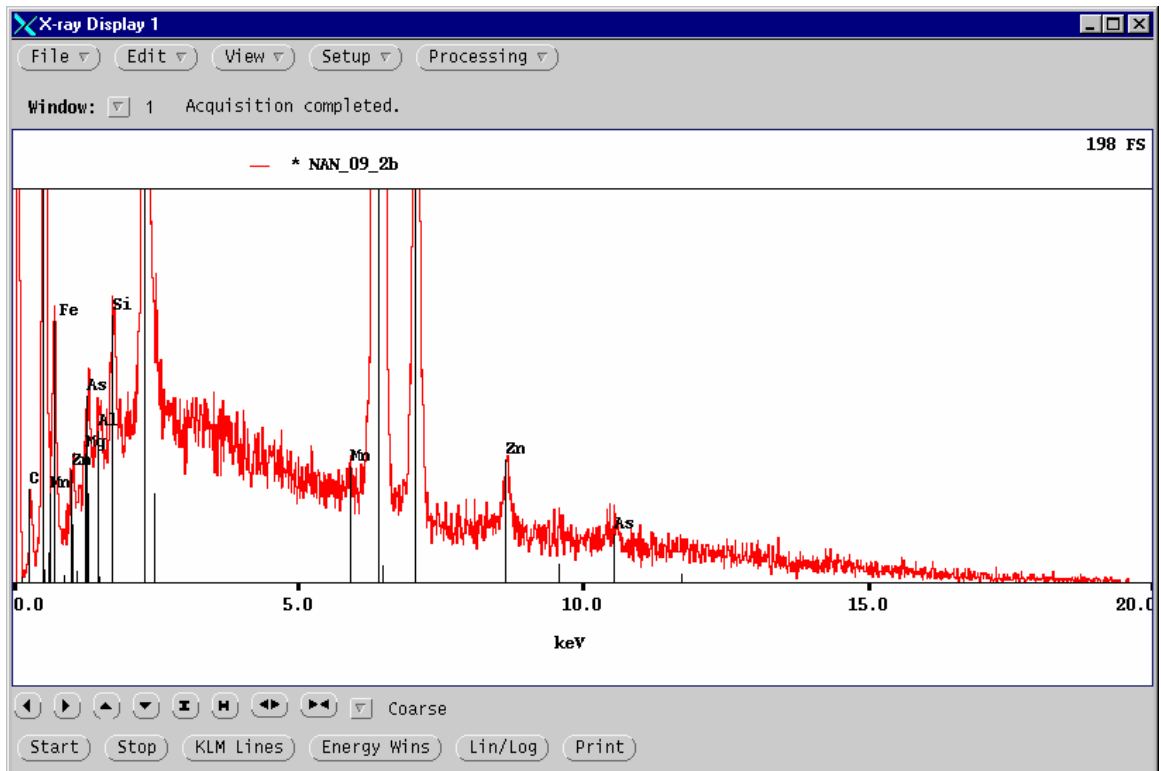
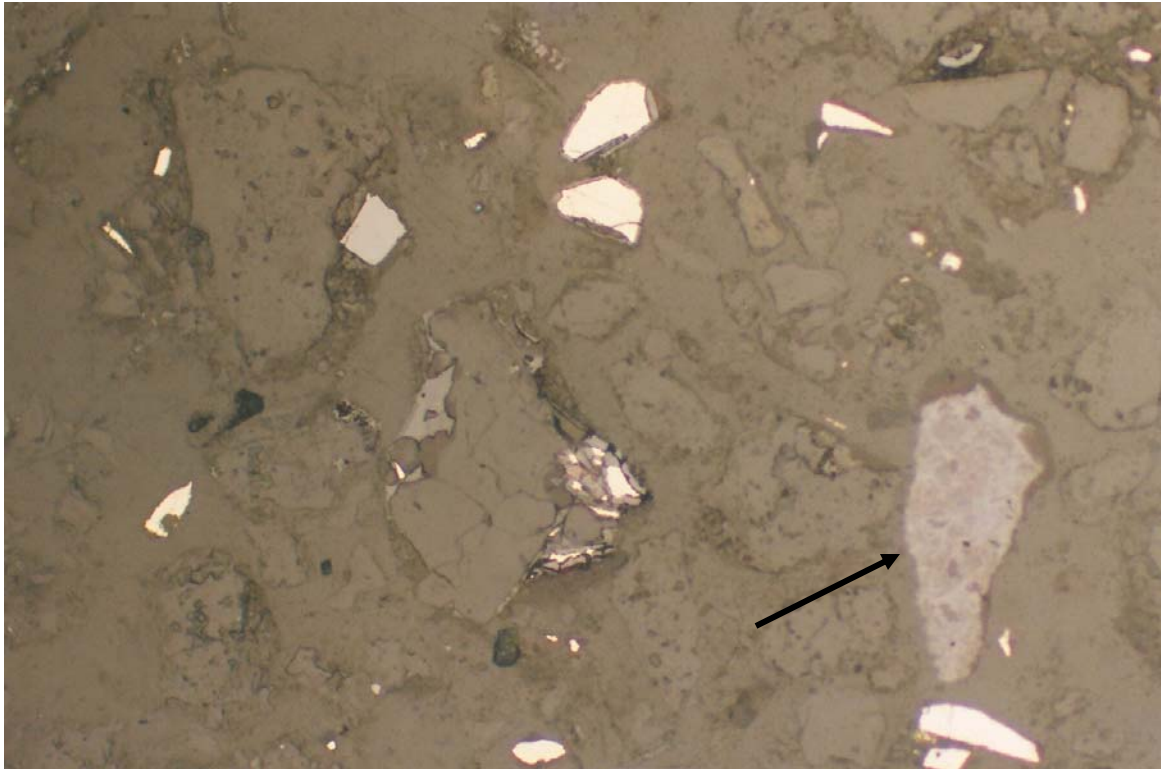


**Figure 43.** Sample 009 in plain reflected light, width of field 0.625 mm. Just below centre is altered pyrite; the expanded-scale EDS spectrum is for the Fe-oxyhydroxide rim, which contains trace amounts of Zn and As. The arrow points to a heterogeneous Fe-oxyhydroxide particle for which the spectrum is in Figure 44.

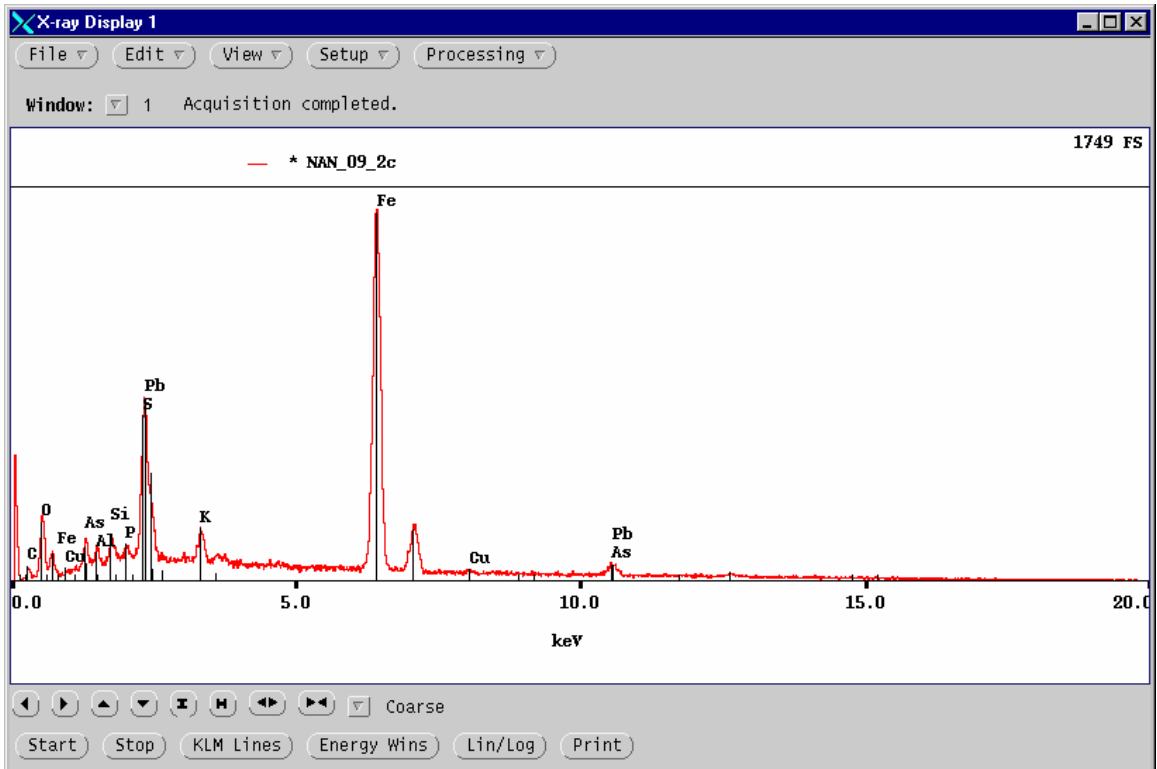


**Figure 44.** The EDS spectrum is for the particle at the arrowhead in Figure 43. The composition corresponds to that of plumbojarosite. The photo (plain reflected light, width of field 0.625 mm) shows, below centre, an elongate grain of grey sphalerite with a distinct alteration rim.

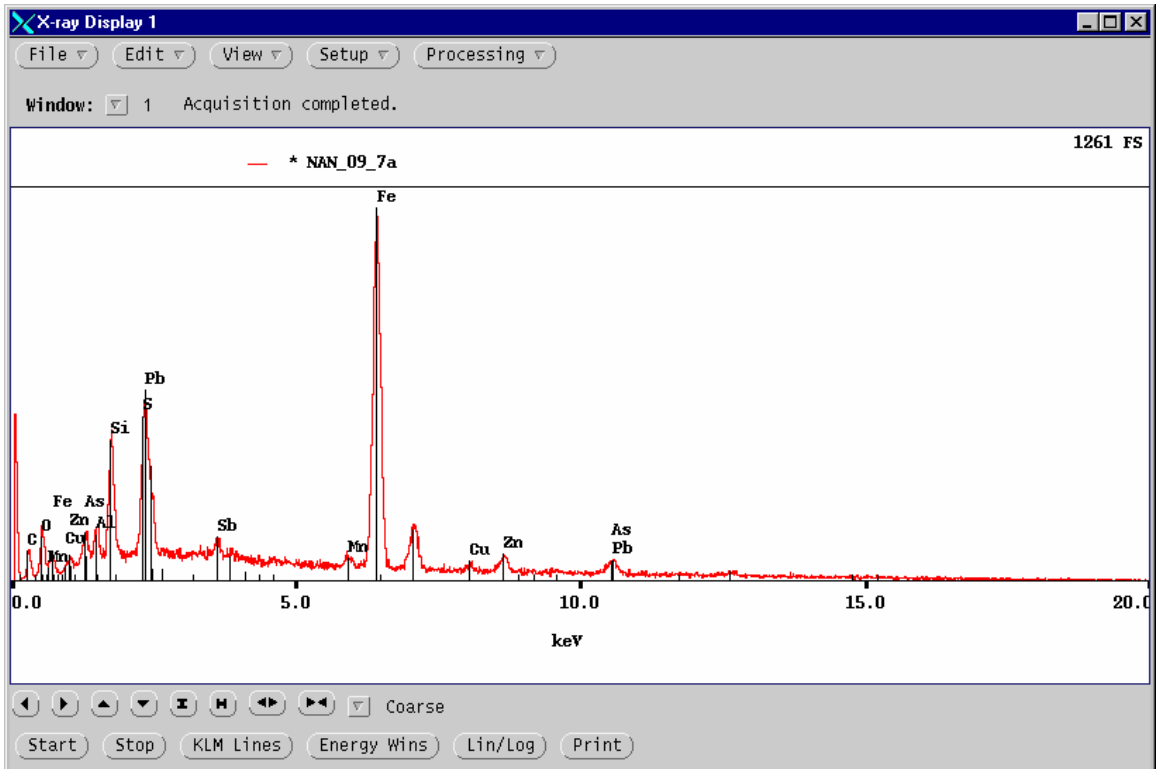
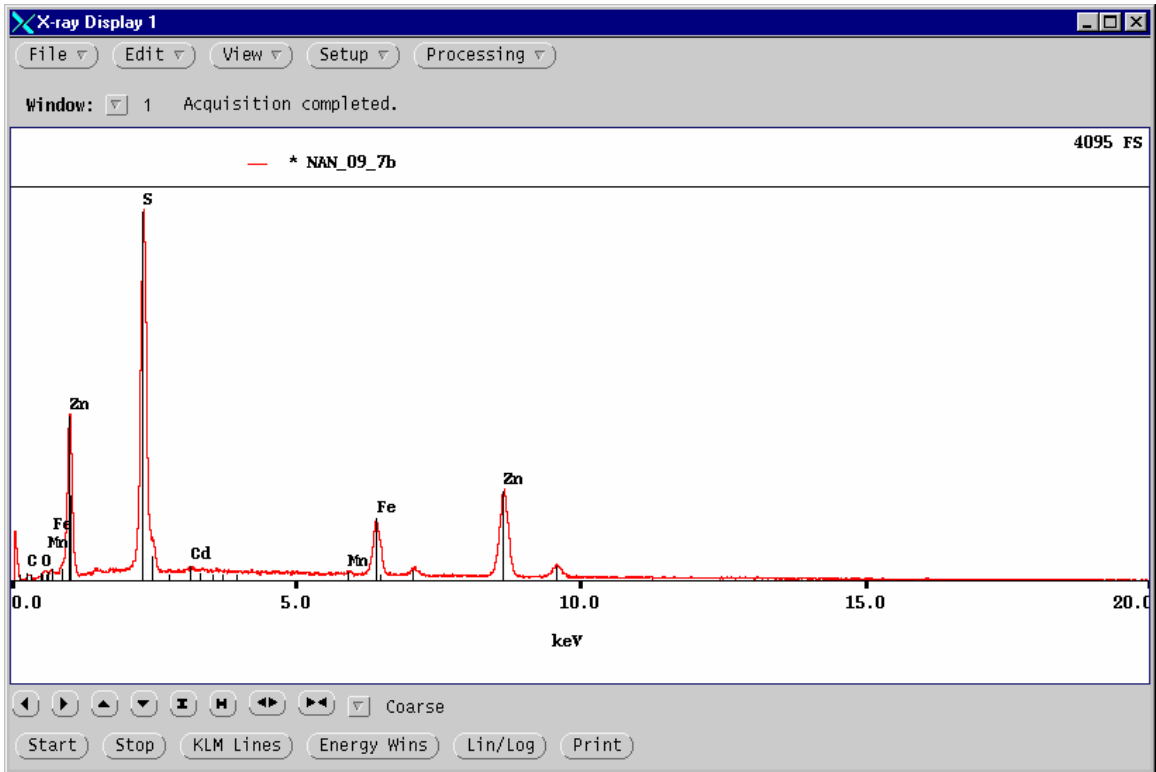


**Figure 45.** The upper spectrum is of the sphalerite grain shown in Figure 44. The lower spectrum is of the sphalerite alteration rim, which apparently consists of plumbojarosite, as in the Figure 44 spectrum.

*APPENDIX 1*

***Analysis of Four Samples Using the Rietveld Method and X-ray  
Powder Diffraction Data.***

---

***J.L. Jambor, Ph.D.  
Leslie Research and Consulting  
316 Rosehill Wynd  
Tsawwassen, B.C. V4M 3L***

---

---

***Mati Raudsepp, Ph.D.  
Elisabetta Pani, Ph.D.***

***Dept. of Earth & Ocean Sciences  
6339 Stores Road  
The University of British Columbia  
Vancouver, BC V6T 1Z4***

***November 16, 2005***

## EXPERIMENTAL METHODS

The samples **NAN-04B** and **NAN-09** were reduced to the optimum grain-size range for quantitative X-ray analysis (<5  $\mu\text{m}$ ) by grinding under ethanol in a vibratory McCrone Micronising Mill (McCrone Scientific Ltd., London, UK) for 7 minutes. Fine grain-size is an important factor in reducing micro-absorption contrast between phases. The samples **NAN-07** and **NAN-8** were ground into fine powder and smeared on to a glass slide with ethanol.

Step-scan X-ray powder-diffraction data for all the samples were collected over a range  $3\text{-}80^\circ 2\theta$  with  $\text{CoK}\alpha$  radiation on a standard Siemens (Bruker) D5000 Bragg-Brentano diffractometer equipped with a diffracted-beam with a Fe monochromator foil, 0.6 mm ( $0.3^\circ$ ) divergence slit, incident- and diffracted-beam Sollers slits and a Vantec-1 strip detector. The long fine-focus Co X-ray tube was operated at 35 kV and 40 mA, using a take-off angle of  $6^\circ$ .

## RESULTS

The X-ray diffractograms of all the four samples were analyzed using the International Centre for Diffraction Database PDF-4 using Search-Match software by Siemens (Bruker). X-ray powder-diffraction data of the two samples **NAN-04B** and **NAN-09** were refined with Rietveld Topas 3 (Bruker AXS). The results of quantitative phase analysis by Rietveld refinements are given in Table 1. These amounts represent the relative amounts of crystalline phases normalized to 100%. The Rietveld refinement plots are shown in Figures 1-2.

The X-ray diffractograms for samples **NAN-07** and **NAN-8** are shown in Figures 3-4.

**Sample NAN-07** consists of quartz,  $\text{SiO}_2$ , muscovite,  $\text{KAl}_2\text{AlSi}_3\text{O}_{10}(\text{OH})_2$  and gypsum,  $\text{CaSO}_4 \cdot 2\text{H}_2\text{O}$ , with minor clinocllore,  $(\text{Mg},\text{Fe}^{2+})_5\text{Al}(\text{Si}_3\text{Al})\text{O}_{10}(\text{OH})_8$ , pyrite,  $\text{FeS}_2$ , jarosite,  $\text{KFe}_3^{3+}(\text{SO}_4)_2(\text{OH})_6$ , dolomite,  $\text{CaMg}(\text{CO}_3)_2$ , kaolinite,  $\text{Al}_2\text{Si}_2\text{O}_5(\text{OH})_4$  and trace of actinolite,  $\text{Ca}_2(\text{Mg},\text{Fe}^{2+})_5\text{Si}_8\text{O}_{22}(\text{OH})_2$ .

**Sample NAN-8** consists of quartz,  $\text{SiO}_2$ , muscovite,  $\text{KAl}_2\text{AlSi}_3\text{O}_{10}(\text{OH})_2$  and gypsum,  $\text{CaSO}_4 \cdot 2\text{H}_2\text{O}$ , with minor jarosite,  $\text{KFe}_3^{3+}(\text{SO}_4)_2(\text{OH})_6$ , dolomite,  $\text{CaMg}(\text{CO}_3)_2$ , pyrite,  $\text{FeS}_2$ , kaolinite,  $\text{Al}_2\text{Si}_2\text{O}_5(\text{OH})_4$ , clinocllore,  $(\text{Mg},\text{Fe}^{2+})_5\text{Al}(\text{Si}_3\text{Al})\text{O}_{10}(\text{OH})_8$ , calcite,  $\text{CaCO}_3$ , and epidote,  $\text{Ca}_2(\text{Fe}^{3+},\text{Al})_3(\text{SiO}_4)_3(\text{OH})$ .

Table 1. Results of quantitative phase analysis (wt.%)

	Ideal Formula	<b>NAN-04B</b>	<b>NAN-09</b>
Quartz	SiO <sub>2</sub>	28.0	68.3
Muscovite	KAl <sub>2</sub> AlSi <sub>3</sub> O <sub>10</sub> (OH) <sub>2</sub>	19.4	13.5
Clinchlore	(Mg,Fe <sup>2+</sup> ) <sub>5</sub> Al(Si <sub>3</sub> Al)O <sub>10</sub> (OH) <sub>8</sub>		1.9
Kaolinite	Al <sub>2</sub> Si <sub>2</sub> O <sub>5</sub> (OH) <sub>4</sub>	2.8	
Calcite	CaCO <sub>3</sub>	42.9	0.4
Gypsum	CaSO <sub>4</sub> ·2H <sub>2</sub> O	3.5	2.2
Jarosite	KFe <sub>3</sub> <sup>3+</sup> (SO <sub>4</sub> ) <sub>2</sub> (OH) <sub>6</sub>	0.6	5.1
Pyrite	FeS <sub>2</sub>	2.9	7.2
Goethite	α-Fe <sup>3+</sup> O(OH)		1.5
Total		100.0	100.0

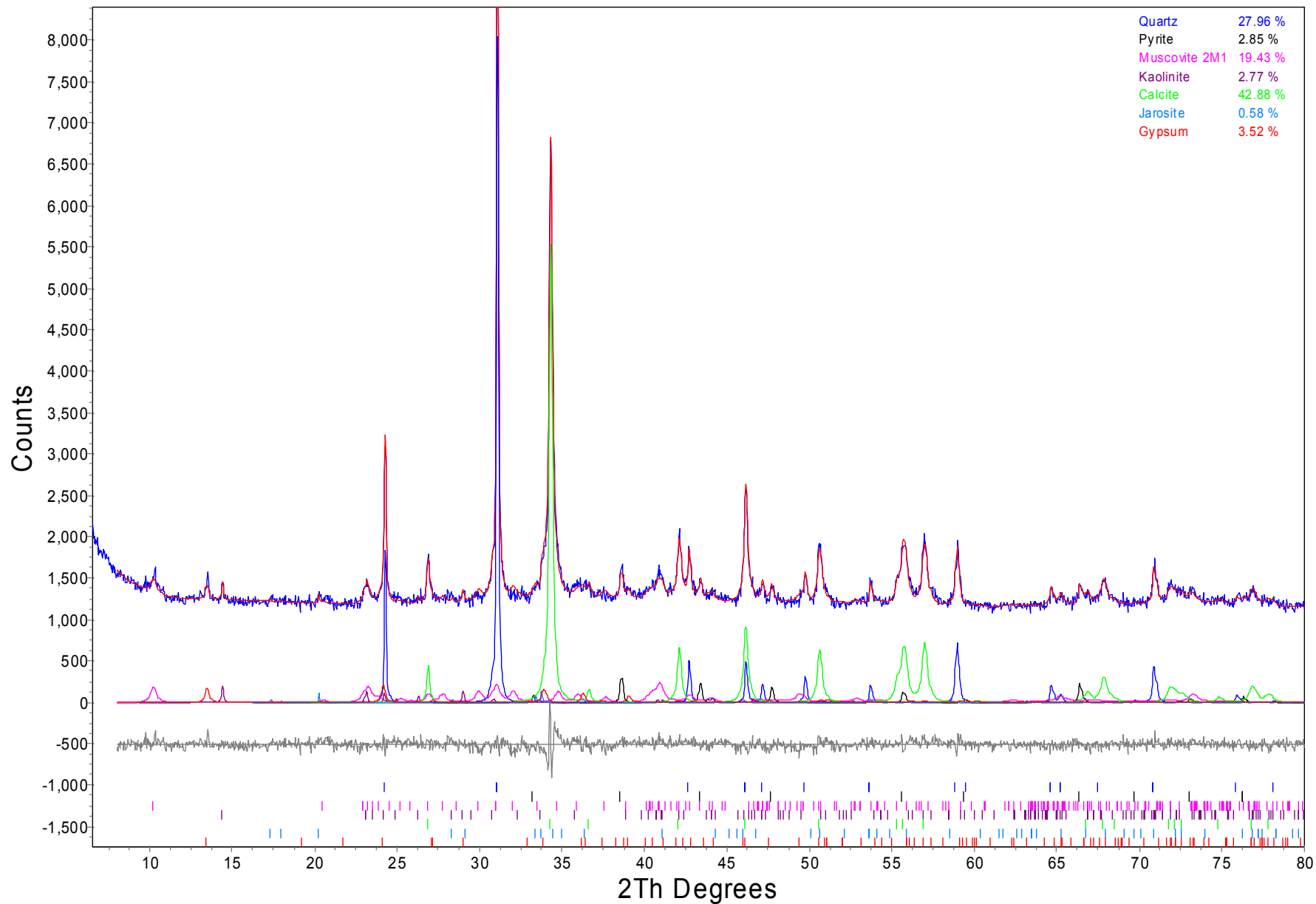


Figure 1. Rietveld refinement plot of sample **NAN-04B** (blue line - observed intensity at each step; red line - calculated pattern; solid grey line below – difference between observed and calculated intensities; vertical bars, positions of all Bragg reflections). Coloured lines are individual diffraction patterns of all phases.

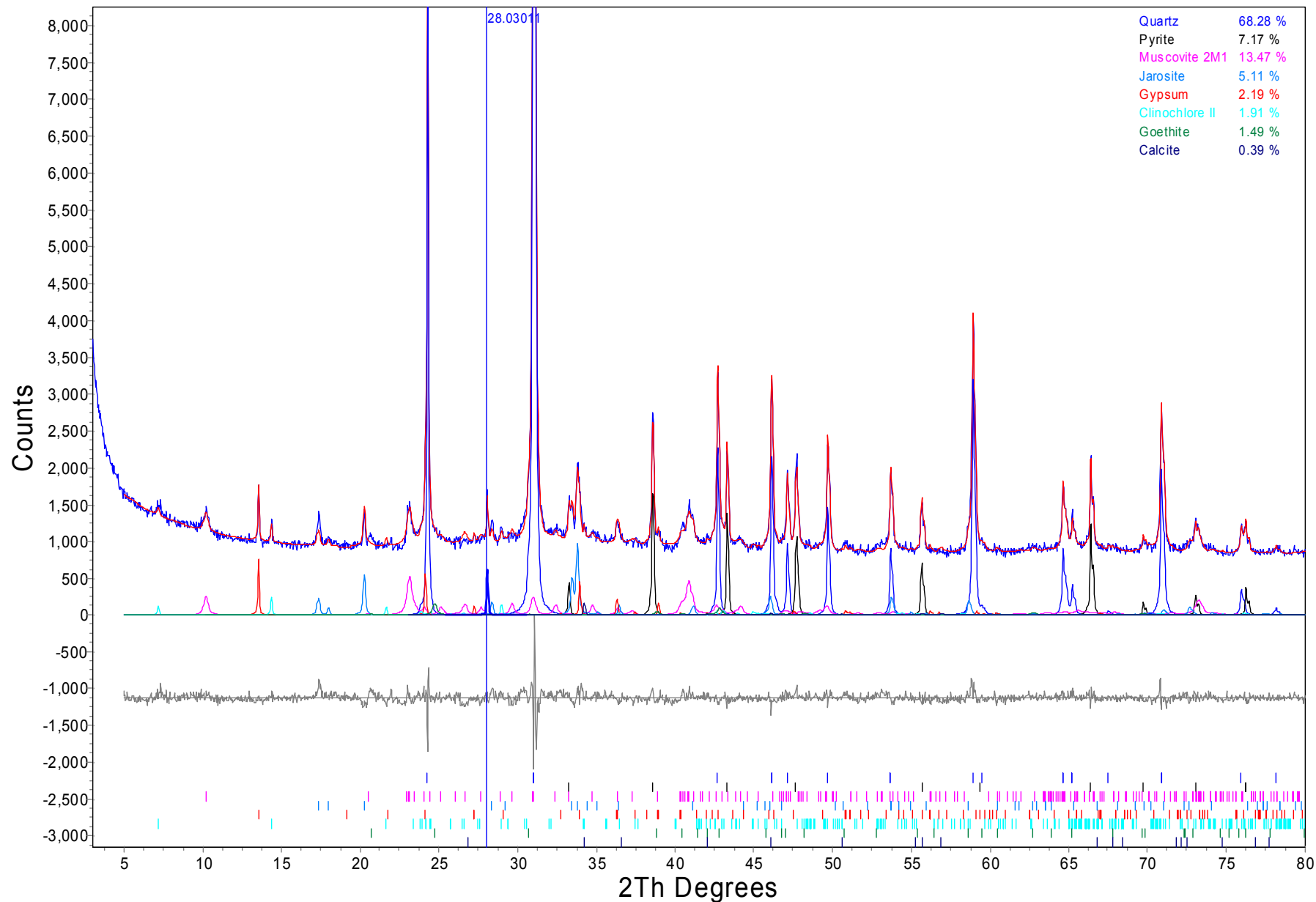


Figure 2. Rietveld refinement plot of sample **NAN-09** (blue line - observed intensity at each step; red line - calculated pattern; solid grey line below - difference between observed and calculated intensities; vertical bars, positions of all Bragg reflections). Coloured lines are individual diffraction patterns of all phases.

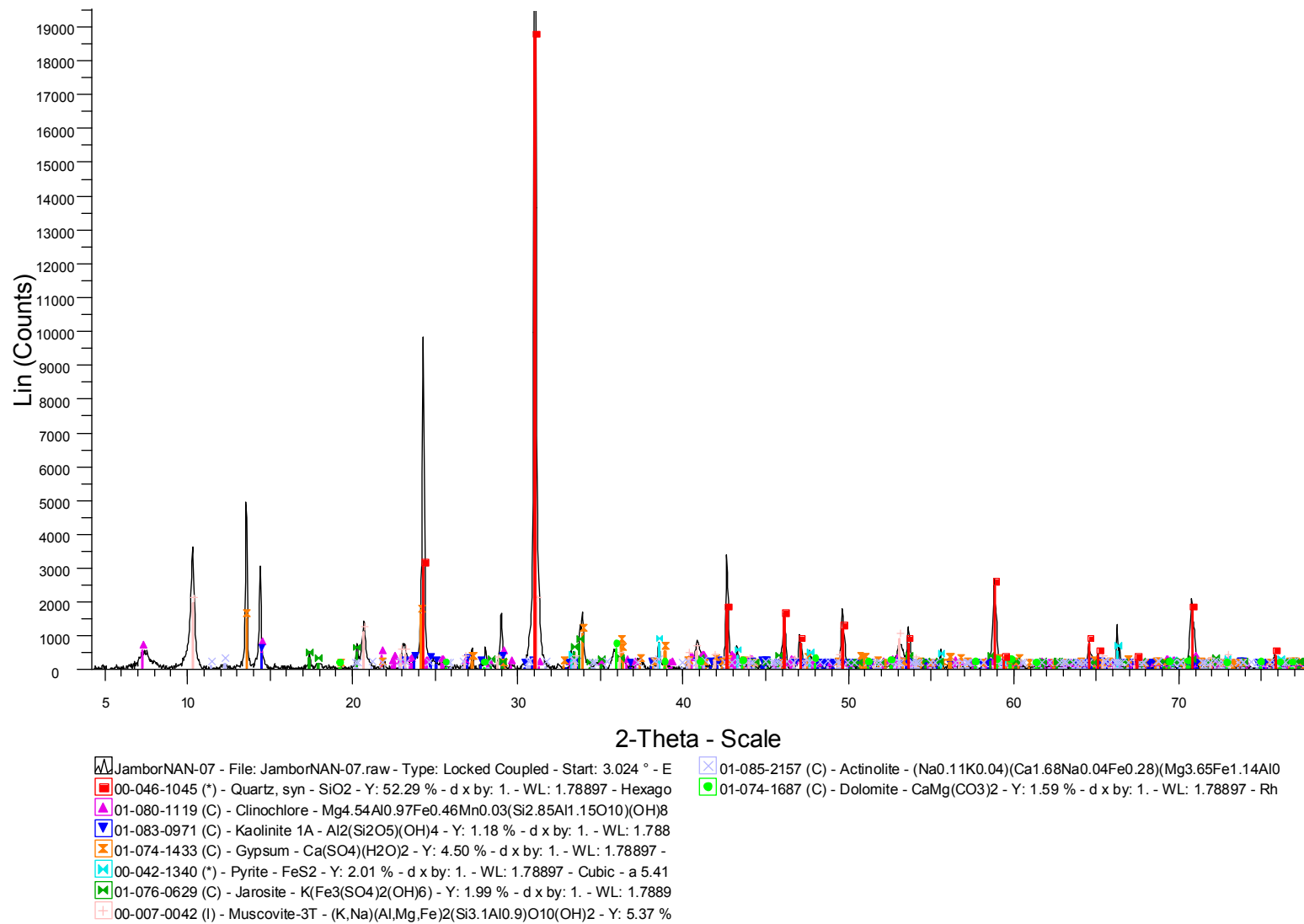


Figure 3. X-ray diffractogram of sample NAN-07 (Background subtracted).

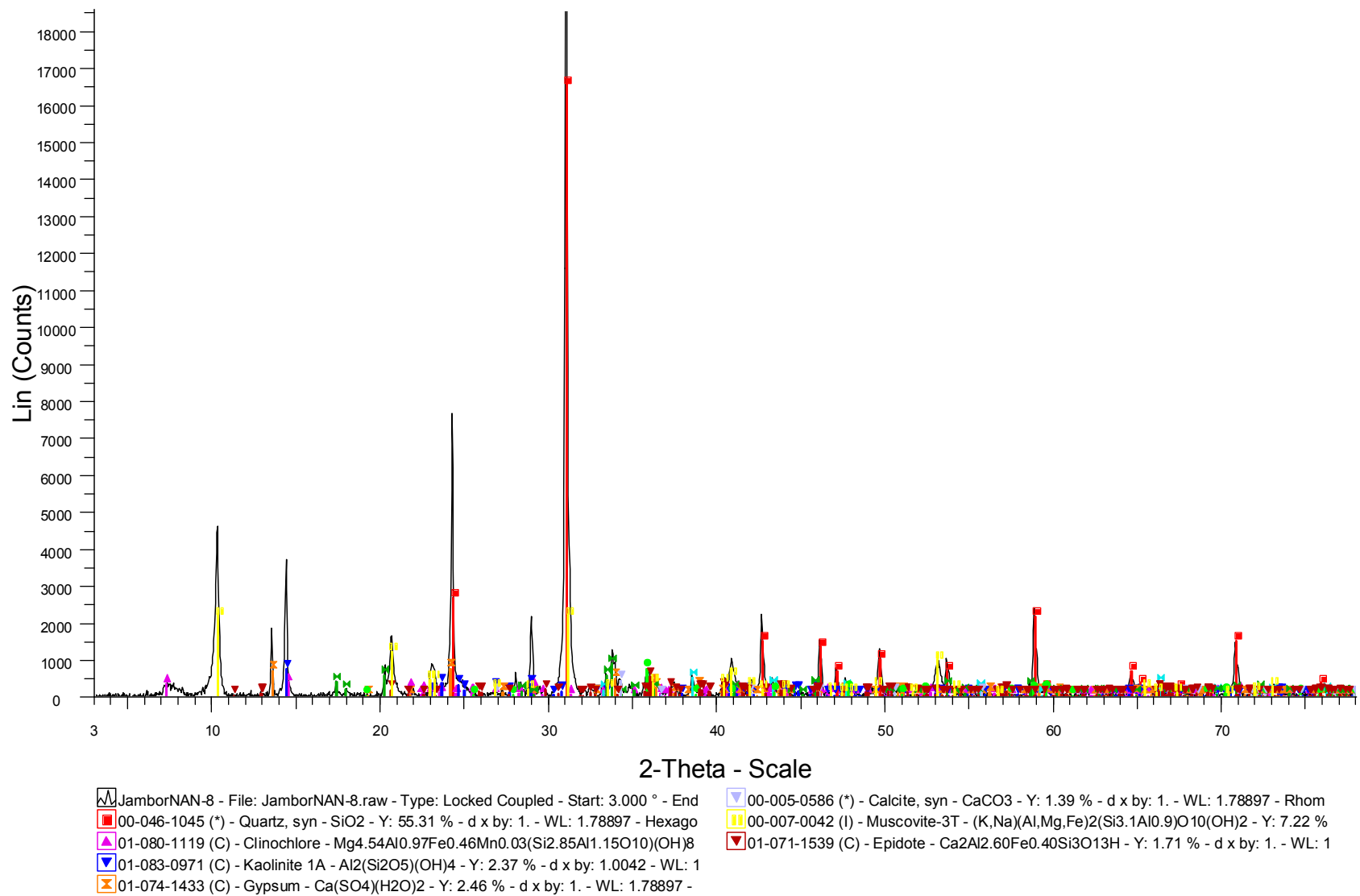


Figure 4. X-ray diffractogram of sample **NAN-8** (Background subtracted).